IGF2BP1 is the First Positive Marker for Anaplastic Thyroid Carcinoma and an Enhancer of a Targetable Gene Expression Signature

Dissertation

zur Erlangung des akademischen Grades

doctor rerum naturalium

(Dr. rer. nat.)

der

Naturwissenschaftlichen Fakultät I – Biowissenschaften –

der Martin-Luther-Universität Halle-Wittenberg,

vorgelegt

von Herrn Jacob Haase

geboren am 31.03.1989 in Karl-Marx-Stadt

Gutachter:
1.   Prof. Dr. Stefan Hüttelmaier
2.   Prof. Dr. Sonja Kessler
3.   Prof. Dr. Julian König

Tag der Verteidigung: 11. Dezember 2020

TABLE OF CONTENTS

Danksagung
Curriculum Vitae
List of publications, held presentations and poster
Erklärung

1. INTRODUCTION

1.1 The thyroid gland

The thyroid gland belongs to the endocrine system, which consists of richly vascularized ductless organs that produce hormones. In humans, the thyroid gland typically lies lateral to the trachea, near the base of the laryngeal cartilages (Figure 1). It is a butterfly shaped organ with a right and left lobe, joined by the *Isthmus*, which forms a bridge across the ventral and anterior aspect of the trachea. It is composed of two hormone-secreting cell types, follicular cells (thyrocytes) and parafollicular cells (C cells). The functional subunit of each thyroid gland is the follicle, formed by a monolayer of follicular cells. These structures contain protein-rich colloid, primarily consisting of thyroglobulin as storage form of thyroid hormones triiodothyronine (T3) and tetraiodothyronine (T4), but also other substances, including proteolytic enzymes as well as iodine. Further, C cells secrete calcitonin, a hormone that modulates blood calcium levels (Kondo et al., 2006; La Perle and Jordan, 2012).
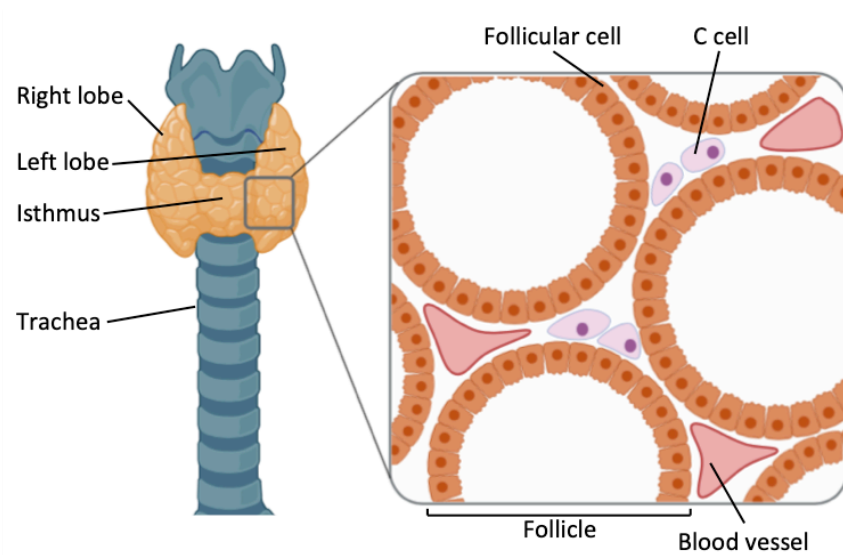
Figure 1. Schematic of the thyroid gland structure. The thyroid gland, consisting of two lobes, is located lateral to the trachea near the base of the laryngeal cartilages. It comprises numerous follicles, formed by a monolayer of follicular cells and filled with colloid. Upon hydrolysis of iodinated thyroglobulin, T3 and T4 get released into the blood stream. C cells, not part of the follicular unit, synthesize and secrete calcitonin. Schematic modified from (Boron and Boulpaep, 2012; La Perle and Jordan, 2012).

1.2 Thyroid-related diseases

The cause of thyroid diseases can be various, in general occur due to malnourishment, which can lead to iodine deficiency. Clinically presented malfunction can be a consequence of Basedow's disease or Hashimoto Thyreoiditis, but also hypothyroidism and hyperthyroidism (Monaco, 2003; Vanderpump, 2011). Furthermore, the thyroid gland can be the host of several malignancies, symptomatically presented by palpable swelling in the front of the neck and difficult swallowing (Nguyen et al., 2015).

Multiple studies report several causes for thyroid cancer. Although under debate, smoking, increasing nitrate uptake and a lack of physical activity or obesity are reported to increase the risk for thyroid cancer. Nnon-debatable is the exposition to ionizing radiation (Gangolli et al., 1994; Kitahara et al., 2012; McTiernan et al., 1998; Schmid et al., 2013; Williams, 2008). Incidences like the Chernobyl (Belarus) power plant accident in 1986 or nuclear strikes on Nagasaki and Hiroshima (Japane), but also nuclear medicine report a severe increase in thyroid cancer (Cardis et al., 2005; Furukawa et al., 2013; Lin, 2010). Presumably, the localization of the thyroid gland within the body and its tendency to radioactive iodine uptake gives an increased probability of thyroid gland irradiation (Ron et al., 2012).

Thyroid cancer represents 3.4 % of all cancers and its incidence steadily increases, whereas it is estimated that, by 2030, it will be the fourth leading cancer diagnosis. According to the World Health Organization the worldwide mortality rate (approx. 7 %) is very low, confirming an effective management by surgical resection with or without radioactive-iodine ablation (Figure 2) (Ferlay et al., 2019; Kondo et al., 2006; Rahib et al., 2014; Rusinek et al., 2017).
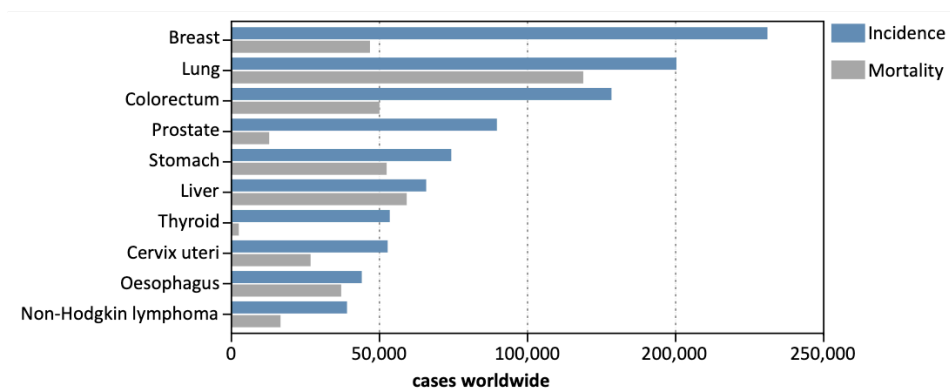
Figure 2. Incidence and mortality numbers of the most common cancers worldwide in 2018.

Thyroid tumors can either be benign (in general follicular thyroid adenomas, FTA) or malignant (in general carcinomas). The vast majority (approx. 97 %) of thyroid carcinomas are of follicular cell-origin, whereas around 3 % derive from C cells, referred to as medullary thyroid carcinoma (MTC) (Kondo et al., 2006). The latter, a neuro-endocrine tumor, is managed differently and will not be further discussed in the present study.

Follicular cell-derived carcinomas are classified into four major subtypes based on histopathological characteristics: Papillary thyroid carcinomas (PTC; incidence, 80-90%), follicular thyroid carcinomas (FTC; incidence, 10-15%) and poorly differentiated (PDTC; incidence, 1-6%) as well as anaplastic thyroid carcinomas (ATC; incidence, 1-2%) (Kondo et al., 2006; Viola et al., 2016). In contrast to the majority of well-differentiated thyroid carcinomas (WDTC) including PTC and FTC, ATC account for the vast majority of thyroid cancer-associated deaths (Smallridge et al., 2012; Tiedje et al., 2018). The survival rates of patients affected by thyroid carcinoma are highly variable and depend on the histotype and the degree of differentiation (Viola et al., 2016). However, tumoral progression involves several genetic alterations at certain steps of increasing dedifferentiation (Figure 3). The
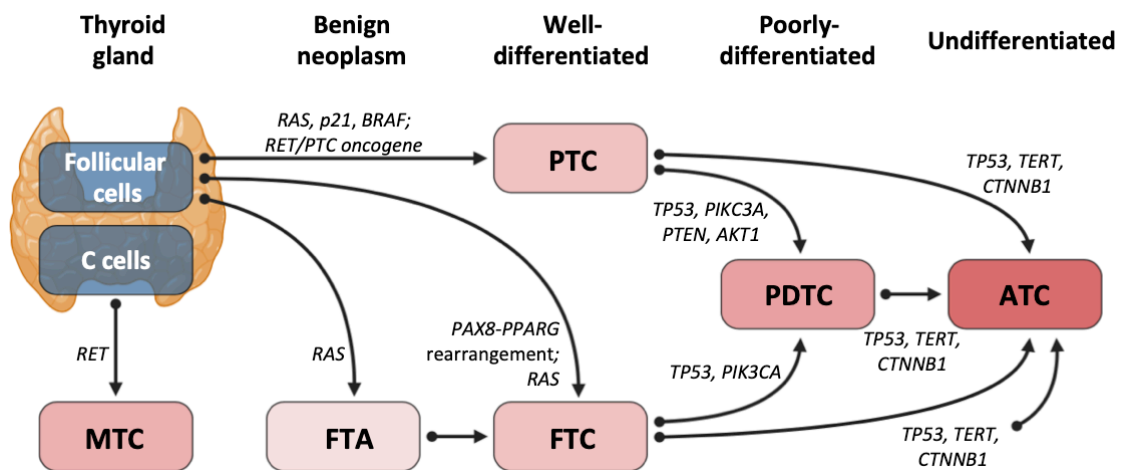
Figure 3. Model of the multistep thyroid carcinogenesis. In general, benign thyroid tumours are FTA, frequently carrying *RAS* mutations. MTC often have mutations in the proto-oncogene *RET*. *RAS* mutations and *PAX8–PPARG* rearrangements have frequently been associated with FTC. PTC are often reported with RET/PTC oncogene rearrangements or *RAS/p21/BRAF* point mutations. A progression to PDTC can be associated with mutations of *AKT1, PTEN* or *PIKC3A* and in few cases in *TP53* or *CTNNB1*. Frequently observed for ATC are *TP53-* or TERT and *CTNNB1* mutations. Note, that ATC can either arise *de novo* or as aggravation of WDTC/PDTC. Schematic modified from (Fagin and Wells, 2016; Pallante et al., 2014).

hypothesis of a multistep carcinogenesis is supported by evidence for an accumulation of oncogenic mutations with growing malignancy. Thus, by histological analysis ATC are frequently, but not consistently, observed with PTC, FTC or PDTC compartments [reviewed in (Fagin and Wells, 2016; Kondo et al., 2006)].

1.3 Well-differentiated thyroid carcinoma

WDTC, including PTC and FTC, present with an excellent prognosis as the survival probability is above 90% within 5 years upon diagnosis. Initially, a PTC diagnosis was defined by architectural criteria and now is confined on nuclear features. At present, more than 10 different histological variants are described. FTC are characterized by haematogenous spread and miss the typical nuclear features from PTC (Haugen et al., 2016; Kondo et al., 2006).

Recent studies suggest that the majority of genes being responsible for the development of PTC or FTC are involved in the MAP-kinase signaling pathway (Fagin and Wells, 2016; Landa et al., 2016). In more detail, 13% of all PTC-driving mutations occur within genes of the RAS-family and in 60% of all cases BRAF is mutated, leading to constitutive activation. An unfavourable consequence of BRAF-mutations is the generally observed reduced expression of iodine-metabolism involved genes within these tumors (Landa et al., 2016). RET rearrangements in PTC are described to lead to oncogenic chimera, causing MAP-kinase pathway induction (Fagin and Wells, 2016). FTC are predominantly reported to derive from RAS mutations, but also PAX8/PPARγ-fusions were observed (Nikiforova et al., 2003).

The therapeutic approach for WDTC is always risk-adapted to the individual patient. Nonetheless, the conventional treatment includes thyroidectomy and adjuvant radioiodine (I^{131}) ablation. In general, patients will be cured. But surgically inoperative recurrence and refractoriness to radioiodine in some WDTC is a hurdle to be solved (Schmidbauer et al., 2017).

1.4 Poorly-differentiated thyroid carcinoma

Poorly differentiated thyroid carcinomas are morphologically and behaviorally intermediate between well-differentiated and undifferentiated thyroid carcinomas

(Kondo et al., 2006). Albeit PDTC diagnosis remains controversial, it is currently assumed that these tumors still retain a sufficient grade of differentiation to express thyroglobulin as well as NKX2.1 and form follicular structures, but lack classical morphologic characteristics of WDTC. In addition, PDTC are reported to lack the marked pleomorphism of anaplastic thyroid carcinoma (Burman, 2014; Kondo et al., 2006). Unfortunately, the rarity and heterogeneity of this malignancy impeded the gain of knowledge regarding genetics and transcriptomics. Interestingly, one of the few recent studies reported the presence of similar mutations shared by WDTC and ATC. This finding supports the hypothesis of a multistep carcinogenesis of thyroid cancers. Thus, PDTC presented with mutations within the *TP53-*, as well as within the *BRAF* gene (Burman, 2014; Landa et al., 2016). Despite appropriate treatment, patients diagnosed with PDTC often have a fast and fatal outcome. The 5-year survival rate is below 20 %. A complete thyroidectomy is recommended, whereas the appropriate use of radioiodine or chemotherapy is still under debate. The vast majority of PDTC are associated with regional metastases. In addition, distant metastases, preferentially to lung and bones, are common (Dettmer et al., 2011).

1.5 Anaplastic thyroid carcinoma

The anaplastic variant of thyroid carcinomas is a rare cancer with fatal progression, making it a clinical emergency. ATC have a dismal prognosis with a mean survival rate of six months. Thus, it accounts for approx. 50 % of thyroid disease-related deaths. Accordingly, all ATC are classified as stage IV diseases. The major risk factors for ATC are age and female sex. In accordance, the majority of ATC patients are within their sixth decade of life. Hence, operations are more often accompanied by increased complications. Younger patients (age < 50 years) show higher survival rates, which still do not exceed three years [reviewed by (Molinaro et al., 2017; Patel and Shaha, 2006)].

Clinical presentation: ATC present as fast growing, large, necrotic and heamorrhagic mass and preservation of respiratory ducts is the major defiance. Local mechanical compression leads to hoarseness, dysphagia, pain or expiratory stridor. Hence,

suffocation is the most commonly observed cause of death. In 90% of cases, tissues in close proximity, commonly including skin or trachea, bones, brain or lung, get infiltrated. At the time of diagnosis distant metastases are usually observed in 50 % of cases, whereas approx. 25 % will develop metastases at a later time point. Patients usually do not benefit from radioiodine treatment, chemotherapy or traditional radiotherapy (Molinaro et al., 2017).

Histopathology: The pathogenesis of ATC, compared to WDTC, is rather unclear, less uniform and thus, can even vary within the same tumor. Reports suggest that they may arise directly from WDTC or PDTC, as they are frequently observed to coexist. This is still under debate, but supported by an increasing rate of reports. Histologically, three subtypes of cells are concluded according to the shape of majorly appearing cell types: splindle, giant or squamoid cells. But none of these can clearly exclude ATC from MTC, PDTC or metastatic WDTC. Further, increased mitotic activity, aneuploidy, but also extensive necrosis and invasion are indicative. Thus far, immunohistochemistry (IHC) is commonly used to exclude epithelial differentiation, but does not exclude an ATC diagnosis. To date, not a single marker exists to clearly discriminate ATC from WDTC or PDTC, although the expression of cytokeratins, NKX2-1 or thyroglobulin, which are essentially lost in ATC, strongly support a diagnosis. Unfortunately, it is important to properly distinguish, as therapeutic approaches and chances of survival are substantially different [reviewed by (Fagin and Wells, 2016; Molinaro et al., 2017; Ragazzi et al., 2014; Smallridge et al., 2012)].

Genetics and transcriptomics: On the molecular level ATC present with an increased mutational burden, underscoring their extreme virulence (Pozdeyev et al., 2018). For neoplastic transformations *BRAF, RAS* genes or the *TERT* promoter are frequently observed to undergo activating mutational events, supporting a theory of WDTC-derivation. In 70 % of cases, ATC presents with inactivating mutations of the tumor suppressor TP53, suggesting it as a cellular gatekeeper during progression from WDTC to ATC. Further, but in minor cases components of WNT-, mTOR-, PI3K- or AKT-signaling, as well as epigenetic regulation, like histone methyltransferases, have been described (Fagin and Wells, 2016; Levine, 1997).

These insights, however, barely improved patient outcome. Unfortunately, the molecular characteristics of ATC have not been fully elucidated yet. The vast majority of studies have reported that multiple mutational hits, either in oncogenes or in tumor suppressor genes, are implicated in ATC development (Molinaro et al., 2017). Alternative approaches dealing with comparative RNA expression data are substantially limited due to a poor understanding of the ATC transcriptome. In general, such analysis are sparse and ATC remained excluded from studies of thyroid cancer reported by the TCGA (Cancer Genome Atlas Research, 2014). At present, only one comprehensive transcriptome analysis, based on RNA-seq was published, but the authors missed to elucidate molecular factors exclusive for this malignancy (Yoo et al., 2019). This substantially limits the investigation of transcriptomic changes underlying the progression of thyroid carcinomas and the design of novel therapeutic strategies. Meager gene expression data, partially supported by histophathological analysis, indicate that ATC are distinguished from WDTC by a severe loss of thyroid markers involved in iodine metabolism and a pro-mesenchymal dedifferentiation (Landa et al., 2016). The latter is associated with severe deregulation of epithelial-mesenchymal-transition (EMT) regulators. Whereas EMT-promoting transcription factors like MYC, SNAI1/2, TWIST1/2 and ZEB1/2 are enhanced in ATC, pro-epithelial microRNAs (miRNAs) of the miR-200 family as well as the tumor-suppressive let-7 miRNA family are decreased (Braun et al., 2010; Jung et al., 2015). Consistent with this EMT-like progression, ATC gain (cancer) stem cell-like characteristics. These include the upregulation of EMT- and stemness drivers like ZEB1/2, CD133, OCT4 (POU5F1) and the RNA-binding protein LIN28B. The latter promotes the downregulation of the tumor suppressive let-7 miRNA family, as reported in ATC (Braun et al., 2010; Guo et al., 2014; Jung et al., 2015). Notably, although poorly understood, the transcriptomic changes underlying the establishment of stem cell and EMT-like gene expression signatures were proposed to promote the severe therapy resistance observed in ATC (Guo et al., 2014; Tiedje et al., 2018).

The entire set of molecular ATC characteristics represents potential targets of clinical significance for future therapy and very few rationales have successfully been evaluated by the U.S. food and drug administration (FDA) (Subbiah et al., 2018).

Conventional and novel therapies: An ATC diagnosis requires immediate decisions regarding an appropriate treatment. Feasible options include surgery, radio- and/or chemotherapy, in general applied as multimodal approach (Smallridge et al., 2012). However, the procedure remains inefficient for patients with advanced, metastatic ATC (stage IVC). The only remaining option is palliative care to improve quality of life. Nonetheless, the major goal should always be to achieve a potentially curative resection, followed by adjuvant chemotherapy or radiotherapy. The latter has not shown to be of significant benefit for ATC patients in general. However, in combination with surgery and chemotherapy, radiotherapy at least prolonged short-term survival in some patients (Viola et al., 2016). Furthermore, the efficient use of radioiodine is only applicable in rare cases for ATC treatment. As ATC cells are highly dedifferentiated, the majority of ATC lack expression of sodium/iodide symporter (SLC5A5), which is essential for the uptake of iodine into the follicular cells (Are and Shaha, 2006).

Aside from that, conventional chemotherapy options have barely changed for 40 years. Since then, the combined application of doxorubicine with platins is still a standard approach and only very few additional agents were identified to effectively inhibit ATC growth with clinical significance (Molinaro et al., 2017). Recently, a combinatorial therapy for BRAF^{V600E}-positive ATC was approved, including a tyrosine kinase (e.g. BRAF) inhibitor with a MEK1/2 inhibitor. Unfortunately, the study could not provide a significant improvement of patient survival, but an increase in life quality by a temporary response to the treatment (Subbiah et al., 2018). Such approaches are promising. Thus, still novel treatment modalities have to be found and evaluated.

1.6 Regulation of gene expression in cancer

Cancer is a genetic disease. Thus, each individual neoplasm can potentially be unique, due to the multitude of possible detectable mutations, alone or in combination within the genome. These changes include coding mutations, changes in the sequence of promoters or enhancers, insertions and deletions in DNA, copy number variations (CNV), and chromosomal translocations. The consequences are defects in regulatory circuits that govern normal cell proliferation and homeostasis (Hanahan and Weinberg, 2000; Harris and McCormick, 2010). The molecular effect generating

the phenotype from a distinct genotype can be diverse and depends on a multitude of aspects. From a simplified view, a mutation generally causes a phenotype by affecting molecular switches, which can further alter a distinct gene expression program by regulating the presentation of DNA (epigenetics) or the direct generation of messenger RNAs (mRNA; transcription) by affecting the transcriptional or post-transcriptional level (Audic and Hartley, 2004; Bradner et al., 2017).

1.6.1 Epigenetics

Epigenetics is referred to as a mechanism that, inheritable, reversibly changes gene expression without altering DNA sequences. This mechanism controls the transcriptional availability of distinct genomic regions through changes in marking and packaging of the chromatin. This includes direct modifications of DNA, like cytosine-5 methylation preferably at CpG islands, as well as nucleosome positioning and several different histone modifications. The major feature of epigenetics is that the marks can be stably maintained, yet adapt to the current needs of a cell. This mechanism involves distinct writer and eraser proteins and is gathered by reader proteins to convey the signal [reviewed in (Shen and Laird, 2013)].

DNA methylation, a mark for silenced gene expression at CpG islands (cytosine- and guanine-rich sequences spanning more than half of the human transcription start sites), is catalyzed and maintained by DNA methyltransferases (writers), including DNMT3A, DNMT3B and DNMT1 (Figure 5). Demethylation in turn is "erased" by the DNA methylases TET1-3 (Shen and Laird, 2013). Interestingly, CpG island-methylation represents a dynamic epigenetic mark that undergoes extensive changes during cellular differentiation. Thus, frequently observed hypermethylation of CpG islands at promoters of tumor suppressor genes is an important mechanism for gene inactivation in cancer (Esteller, 2002; Meissner et al., 2008).

The repertoire of post-translational histone modifications primarily includes methylation and acetylation, but also many others like phosphorylation, which are coordinated by the respective writers and erasers. The modifiers act in complexes, such as the activating Trithorax group (TrxG) complex and the repressive Polycomb complexes (PRCs). These outweigh each other in terms of developmentally regulated genes, which have also been implicated in cancer. The TrxG complex generates

activating lysine mono-, di- or trimethylation of histones residues, most prominently at lysine 4 of histone H3 (H3K4me1/2/3).
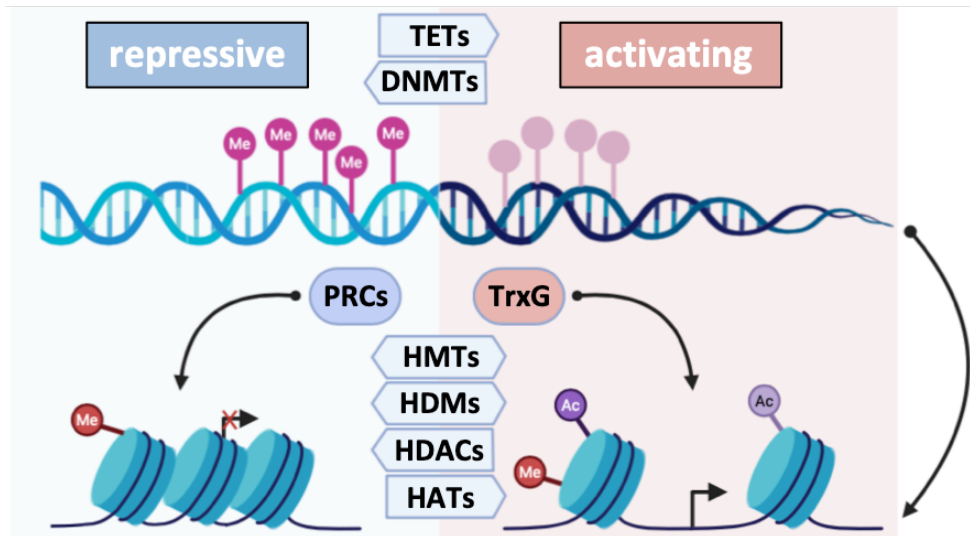
Figure 4. Schematic summarizing the major epigenetic repressive and activating mechanisms of gene expression. Writing and erasing mechanisms include the generation of 5-methylcytosine at CpG-islands by DNA-methyltransferases (DNMT), reversed by TET proteins. Well defined writers and erasers of histone modifications either belong to the repressing Polycomb-repressive complexes 1 or 2 (PRC), or to the activating Trithorax group, involving (histone) histone methyltransferases (HMT), -demethylases (HDM), but also -acetyltransferases (HAT) and -deacetylases (HDAC). Schematic modified from (Mills, 2010)

The enzymatically active core proteins comprise the histonemethyltransferases MLL1-5, SETD1A/B or SMYD1-3. The TrxG-histonedemethylase KDM6A removes the repressive marks H3K27me1/2/3. These marks are originally generated by the PRC2, consequently blocking RNA polymerase II elongation. Aside from that, histone acetylation is generally seen as activating mark by blocking PRC-binding. [reviewed by (Mills, 2010; Shen and Laird, 2013)]. The *written* marks get recognized by reader proteins, which convey information for different cellular functions. Amongst, WD40, plant homeodomain (PHD), Tudor or the bromodomain and extra-terminal domain (BET) protein family are well described (Musselman et al., 2012).

1.6.2 BET-inhibitors

A promising new class of compounds, being tested in pre-clinical studies on ATC, targets Bromodomain extra-terminal proteins (BET), which belong to the bromodomain (BRD) family. These BET-inhibitors (BETi) are most often pan-inhibitors, targeting BRD2, BRD3, BRD4 and BRDT. BET proteins bind to

acetylated histone tails to regulate transcription of primarily pro-survival genes while participating in super-enhancer complexes or at promoters (Figure 4). Thus, either an increase of BET expression, or changed histone acetylation is frequently observed in cancer. A key finding from multiple studies was the BET-dependent promotion of aberrant expression of the MYC oncogene, but also of FOSL1, CDK4 or CDK6 in different solid and hematologic malignancies. [reviewed in (Alqahtani et al., 2019)].
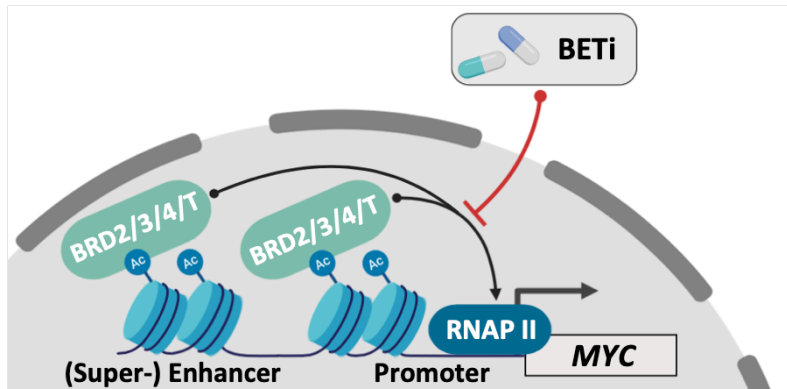
Figure 5. Schematic of the mechanism of BET protein action and inhibition. By recognizing acetylated histone residues, BET proteins (BRD2/3/4/T) stimulate the transcription process by recruiting chromatin remodeling enzymes and protein complexes and by associating with the transcriptional machinery (RNA polymerase II; RNAP II) of pro-oncogenic genes like MYC at (super-) enhancer or promoter regions. The interaction with histone residues can be inhibited with specific compounds (BETi), thus halting the transcriptional cascade. Schematic modified from (Stathis and Bertoni, 2018).

Several lines of evidence from preclinical ATC studies indicated the efficient inhibition of proliferation by using BETi *in vitro*. In accordance, the widely used BETi JQ1 was evaluated in a transgenic mouse model for ATC. The study revealed improved survival, along with a strong reduction in tumor growth and a significant decrease of MYC expression (Enomoto et al., 2017; Zhu et al., 2017). A combinatorial approach with MEK-inhibition showed even more promising results (Zhu et al., 2018). Unfortunately, JQ1 is not suitable for patient application due to its short half-life and severe side effects (Trabucco et al., 2015). Thus, the efficiency and safety of novel BETis, also including BET proteolysis targeting chimeras (PROTACS), are already getting evaluated in clinical trials for different malignancies (Stathis and Bertoni, 2018).

1.6.3 Transcription

Besides epigenetics, eukaryotic gene expression is regulated by a diverse range of proteins either being implemented into the general transcription apparatus (with RNA

polymerase II as its essential core) or affect the assembly and the recruitment of its cofactors. Major regulators, termed transcription factors, bind cooperatively to enhancer or promoter DNA elements to facilitate their function. A transcription factor employs at least a sequence-specific DNA-binding domain (e.g., zinc finger, basic helix-loop-helix) and an activation/repression domain for the interaction with its various cofactors (Bhagwat and Vakoc, 2015). The identity of a differentiated cell type is in general under the control of selectively expressed transcription factors, which are able to drive gene expression programs that define the respective cell identity (Bradner et al., 2017).

In any form of human cancers, transcription factors were reported as deregulated. The respective genes are often gained/amplified, deleted, translocated or subjected to point mutations, resulting in gain- or loss-of-function. A prominent example is the tumor suppressor gene *TP53* (tumor protein 53) as the most commonly altered gene across all cancers. Moreover, the family members of the MYC (MYC, MYCN, MYCL) oncoprotein family are frequently reported to show aberrant expression (Chen et al., 2018). Their expression is tightly controlled in normal cells, but induction in malignant cells can be induced upon various events, including retroviral promoter insertion, chromosomal translocation/amplification, activation of *MYC* gene-enhancers, mutation of upstream signaling pathways and post-transcriptional regulation that enhance MYC mRNA stability or translation [reviewed in (Chen et al., 2018; Dani et al., 1984)].

1.6.4 The MYC cncogenes are master transcription factors

MYC is a basic region helix-loop-helix leucine zipper (bHLHZ) domain transcriptional regulator. Each MYC protein belongs to the MYC/MAX/MAD network by forming a heterodimer complex with the bHLHZ protein MAX. This complex is able to specifically recognize and bind to E-box DNA sequences (consensus 5'-CACGTG-3'), which is usually located within promoter regions with high CpG content. For the efficient regulation and recruitment of cofactors the MYC proteins comprise a transactivation domain, which contains the two conserved elements Myc box 1 and 2. But MYC protein function can also get antagonized by the bHLHZ MAD proteins.

MYC has the ability to activate transcription by indirectly affecting chromatin structures, controlling the recruitment of other transcriptional regulators and exerts influence on the assembly of the RNA polymerase complex. Thus, MYC proteins are master regulators of transcription (Vervoorts et al., 2006). This is further underlined by MYCs capability to reprogram cells into a pluripotent state, together with KLF4, SOX2 and POU5F1 (OCT3/4) (Takahashi and Yamanaka, 2006).

In cancer, mutations of MYC cofactors (including components of the SWI/SNF, p300/CBP or Mediator complex) frequently contribute to tumorigenesis. But there are countless mechanisms driving aberrant gene expression of MYC proteins in transformation events (Bhagwat and Vakoc, 2015). Among these mechanisms, the genetic amplification of the *MYCN* locus in high-grade neuroblastic cancers or the post-transcriptional stabilization of the MYC mRNA by the insulin-like growth factor 2 mRNA-binding protein 1 (IGF2BP1) have been recently reported (Bell et al., 2015; Noubissi et al., 2006). The importance of MYC proteins in the myriad of malignancies justifies consideration as therapeutic targets. Unfortunately, until today no small molecule has been developed to directly inhibit MYC function. But it emphasized to find a promising indirect approach, which has emerged over the last decade – BETi (see chapter 1.6.2).

1.6.5 Post-transcriptional regulation of protein coding genes

Post-transcriptional regulation controls the fate of mature mRNAs via editing, localization, and finally translation or turnover. These processes largely rely on the expression and localization of the respective RNA binding proteins (RBP) (Mitchell and Parker, 2014; Muller-McNicoll and Neugebauer, 2013; Singh et al., 2015). The diversity of post-transcriptional regulation ensures precise mechanisms from embryonic development, to heart muscle function or learning. Thus, the half-life of an RNA can vary from several minutes to weeks and translation can be restricted to spatially defined regions to enable neuronal plasticity or cell migration (Gehring et al., 2017). Since the era of transcriptomics and proteomics, many RBPs have been identified.

An RBPs function is facilitated by binding to sequence motifs, structures or by the recognition of nucleotide modifications via one or multiple RNA-binding domains,

such as the hnRNP K homology domain (KH), the RNA recognition motif (RRM) or the DEAD box helicase domain (Hentze et al., 2018). Over the last 5 years high-throughput approaches provided a clearer overview on the variety of RBPs among all human protein coding genes. At present $> 1,500$ proteins seem to be specific for RNA. CLIP (cross-linking immunoprecipitation) technologies or approaches like XRNAX/RNA-interactome capture combined leading-edge techniques with next-generation sequencing and mass-spectrometry for identification of RBPs. Thus, multiple proteins have been identified, although their canonical function did not suggest association with RNA (Gerstberger et al., 2014; Lin and Miles, 2019; Trendel et al., 2019).

By associating with their target mRNAs RBPs can form large and dynamic complexes – the messenger ribonucleoprotein complexes (mRNPs). From the start of transcription, three co-transcriptional processes take place. A 7-methylguanosine (m7G) will be added 5' of the very first nucleotide ('capping'), which provides a platform for association with export factors (nuclear export) and the translation machinery later on. During the continuing process of transcription, splicing will remove introns from the majority of protein-coding pre-mRNAs. As soon as the RNA polymerase II reaches and reads through a polyadenylation site, cleavage and polyadenylation will take place. The export of a mature mRNA from the nucleus through the nuclear pore complex involves the remodelling of the mRNP. When the mRNP complex reaches the cytoplasm, the composition of proteins is again reassembled, according to the mRNAs fate [reviewed in (Gehring et al., 2017)].

In the cytoplasm, post-transcriptional regulation encompasses three major purposes: localization, decay and translation. MRNA localization plays a central role during cell migration or to facilitate neuronal plasticity. Thus, the chicken version of the oncofetal IGF2BP1 inhibits β-actin translation during the transport in neurons. Once the mRNP reaches its destination in axons, phosphorylation causes IGF2BP1 dissociation and the local translation of β-actin (Huttelmaier et al., 2005). MRNA decay can have various facets, whereas the major pathway in eukaryotic cells depends on the shortening of the poly(A)-tail, followed either by 5'-3' or 3'-5' exonucleolytic cleavage. Further, destabilizing micro RNAs (miRNAs), incorporated into the multi-protein RNA-induced silencing complex (RISC), specifically recognize *cis*-elements within 3'UTRs and trigger endonucleolytic cleavage via the Argonaut (AGO1-4) proteins or recruit a

deadenylation complex. In contrast, the stabilizing AU-rich elements get bound by ELAVL1, which prevents mRNA decay (Garneau et al., 2007). Finally, translation ultimately depends on the association of the eukaryotic initiation factor 4F (eIF4F) complex with an mRNAs 5'-cap. This complex represents a bridge between the 5' and 3' end by binding to poly(A)-binding proteins (PABP). Further translation is initiated by the recruitment of the ribosomes (Jackson et al., 2010).

Throughout the last decade, one particular topic in terms of post-transcriptional regulation raised attention – RNA modifications and their implications in diseases.

1.6.6 N6-methyladenosine – writer, eraser and reader proteins

Initially, modified nucleotides of transcripts were already discovered in the 1960's, but the awareness just peaked within recent years, as the research field was revived after the identification of the first RNA N6-methyladenosine (m6A)-demethylase, the fat mass and obesity-associated protein (FTO). It is assumed that the evolutionarily conserved m6A is the most prevalent RNA modification in eukaryotic cells. Thus, it is implicated in important developmental processes, but also diseases (including cancer) by affecting splicing, stability control and translation of tRNAs, rRNAs, long noncoding RNAs and mRNAs. Due to its impact on post-transcriptional regulation this new layer is termed "epitranscriptomics". By using m6A-specific antibodies for immunoprecipitation-sequencing (m6A-Seq), approx. 25% of all human mRNAs are being modified. Interestingly, in these m6A is enriched in close proximity to stop codons and 3'UTRs.

The generation of the modification is catalyzed by a well characterized methyltransferase (writer) complex (Figure 6). The catalytic core is represented by the methyltransferase-like 3 (METTL3) protein. But METTL14 and the cofactors WTAP, RBM15, RBM15B, HAKAI, VIRMA (KIAA1429), and ZC3H13 were reported to be of great importance. METTL14 lacks catalytic activity, but remains essential for proper function of the complex by representing an allosteric adaptor for METTL3. WTAP, RBM15B, VIRMA and ZC3H13 affect the localization of the complex and the specificity to the consensus motifs. METTL16 is another enzymatically active methyltransferase with specificity for a different consensus motif, which is present in a small amount of mRNAs and the U6 snoRNA [reviewed in (Zaccara et al., 2019)].
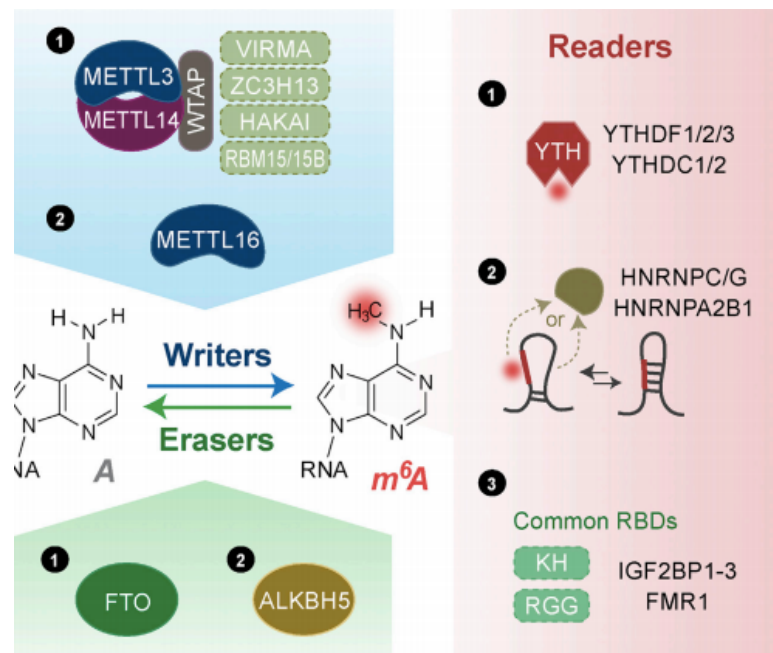
Figure 6. Schematic summarizing the identified m6A effectors. **Writers** (highlighted in blue): The writer complex is composed of (1) METTL3 and METTL14 and the additional adaptors WTAP, VIRMA, ZC3H13, HAKAI, and RBM15/15B. (2) METTL16 is another enzymatically active methyltransferase with specificity for a different consensus motif, being present in a small number of mRNAs and the U6 snoRNA. **Erasers** (highlighted in green): m6A on mRNAs can be removed by (1) FTO, whereas its function is under debate, and (2) ALKBH5. **Readers** (highlighted in red): Reader proteins can either (1) bind directly to m6A (YTHDs), favor (2) m6A-induced structures (HNRNPc, G or A2B1) or rely on an (3) m6A-dependent mechanism yet to be characterized (FMR1 and IGF2BPs). Schematic from (Shi et al., 2019).

The writing of m6A can also be reversed (erased) by, to date, two identified demethylases – the before-mentioned FTO and ALKBH5. Certainly, the function of FTO was under debate and it was proved that it removes m6Am, a very similar modification to m6A at the very first adenosine of an mRNA, but not m6A itself. Thus, at present ALKBH5 is the only 'real' m6A eraser (Mauer et al., 2017). Eventually, m6A-dependent effects are mediated by an expanding list of m6A readers. These include the directly binding YTH-domain containing proteins YTHDC1, 2 and YTHDF1-3. Proteins most likely binding due to m6A-mediated structural changes of non-coding or mRNAs, or by another unknown mechanism, are HNRNPC, G and A2B1, IGF2BP1-3, or FMR1. The HNRNPs affect splicing of targeted RNAs or miRNA processing and FMRP and the IGF2BPs are implicated in maintaining mRNA stabilization (Zaccara et al., 2019).

1.7 RNA-binding proteins in cancer

As pivotal part of highly sensitive mechanisms at the post-transcriptional level, changes in abundance or somatic mutations of RBPs have been reported to induce or promote human diseases, including neurodegenerative and cardiovascular disorders, or cancer. For the latter, publications are increasing on reporting RBPs to be changed in expression or function. However, current understanding on these alterations is rather confined (Kechavarzi and Janga, 2014; Neelamraju et al., 2015; Pereira et al., 2017). The aberrant expression or mutation of RBPs can modulate cancer cell growth and proliferation, immune evasion, apoptosis, metastasis/invasion and thus is frequently associated with prognosis. A single RBP is often associated with a variety of different RNAs. For instance, germline mutations within the *DICER1* gene resulted in pre-miRNA processing defects, followed by an altered expression of many target RNAs, as described for several malignancies. SAM68 regulates alternative splicing of the CD44 pre-mRNA and thus, stimulates proliferation (Hong, 2017). Often RBPs present without enzymatic activity, or their tertiary structure is dynamic and thus, are often of low interest in terms of targeted inhibition (Disney et al., 2018; Hermann, 2002; Warner et al., 2018). Nonetheless, at present a controversial topic is the targeting of METTL3 (see chapter 1.7.5) function (Cully, 2019). Further, RBPs with an 'oncofetal'-like expression pattern reveal therapeutic target potential, as their expression is predominantly detectable during developmental processes and is absent or very low in differentiated cells. In this respect, MSI1 and MSI2 proteins are linked to cancer progression, cancer stem cells and unvafourable prognosis in medulloblastoma, glioma, breast, ovarian cancer or AML (Fox et al., 2015; Kudinov et al., 2017). In GBM, the most lethal form of glioma, MSI1 was recently shown to be involved in chemo-resistance and as a modulator of cell adhesion and metastasis (Potschke et al., 2020; Uren et al., 2015). Hence, recently Luteolin in GBM, as well as Ro 08–2750 in AML have been shown to selectively target MSI1 or MSI2, respectively (Minuesa et al., 2019; Yi et al., 2018). The LIN28A and LIN28B proteins are regulators of developmental timing and are generally defined as promoters of pluripotency by regulating *let-7* miRNA maturation (Yu et al., 2007). In accordance, LIN28A and LIN28B expression is associated with advanced disease, more aggressive tumors and poor prognosis in T-cell lymphoma,

neuroblastoma, hepatoblastoma, or colorectal adenocarcinomas (Beachy et al., 2012; Molenaar et al., 2012; Nguyen et al., 2014; Tu et al., 2015; Wang et al., 2018). Another RBP with a significant role in cancer is ELAVL1, better known as Human Antigen R (HuR), which is found to be overexpressed in multiple malignancies. In these it enhances the stability of several AU-rich element (ARE)-containing mRNAs, which are predominantly ‚pro-oncogenic' (Bakheet et al., 2018; Hitti et al., 2016). Further, two members of the IGF2BP family, IGF2BP1 and IGF2BP3, are well characterized 'oncofetal' RBPs (Degrauwe et al., 2016).

1.8 The IGF2BPs – a family of multi-faceted RNA-binding proteins

The IGF2BPs are a highly conserved family of mostly cytoplasmic RBPs and, as yet, have been studied in multiple contexts, predominantly in studies addressing malignancies. In recent years, different terminologies have been used for the members of this family, including Vg1-RBP/Vera, IMP1-3, CRD-BP, KOC, ZBP-1, p62, CT98, or VICKZ1-3, all of which refer to a certain identified function, molecular weight or cancer background [reviewed by (Bell et al., 2013; Degrauwe et al., 2016)]. However, the official gene names IGF2BP1-3 will be used throughout study (which derived from their ability to bind the IGF2 mRNA), to prevent any confusion. In literature, IGF2 mRNA regulation plays a subordinate role. Nonetheless, their names lead to the assumption that the major function is the binding of RNAs. In more detail, IGF2BPs associate with a plethora of target mRNAs, as revealed by CLIP studies, but also with non-coding RNAs (ncRNAs), including H19 or HULC (Conway et al., 2016; Hafner et al., 2010; Hammerle et al., 2013; Jonson et al., 2014; Runge et al., 2000; Van Nostrand et al., 2016). Of note: IGF2BPs do not have any enzymatic activity. They presumably orchestrate an RNAs fate only by their appearance in the respective RNP complex upon binding to the RNA, like many other RBPs do (Degrauwe et al., 2016; Schoenberg and Maquat, 2012). The IGF2BPs bind their target transcripts via highly conserved domain structures, including two RNA-recognition-motifs (RRM1, 2) and four hnRNPK homology domains (KH1-4) (Figure 5A). As yet, studies reported that the RNA-binding is mainly facilitated via the KH-domains, but the most recent study found evidence that the role of the RRM1 and 2
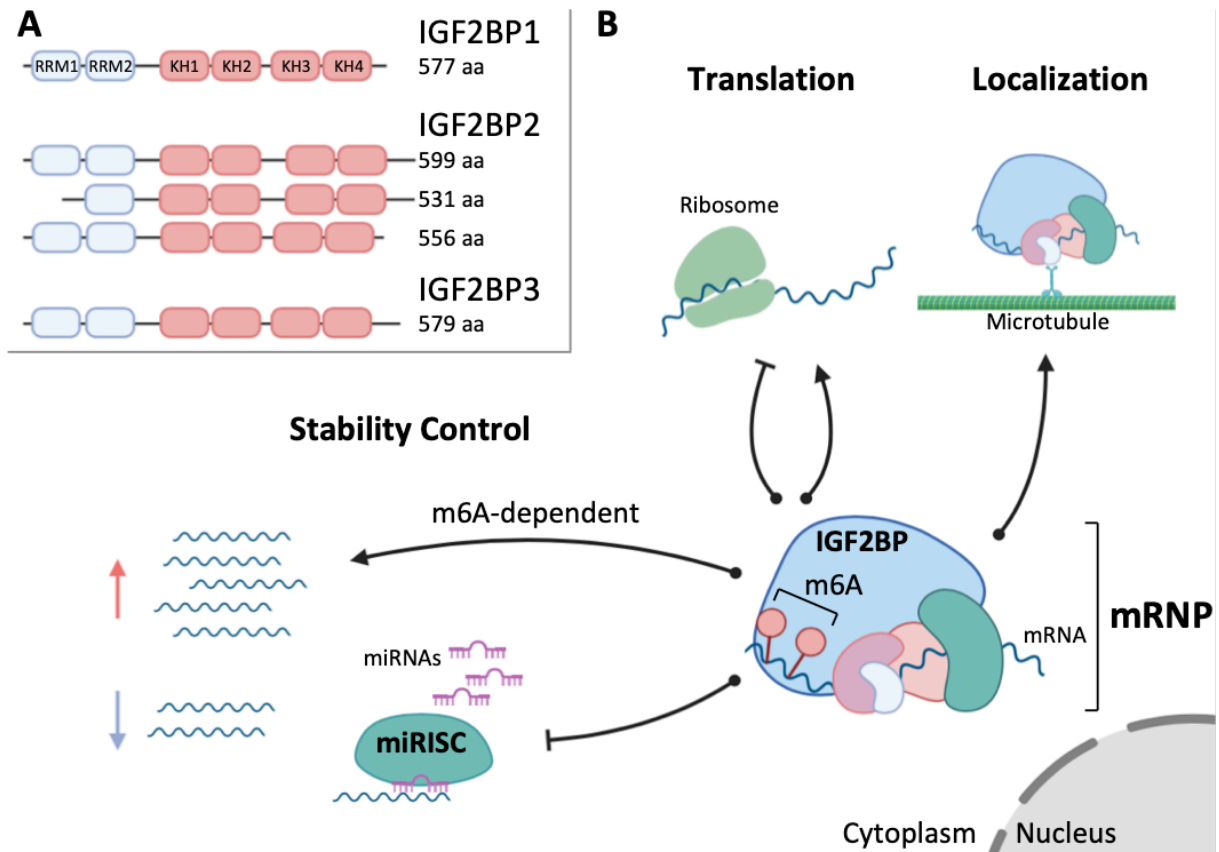
Figure 7. IGF2BPs are RBPs with multiple functions. **A)** Domain structure schematics of human IGF2BPs are shown. Following proteins are presented: IGF2BP1 (UniProt-ID: Q9NZI8-1); IGF2BP2 (IDs: Q9Y6M1-2, Q9Y6M1-6 - product of alternative translational inititiation, Q9Y6M1-1 - product of alternative splicing) (Le et al., 2012); IGF2BP3 (ID: O00425-1). RNA-recognition motif (RRM blue); hnRNP-K homology domain (KH, red). **B)** IGF2BPs associate with target mRNAs in an m6A-dependent manner and with other RBPs into mRNPs (mostly cytoplasmic), to determine an mRNAs fate. The major function of IGF2BPs relies in promoting increased mRNA stability by preventing association with the miRISC. Increased stability is also facilitated in an m6A-dependent manner. In addition, IGF2BPs inhibit and promote translation, again a dependency of m6A is reported. Moreover, localization of mRNAs can be regulated. Schematic modified from (Bell et al., 2013; Huang et al., 2018a).

have been underestimated (Chao et al., 2010; Farina et al., 2003; Nicastro et al., 2017; Nielsen et al., 2004; Schneider et al., 2019; Wachter et al., 2013). To date, it is known that the binding to a myriad of target mRNAs is supported by m6A (Figure 5B). But the way of association is still under debate, as IGF2BPs do not contain any classical m6A-recognizing domains (Huang et al., 2018a; Zaccara et al., 2019). Nonetheless, the major mechanisms by which the IGF2BPs regulate RNA turnover, translation or localization, are determined by the region they target.

Amongst the earliest findings it was shown, that in *Xenopus leavis*, Vg1-RBP/ Vera (the orthologue of the mammalian IGF2BP3), facilitates the spatio-temporal control of translation of the Vg1 mRNA to the vegetal cortex of oocytes (Yisraeli, 2005). A

comparable function is mediated by chicken orthologue of IGF2BP1 and the ACTB mRNA in a neuronal context, as above-mentioned (Huttelmaier et al., 2005). Further, the phosphorylation of IGF2BP1 at serine 181 by mTORC2 leads to IGF2-leader 3 mRNA translational initiation by internal ribosomal entry (Dai et al., 2013). But IGF2BPs do not only regulate translation and localization. The regulation of m6A- and miRNA-dependent mRNA turnover emerged as the most important functions for IGF2BPs over the last years (Degrauwe et al., 2016; Lan et al., 2019). Thus, Huang et al. identified thousands of transcripts potentially being stabilized by IGF2BP1-3 in a conserved manner by the occurrence of m6A. Amongst, the MYC mRNA contains a coding region determinant, which is specifically recognized by the IGF2BPs and thus, stabilization of the mRNA is mediated in dependency of m6A (Huang et al., 2018a). In addition to that, sequestration and 'shielding' of nascent mRNAs from the RISC is proposed to be a major mechanism to prevent miRNA-dependent silencing of gene expression. Thus, IGF2BP1 and 3 have been shown to specifically promote the expression of let-7 miRNA family targets HMGA2 and LIN28B by blocking RISC association (Busch et al., 2016; Jonson et al., 2014). Müller et al. were able to identify several additional IGF2BP1 target mRNAs, including SIRT1, which is prone to RISC-mediated silencing via miR-22-3p (Muller et al., 2018). Interestingly, an interdependence of m6A and miRNA-targeting could be possible for the serum responsive factor (SRF). In this regard, IGF2BP1 preferably stabilizes the transcript by recognizing its m6A-modified 3'UTR, whereas this event is closely linked to the repelling of miR-23a/b- and miR-125a/b-incorporating RISC (Muller et al., 2019).

1.8.1 IGF2BPs in development and physiology

The expression of IGF2BPs can be observed first between zygote and embryonic stages. During the development, the IGF2BPs are expressed in most tissues, peak around embryonic day 12.5 in mice and decreases towards birth, whereas their highest expression is observed in neuronal and epithelial cells. IGF2BP1 and IGF2BP3 are virtually absent from then on. Thus, both are also termed 'oncofetal' RBPs, although IGF2BP1 persists in the adult testis and lower IGF2BP3 mRNA was also observed in lung, spleen, kidney and gut. IGF2BP2 expression follows a similar trend during development, as its two paralogs do. But it persists in several adult

organs [reviewed by (Bell et al., 2013; Degrauwe et al., 2016)]. The general IGF2BP expression pattern seems to be conserved in the animal kingdom, as *Xenopus laevis* (frog), *Danio rerio* (zebrafish), *Drosophila melanogaster* (fruitfly), rodents and humans show high similarities in the tight control of IGF2BP expression (Hansen et al., 2004; Mueller-Pillasch et al., 1999; Nielsen et al., 2001; Nielsen et al., 2000; Yaniv and Yisraeli, 2002).

To study the physiological role of IGF2BP1, respective KO mice were used. These animals presented with impaired gut development, dwarfism (40 % reduced size) and increased perinatal mortality. Alongside, impaired IGF2 mRNA translation was observed (Hansen et al., 2004). The aberrant expression of the neuronal dIMP in Drosophila or ZBP1 in rats suggested that it is required for appropriate branching and synaptogenesis (Boylan et al., 2008; Perycz et al., 2011). Further, as already mentioned (see chapter 1.7.4), the chicken orthologe IGF2BP1 controls ACTB mRNA translation in a spatiotemporal-manner. IGF2BP1 'cages' the respective mRNA in cytoplasmic mRNP complexes, which are necessary for the transport into developing axons and dendrites. At the destination, the SRC kinase phosphorylates IGF2BP1, leading to the dissociation from the ACTB mRNA and the subsequent translation to promote growth cone guidance (Eom et al., 2003; Huttelmaier et al., 2005; Leung et al., 2006). Consistent with its importance during neuronal development, another study suggested IGF2BP1 to maintain stem cell properties in fetal brains (Nishino et al., 2013). In addition to the regulation of neural stem cells, IGF2BP1 was recently shown to promote survival and adhesion of induced pluripotent stem cells (Conway et al., 2016; Degrauwe et al., 2016). In contrast to IGF2BP1 and 3, the homolog IGF2BP2 revealed to be ubiquitously expressed in adults, as frequently reported [reviewed by (Bell et al., 2013; Cao et al., 2018; Degrauwe et al., 2016)]. However, several *in vivo* studies link IGF2BP2 to (neuronal) stem cell maintenance and blockage of differentiation, but also metabolism. This was recently evidenced with IGF2BP2-knockout mice, which revealed smaller size, but also increased resistance to obesity (Dai et al., 2015). Interestingly, a liver-sepcific overexpression resulted in steatosis, linking IGF2BP2 to hepatic pathophysiology and diseases (Tybl et al., 2011). IGF2BP3 was shown to might drive a post-transcriptional program during pancreas development and hematopoiesis. But sufficient models do not exist. Thus

the impact on organ development and physiology for IGF2BP3 remains elusive (Degrauwe et al., 2016; Palanichamy et al., 2016; Wagner et al., 2003).

1.8.2 IGF2BP1 in cancer

IGF2BPs are reported to be expressed in multiple tumor types, where they significantly contribute to stem cell-like cancer properties. Thus, IGF2BP1 and 3 are termed 'oncofetal'. All three homologs regulate cell motility, adhesion and stabilize oncogenes and pluripotency factors to facilitate tumor progression (Degrauwe et al., 2016).

IGF2BP3 is the most widely studied family member in the cancer context. Its expression was found to be associated with increasing severity and invasiveness in multiple entities, including carcinomas deriving from the pancreas, liver, gallbladder or bile duct, to only name a few (Gress et al., 1996; Jeng et al., 2008; Levy et al., 2010; Shi et al., 2013). Along with IGF2BP3, IGF2BP1 was identified to be amongst the most highly upregulated RBPs in hepatocellular carcinoma (Gutschner et al., 2014). In accordance, IGF2BP1 expression is also correlating with poor prognosis in lung, breast, ovarian cancers, neuroblastoma or melanoma (Bell et al., 2015; Fakhraldeen et al., 2015; Fortis et al., 2017; Kato et al., 2007; Kobel et al., 2007). The oncogenic potential of IGF2BP1 was recently demonstrated with transgenic mice expressing IGF2BP1 in the mammary epithelial cells. 95 % of all mice developed tumors after approx. one year (Tessier et al., 2004). Interestingly, together with a constitutively active mutant version of the murine *Kras* gene ($Kras^{G12D}$), IGF2BP1 drives aggressive lung adenocarcinoma in synergy *in vivo* (Rosenfeld et al., 2019).

Although mechanisms of IGF2BP1 upregulation or *de novo* expression in cancers remain largely elusive, studies in stem and cancer cells suggest that IGF2BP1 synthesis is substantially controlled at the epigenetic level and enhanced by MYC- and CTNNB1-driven transcription (Gu et al., 2008; Mahaira et al., 2014; Manieri et al., 2012; Noubissi et al., 2010). Besides transcriptional control, IGF2BP1 is reported to be a target of miRNA-dependent regulation. Its comparably long 3'UTR harbours multiple miRNA-recognition elements (MREs) (Huang et al., 2018b). In liver cancer, the miR-625 and miR-196b suppress invasion and metastasis, as well as proliferation and apoptosis by directly targeting IGF2BP1 expression, respectively

(Rebucci et al., 2015; Zhou et al., 2015). Most prominently, at least five MREs for the let-7 miRNA family are reported within the IGF2BP1 3'UTR. Thus, alternative polyadenylation of the IGF2BP1 3'UTR is a mechanism to avoid miRNA attack (Mayr and Bartel, 2009). Interestingly, its shortening seems to be largely dispensable as transcripts with the full-length 3'UTR are frequently expressed in ovarian cancer cell lines and analyzed patient samples (Busch et al., 2016). In turn, IGF2BP1 stabilizes another major let-7 miRNA family target, LIN28B, which is a suppressor of let-7 miRNA maturation. Finally, the interplay of LIN28B and IGF2BP1 enhances the expression of the architectural transcription factor HMGA2 by reducing the targeting let-7 miRNA family expression and simultaneously shielding from the miRISC by IGF2BP1, as also shown for IGF2BP3 (Busch et al., 2016; Jonson et al., 2014).

In cancer cells, the mainly 3'end-dependent impairment of target mRNA degradation is the major role of IGF2BP1. Besides the before mentioned transcripts, *in vivo* and *in vitro* studies identified multiple cancer-related mRNAs, including PTEN, MDR1, MKI67, GLI1 and CD44, all of which are stabilized by association with IGF2BP1. Collectively, these findings indicate that IGF2BP1 promotes a metastatic, mesenchymal and stem cell-like tumor cell phenotype at the post-transcriptional level (Gutschner et al., 2014; Noubissi et al., 2009; Sparanese and Lee, 2007; Stohr et al., 2012; Vikesaa et al., 2006). Moreover, the stabilization of transcription factors like HMGA2, MYC and SRF suggests IGF2BP1 as a post-transcriptional enhancer of 'oncogene-driven' gene expression in cancer (Busch et al., 2016; Huang et al., 2018a; Muller et al., 2019).

The profound oncogenic potential and the fact that IGF2BP1 is barely expressed in any other healthy tissue, except for testis, emphasizes the capability in targeted therapy. Thus, a recent study presented a small molecule, specifically targeting IGF2BP1 – BTYNB. The use of this compound significantly reduced cancer cell proliferation *in vitro*, by decreasing the expression of MYC and other target transcripts in IGROV-1 and SK-MEL2 cells (Mahapatra et al., 2017). Although at present only *in vitro* data is available, BTYNB represents a promising compound for future mechanistic studies and clinical evaluation.

1.9 Aims of the study

Anaplastic thyroid carcinoma (ATC) is the most lethal malignancy of the thyroid. Markers and drivers remain unknown, inhibiting advances in reliable diagnosis and treatment. Therefore, the here presented study focused on two major aims:

I) The identification of novel molecular markers, reliably distinguishing ATC from any other thyroid carcinoma of follicular origin for diagnostic purposes.

II) Taking advantage of the mechanisms, facilitated by the candidate marker, for future targeted therapy options.

In order to ascertain these aims, following objectives have been defined:

I) A retrospective analysis of a test cohort by RNA-sequencing will be used to identify exclusive markers for ATC, followed by a validation with two independent thyroid cancer cohorts by immunohistochemistry (IHC) to highlight a possible diagnostic value.

II) Beyond the putative marker potential of the most promising candidate gene, the molecular cause of its ATC-specific expression, as well as its oncogenic potential should be investigated via experimental *in vitro* and *in vivo* tumor models.

III) The mechanistic details of a putative pro-oncogenic action will be analyzed, as these could provide a rationale for effective ATC therapy options.

IV) In a final step, directly and indirectly targeting compounds will be evaluated *in vitro* by comparative analysis of potency, efficacy and synergy in combination.

2. MATERIALS AND METHODS

2.1 Material

2.1.1 Patient samples

For the test cohort ten human primary ATC, six PTC and six FTC samples were collected from 1999 to 2012 at the University clinic of Halle, Germany with consent from the Clinical Investigation Ethical Committee. In addition, six normal thyroid (NT) samples served as healthy controls. Specimens were formalin-fixed and paraffinized for IHC, or snap frozen in liquid nitrogen and stored at -80 °C. All samples were re-evaluated histologically and with review of patient records by two pathologists (Dr. Nikolaos Pazaitis and Prof. Claudia Wickenhauser, Institute of Pathology, University clinics Halle).

An independent in-house tissue microarray (TMA I) contained 147 primary thyroid cancer samples (20 ATC, 16 PDTC, 82 PTC, 29 FTC) and 108 paired normal thyroid tissue samples of all entities. A commercial microarray (TMA II, TH8010a, Biomax) contained six primary ATC, 44 PTC, twenty FTC and ten unpaired normal tissue samples.

2.1.2 Animals

For animal studies, following strains were used.

Table 1. Mice strains

Name	Genotype	Company/Reference
Crl:NU(NCr)-*Foxn1*^{nu}	*Foxn1*$^{-/-}$	Charles River
TgCreER^{T2}	*TgCreER*$^{T2+}$	Dr. Lars Möller (UK Essen)
LSL-*IGF2BP1*	*Rosa26*$^{LSL\text{-}IGF2BP1/wt}$	this study/Taconic Bioscience
LSL-*KRAS*^{G12D}	*Kras*$^{LSL\text{-}G12D/wt}$	Dr. Patrick Michl (UK Halle)
TgCreER^{T2}*;* LSL-*IGF2BP1*	*TgCreER*$^{T2+}$*; Rosa26*$^{LSL\text{-}IGF2BP1/wt}$	this study
TgCreER^{T2}*;* LSL-*IGF2BP1;* LSL- *KRAS*^{G12D}	*TgCreER*$^{T2+}$*; Rosa26*$^{IGF2BP1/wt}$*; Kras*$^{LSL\text{-}G12D/wt}$	this study

2.1.3 Bacteria

For cloning purposes, the bacteria strain *Escherichia coli* TOP10 (genotype: F– *mcr*A Δ(*mrr-hsd*RMS-*mcr*BC) Φ80*lacZ*ΔM15 Δ*lac*X74 *rec*A1 *ara*D139 Δ(*ara leu*) 7697 *gal*U *gal*K *rps*L (StrR) *end*A1 *nup*G) was used.

For cultivation of bacteria, LB (lysogeny broth) medium was used, containing 1 % (w/v) Tryptone, 0,5 % (w/v) yeast extract and 1 % (w/v) NaCl. For the generation of LB-Agar, 1,5 % (w/v) Agar was supplemented.

For selection of recombinant clones, respective antibiotics (30 μg Kanamycin/mL or 150 μg Ampicillin/mL) were added to the LB medium.

2.1.4 Cell lines

Cell lines were purchased from ATCC, DSMZ and CLS GmbH.

Table 2. Cell lines

Name	Origin	Reference
HEK293T/17	Human embryonic kidney	DuBridge et al., 1987
8305C	ATC (female, 67 years)	(Ito et al., 1994)
8505C	ATC (female, 78yrs)	(Ito et al., 1994)
C643	ATC (male, 76 years)	(Mark et al., 1987)
BHT-101	ATC (female, 63 years)	(Palyi et al., 1993)

2.1.5 Chemicals, reagents and cell culture consumables

All chemicals used throughout this study were purchased from Thermo Fisher Scientific, Sigma-Aldrich and Carl Roth, unless otherwise stated. Enzymes, including respective reaction buffers, PCR-master mixes, as well as DNA and protein ladders were purchased from Promega, Thermo Fisher Scientific and New England Biolabs. Cell culture dishes and flasks were purchased from TPP (Techno Plastic Products) and cell culture solutions were acquired from Thermo Fisher Scientific (DMEM, FBS, Optimem, GlutaMax, PBS).

2.1.5.1 Buffers and reagents

Table 3. Receipts for buffers and reagents

Name	Receipt
Phosphate buffered saline (PBS)	137 mM NaCl 2,7 mM KCl 10 mM Na_2HPO_4 2 mM KH_2PO_4
PBS-Tween (PBS-T)	PBS 1% Tween-20
Total Lysis buffer	50 mM Tris pH 7,4 50 mM NaCl 1 % (v/v) SDS 2 mM $MgCl_2$ 0,2 % (v/v) Benzonase (Millipore)
RIP buffer	10 mM Hepes pH 7,4 150 mM KCl 5 mM $MgCl_2$ 0,5 % (v/v) NP40
ChIP Lysis buffer	10 mM HEPES, pH 7.9 7.2 mM KOH 150 mM KCl 5 mM MgCl2 0.5 % (v/v) NP-40
Nuclei lysis buffer	50 mM Tris-Cl, pH 8.0 10 mM EDTA 1 % (v/v) SDS
Dilution buffer	10 mM Tris-Cl, pH 8.0 150 mM NaCl 1 mM EDTA 0.1 % SDS 1 % Triton X-100
Low-salt wash buffer	20 mM Hepes, pH 7.9 150 mM NaCl 2 mM EDTA 0.1 % SDS 1 % Triton X-100
High-salt wash buffer	20 mM Hepes, pH 7.9 500 mM NaCl 2 mM EDTA 0.1 % SDS 1 % Triton X-100

LiCl-wash buffer	100 mM Tris-Cl, pH 7.5 500 mM LiCl 1 % NP-40 1 % NaDoc
m6A-IP buffer	20 mM Tris, pH 7.5 140 mM NaCl 0.05 % Triton X-100 5 mM EDTA
m6A-high-salt wash buffer	20 mM Tris, pH 7.5 500 mM NaCl 0.5% Triton X-100 0.5% NaDoc 5 mM EDTA
NuPage Blotting Buffer	50 mM Tris pH 8,5 40 mM Glycin 10 % MeOH 0,04 % SDS
Ponceaus-S	0,1 % (w/v) Ponceau 5 % Acetic Acid Nuclease-free Water
TRIzol	0,8 M Guanidiumthiocyanat 0,4 M Ammoniumthiocyanat 0,1 Natriumacetat pH 5 5 % Glycerin 48 % Roti-Aqua-Phenol Nuclease-free Water
AlamarBlue	75 mg Resazurin 12,5 mg Methylene Blue 164,5 mg Potassium hexacyanoferrate (III) 211 mg Potassium hexacyanoferrate (II) trihydrate 500 ml sterile PBS
Trypsin-EDTA	0,05 % Trypsin 0,4 mM EDTA sterile PBS

2.1.5.2 Small molecule inhibitors

Table 4. Small molecule inhibitors

Name	Company (cat. no.)
ABBV-075 (Mivebresib)	MedChemExpress (HY-100015)
ARV-771 (PROTAC-OTX015)	MedChemExpress (HY-1000972)
ARV-825 (PROTAC-JQ1)	MedChemExpress (HY-16954)
OTC015 (Birabresib)	Biomol (Cay15947)
(+)-JQ1	Biomol (Cay11187)
CPI-203	MedChemExpress (HY-15846)

CPI-0610	Abcam (ab230374)
PLX51107	MedChemExpress (HY-111422)
BTYNB	Biomol (Cay25623)
Tamoxifen	Toronto Research Chemicals (T006000)

2.1.6 Antibodies

Table 5. Primary and secondary antibodies

Primary Antibodies	Species	Company (cat. no.) & Reference
anti-IGF2BP1 (6A9)	mouse	BSBS AB facility (Stohr et al., 2012)
anti-AURKB	rabbit	Cell Signaling (3094)
anti-LIMK1	rabbit	Abcam (ab81046)
anti-RRM2	mouse	Santa Cruz (sc-81850)
anti-p-Histone H3 (Ser10)	mouse	Cell Signalling (9706)
anti-Histone H3	rabbit	Cell Signaling (9715)
anti p-CFL1 (Ser3)	rabbit	Cell Signaling (3313)
anti-CFL1	rabbit	Cell Signaling (3318)
anti-PARP1	rabbit	Cell Signalling (9532)
anti-MYC	mouse	Merck Millipore (06-340)
anti-MYC	rabbit	Cell Marque (395R)
anti-VCL	mouse	Sigma-Aldrich (V9131)
anti-METTL3	rabbit	Proteintech (15073-1-AP)
anti-MAGEA3	rabbit	Merck Millipore (MABC1150)
anti-SNAI2	rabbit	Cell Signaling (9585)
anti-CDH1	rabbit	Abcam (ab40772)
anti-SETD1A	rabbit	Bethyl (A300-289A)
anti-SETD1B	rabbit	Abcam (ab113984)
anti-GAPDH	rabbit	Bethyl (A300-641A)
anti-H3K4me3	rabbit	Abcam (ab8580)
anti-H3K4me27	mouse	Abcam (ab6002)
anti-GFP	mouse	Sigma-Aldrich (11814460001)
anti-m6A	rabbit	SynapticSystems (202003)
anti-IgG	rabbit	Abcam (ab171870)
Secondary Antibodies	**Antigen**	**Company**
mouse-IRDye 680	mouse IgG	Licor (926-68072)
mouse-IRDye 800	mouse IgG	Licor (926-32212)
rabbit-IRDye 680	rabbit IgG	Licor (926-68073)
rabbit-IRDye 800	rabbit IgG	Licor (926-32213)

2.1.7 Vectors and plasmids

Table 6. Cloning vectors and plasmids

Name	Company (cat. no.) & Reference
pCR®-blunt	Thermo Fisher Scientific (K270040)
pmirGLO	(Busch et al., 2016)
pmirGLO-AURKB-3p	this study
pmirGLO-LIMK1-3p	this study
pmirGLO-RRM2-3p	this study
pSG-RFP-BbsI-GFP	Dr. Marcell Lederer
pSG_RFP_IGF2BP1_ex6	(Muller et al., 2018)
pSG_RFP_IGF2BP1_ex7	(Muller et al., 2018)
pSG_RFP_METTL3_ex3-1	this study
pSG_RFP_METTL3_ex3-2	this study
pcDNA_Cas9_T2A_GFP	Addgene (4813)
psPAX2	Addgene (12260)
pMD2.G	Addgene (12259)
pLVX_GFP	(Busch et al., 2016)
pLVX_GFP-IGF2BP1	(Muller et al., 2018)
pLVX_GFP-IGF2BP1mut	(Muller et al., 2018)
pLVX-shRNA2-Control	(Gutschner et al., 2014)
pLVX-shRNA2-I1	(Gutschner et al., 2014)

2.1.8 Oligonucleotides

Oligonucleotides and siRNAs were purchased from MWG Eurofins. Probes were acquired from IDT.

Table 7. Oligonucleotides for molecular cloning

Name	Sequence (5' – 3')	Restrict. site
AURKB-3p_s	GAC**GAATTC**GTGGACCTAAAGTTCCCCGCTT	EcoRI
AURKB-3p_as	GGG**CTCGAG**AAACAAAGGAGGAGGTAGAAAACA	XhoI
LIMK1-3p_s	**GAATTC**GCCAGGGCCACTCAGCTGC	EcoRI
LIMK1-3p_as	**CTCGAG**GTTCTGCGTCTGGGTTTGGTTCC	XhoI
RRM2-3p_s	**GAATTC**ATGAACTGAAGATGTGCCCTTACT	EcoRI
RRM2-3p_as	**CTCGAG**TTAATCACTTAAGACTTGTGCATTATTCAA	XhoI
pSG_RFP-METTL3_ex3-1_s	caccgGAGTTGATTGAGGTAAAGCG	–
pSG_RFP-METTL3_ex3-1_as	aaacCGCTTTACCTCAATCAACTCc	–

pSG_RFP-METTL3_ex3-2_s	caccgTATCTCCAGATCAACATCTG	–
pSG_RFP-METTL3_ex3-2_as	aaacCAGATGTTGATCTGGAGATAc	–

Table 8. Oligonucleotides for RT-qPCR

Gene/Name	Sense (5' – 3')	Antisense (5' – 3')
GAPDH	CATCAAGAAGGTGGTGAAGCAG	TGTCATACCAGGAAATGAGCTT
VCL	TTACAGTGGCAGAGGTGGTG	TCACGGTGTTCATCGAGTTC
RPLP0	CCTCGTGGAAGTGACATCGT	ATCTGCTTGGAGCCCACATT
IGF2BP1	AGTACCAAGAGACCAGACCC	GATTTCTGCCCGTTGTTGTC
AURKB	GGGAACCCACCCTTTGAGAG	GGGGTTATGCCTGAGCAGTT
LIMK1	TGCATGAGCCCAGATGTGAA	CCCAGTGTATCGTGAGGGTC
RRM2	GCCTGGCCTCACATTTTCTAAT	GAACATCAGGCAAGCAAATCA
MYC	GATCCAGACTCTGACCTTTTGC	CACCAGCAGCGACTCTGA
SETD1A	TGACTGGCTCAACGACACTC	TGCTGATGGGGTAGTAGCCT
SETD1B	TTAACGACACGCTCTGGGTC	TGTCGATGGTGTAGAAGCCC
HIST1H2AC	TTTCTCGTGAGCTTAGGCCG	CCTTGCTTACCACGTCCAGA
HIST2H3A	CTACCAGAAGTCCACGGAGC	AAGCGCAGGTCCGTCTTAAA
Rplp0	CCATCAGCACCACAGCCTTC	GGCGACCTGGAAGTCCAACT
Gapdh	CAACGAATTTGGCTACAGCA	AGGGGAGATTCAGTGTGGTG
Eef2	GTGGTGGACTGTGTGTCTGG	CGCTGGAAGGTCTGGTAGAG
Tg	CAAGGGACAACTTTGCCTGC	GCCAGAGAATCCTTGCCACT
Foxe1	TTCACAGCCCCGATTTGGA	ACACGGTGAAGCCTTACGAC
Slc5a5	CCAGTACCTAGAACTGCGCTT	AACCCGGTCACTTGGTTCAG
ChIP_IGF2BP1	GCGACCCTCTCCTGAAGAC	GTCCAGCCCAGATCTCACAT
ChIP_GAPDH	CTGAGCAGTCCGGTGTCAC	GAGGACTTTGGGAACGACTGA
NDP1	–	CCGCCTCCACCGCC
template dTTP	TCGCTCGCTCTTGCCTCGGTCCTTTATTTATTTGGCGGTGGAGGCGG	–
template dATP	ACGCACGCACAAGCCACGGACCAAATAAATAAAGGCGGTGGAGGCGG	–
template dCTP	CCACTCACTCTTACCTCAATCCTTTGTTTGTTTGGCGGTGGAGGCGG	–
template dGTP	GGAGTGAGTGTGAGGTGAATGGTTTCTTTGGCGGTGGAGGCGG	–

Table 9. Probes for RT-qPCR

Name	sequence (5' – 3')
FAM-dTTP	**6FAM**/AGGACCGAG/**ZEN**/GCAAGAGCGAGCGA/**IBFQ**
FAM-dATP	**6FAM**/TGGTCCGTG/**ZEN**/GCTTGTGCGTGCGT/**IBFQ**
FAM-dCTP	**6FAM**/AGGATTGAG/**ZEN**/GTAAGAGTGAGTGG/**IBFQ**
FAM-dGTP	**6FAM**/ACCATTCAC/**ZEN**/CTCACACTCACTCC/**IBFQ**

Table 10. siRNAs

siRNA	Sequence (5' – 3')
Control (siC, miR-cel-239b-5p)	UUUGUACUACACAAAAGUACUG
IGF2BP1 pool	CCGGGAGCAGACCAGGCAA UGAAUGGCCACCAGUUGGA CCAGGCAAGCCAUCAUGAAGCUGAA GGCUGCUCCCUAUAGCUCCUUUAUG GGGAAGAGCUGGAGGCCUA CCAUCCGCAACAUCACAAA AAGCUGAAUGGCCACCAGUUG AACACCUGACUCCAAAGUUCG GUAUGGUACAGUAGAGAAC CCUGAAGAAGGUAGAGCAA GUUCGUAUGGUUAUCAUCA GUGAACACCGAGAGUGAGA
LIMK1 pool	CCAUGGGUGCUCUGAGCAAAU CCCUGAGCUCUCCGGCUUAUA GCAACAGGUAUCGAGGACUCU
AURKB pool	CCUGCGUCUCUACAACUAUUU CUACCUCCUCCUUUGUUUAAU UUAACGCGGCACUUCACAAUU
RRM2 pool	UGUACUCACAAGGCGAUAAUA CCAUGAUAUCUGGCAGAUGUA GCUCAAGAAACGAGGACUGAU
MYC pool	CCCAAGGUAGUUAUCCUUAAA ACUGAAAGAUUUAGCCAUAAU CCAGAGGAGGAACGAGCUAAA
SETD1A pool	CGAGUUCUAUAUUGGACAGAU GCGAUUCGUCUUCCAAAUGUU CGGAAGAAGAAGCUCCGAUUU
SETD1B pool	GGAGAUUACCUAUGACUAUAA GCCGCCACGAACAUCAUUAUG GCUUGUAGAGACGGCUGAUUC
METTL3 pool	GCAAGUAUGUUCACUAUGAAA GUAUGAACGGGUAGAUGAAAU CUACAGAUCCUGAGUUAGAGA

2.1.9 Kits and systems

Table 11. Kits and systems

Name	Company
3D Spheroid Cell Invasion Assay	AMSBIO
AllPrep DNA/RNA Kit	Qiagen
Caspase-Glo® 3/7 Assay System	Promega
CellTiter-Glo® Assay Sytem	Promega
DC Protein Assay	Biorad
Dual-Glo^{TM} Luciferase Assay System	Promega
EpiQuik m6A RNA Methylation Quantification Kit	EpiGentek
Phusion® High-Fidelity PCR Kit	New England Biolabs
Qiagen Plasmid Midi Kit (100)	Qiagen
WIZARD® SV Gel and PCR Clean-Up System	Promega
WIZARD® Plus SV Miniprep Kit	Promega
Zero Blunt^{TM} PCR Cloning Kit	Life Technologies
ZytoChem Plus (HRP) Broad Spectrum (DAB) Kit	Zytomed Systems

2.1.10 Instruments

Table 12. Instruments

Application	Device (Company)
Spectroscopy	Infinite 2000 (Tecan)
SDS-PAGE	NuPAGE MOPS Electrophoresis System (Thermo Fisher Scientific)
Western-Blot	Trans-Blot Turbo Transfer System (BioRad)
Infrared-Scanner	Odyssey Infrarot Scanner (LiCOR)
Luminescence	GloMAX® 96 Luminometer (Promega)
Real-Time PCR	LightCycler® 480 II (Roche)
Flow Cytometry	MACSQuant Analyzer (Miltenyi Biotec)
FACS	FACS Melody (BD)
Thermocycler	Mastercycler gradient (Eppendorf)
Centrigues	Heraeus Biofuge Stratos
	Heraeus Biofuge fresco
	Eppendorf miniSpin
Microscopy	Nikon TE-2000E
	Nikon Eclipse TS100
	IncuCyte (Essen BioScience)
Rotation	Rotator (Snijder)

2.2 Methods

2.2.1 Studies involving patient samples and animal work

2.2.1.1 Immunohistochemistry analysis

Immunohistochemistry (IHC) was performed on 3 μm thick, consecutive sections of formalin-fixed, paraffin-embedded samples with the Bond Polymer refine detection Kit (Leica, DS9800), according to the manufacturer's instructions on a fully automated immunihistochemistry stainer (Leica Bond). Sections were imaged with an Olympus BX50/51 microscope. Two pathologists (Dr. Udo Siebolts and Dr. Marcus Bauer, Institute of Pathology, University clinics Halle), independently and blinded to the clinical data, scored all samples by using a Histoscore, as described previously (Hirsch et al., 2003). In brief, the relative amount of tumor cells being positively stained (%) was multiplied by their intensity from 0 (negative), 1 (weak), 2 (moderate), to 3 (intense). Expression classified into absent (0), low (1-100), intermediate (101-200), or strong (201-300) overall expression.

2.2.1.2 Mouse xenograft studies

Immunodeficient athymic nude mice were obtained from Charles River. All experimental procedures were approved by the Martin Luther University Halle-Wittenberg and the administration office Saxony-Anhalt. For tumor xenograft studies, 2 x 10^6 (C643) or 5 x 10^5 (8305C) cells were mixed with 50% matrigel (Sigma-Aldrich) and 50% FBS-free DMEM and injected subcutaneously in the flank of 6 week old athymic nude mice. Mice were held with access to chlorophyll-free food to avoid background noise in iRFP image acquisition by a Pearl Imager (LICOR). Tumor size and volume, as well as body weight were measured at indicated time points. The mice were euthanized, once the first tumor reached a diameter of 1.5 cm. Tumor volume was calculated using the formula 0.52 x L_1 x L_2^2, where L_1 is the long axis and L_2 is the short axis of the tumor. The number of mice used for tumor xenograft studies was n=6 for each condition. Sex of mice was distributed equally among each condition.

2.2.1.3 Transgenic mouse studies

All experimental procedures were approved by the Martin Luther University Halle-Wittenberg, Germany and the administration office Saxony-Anhalt.

Three different mouse lines were used in the here presented study. 1) LSL-IGF2BP1: Transgenic mice, harbouring the human IGF2BP1 coding sequence (CDS) followed by an internal ribosomal entry-site (IRES) and a near-infrared fluorescent portein (iRFP; as a tracer for imaging) CDS in the *Rosa26* locus, were generated by Taconic Biosciences. A STOP-signal was inserted downstream of the promoter, flanked by two loxP-sites (floxed). 2) LSL-Kras^{G12D}: Mice harbouring one floxed, mutant *Kras* allel (*Kras^{G12D}*) were provided by Dr. Patrick Michl from the University Clinics Halle. 3) TgCreER^{T2}: A driver-line, expressing a Tamoxifen-dependent Cre recombinase exclusively in thyrocytes under control of the thyroglobuline (Tg) promoter (Undeutsch et al., 2014), was used to facilitate specific IGF2BP1 and iRFP, as well as Kras^{G12D} expression in the thyroid. Therefore, LSL-IGF2BP1 animals were mated with TgCreER^{T2} and in addition with LSL-Kras^{G12D} animals to generate LSL-IGF2BP1+; Cre+ and LSL-IGF2BP1; LSL-Kras^{G12D}; Cre+ mice.

To induce the expression of the transgenes, six to eight week old mice received *intra peritonela* Tamoxifen injections (3 mg) on five consecutive days. Subsequently, the Cre recombinase is imported into the nucleus and facilitates the removel of sequences flanked by loxP-sites. From the first day of induction animals were examined daily and sacrificed when termination conditions were reached, according to the animal testing application 2-1464_MLU. Image acquisition was performed with a Pearl Imager (LICOR).

2.2.2 Cell culture

2.2.2.1 Cell culture of adherently growing cells

All cell lines were cultured in Dulbecco's modified Eagle's medium (DMEM) supplemented with 10 % (20 % for BHT-101 cells) fetal bovine serum (FBS) and 1 % GlutaMAX (L-Alanyl-L-glutamin) at 37°C and 5% CO_2. Prior to passaging, the medium was discarded and the cells were washed with PBS. Afterwards, cells were detached by trypsinisation, followed by addition of DMEM supplemented with 10 %

FBS to stop the detaching. Subsequently, cells were counted and seeded into cell culture dishes.

2.2.2.2 Lipofection of DNA and RNA

Transfection with DNA or siRNAs was performed with Lipofectamine 3000 or Lipofectamine RNAiMAX (Thermo Fisher Scientific), respectively according to the manufacturer's instructions. In brief, 2-5 x 10^5 cells in 1.8 ml DMEM were seeded into a 6-well plate. For DNA transfection, 2 μg plasmid DNA and 4 μl P3000 reagent were combined in 100μl serum-free medium (Opti-MEM, Gibco) in a 1.5 ml reaction tube. In a second 1.5 ml reaction tube 4 μl Lipofectamine 3000 were added to 100 μl Opti-MEM. The contents of both tubes were mixed, incubated for 10 min at RT and added to the cell suspension. For siRNA-mediated knockdowns, 15 nM siRNA in 100 μl Opti-MEM in a 1.5 ml reaction tube and 5 μl RNAiMAX in 100 μl Opti-MEM in a second reaction tube were mixed and incubated for 5 min at RT. Subsequently, the content of both reaction tubes were mixed, incubated for 5 min at RT and added to the cell suspension. Downstream analyses were performed 72 h post-transfection, unless otherwise stated.

2.2.2.3 Generation of CRISPR/Cas9-mediated knockout cell lines

Knockout clones were generated using the clustered regularly interspaced short palindromic repeat (CRISPR)/Cas9 technology, as described by multiple sources, including (Zhan et al., 2019). C643 cells were transfected with pcDNA-Cas9-GFP and two small-guideRNA (sgRNA) encoding psg-RFP plasmids by using Lipofectamine 3000, according to the manufacturer's instructions (see chapter 2.2.2.2). 48 h post-transfection, single cells were sorted for fluorescence in 96-well plates with a FACS Melody cell sorter and cultured. Knockout clones were tested by Western blotting. Positive clones were confirmed by sequencing of the genomic region targeted by the sgRNAs.

2.2.2.4 Lentiviral transduction

For production of lentiviral particles 293T/17 cells were transfected by using Lipofectamine 3000 reagent, according to the manufacturer's protocol (see chapter 2.2.2.2). Briefly, 3×10^6 293T cells were plated in a 6-well plate, two packaging plasmids psPAX2 (Addgene) and pMD2.G (Addgene) together with pLVX-GFP, pLVX-GFP-IGF2BP1, pLVX-GFP-IGF2BP1mut, pLVX-iRFP, pLVX-shC-iRFP or pLVX-shI1-iRFP transfer plasmids were diluted in Opti-MEM and transfected into the cells. Growth media was replaced 12 h post-transfection. The lentivirus was harvested 36 and 72 h post-transfection. Upon filtration with a 0.45 μm filter lentiviral particles were concentrated by using 1/3 volume Lenti-X concentrator (Takara Bio), according to the manufacturer's protocol. After overnight incubation at 4°C the lentiviral particles were centrifuged with 2,000 rpm at 4°C for 30 min. The pellets were resuspended in 500 μl PBS and stored at -80°C. The viral titer was determined by fluorescence titering with a flow cytometer (Miltenyi Biotech).

Lentivirus transduction for downstream experiments was accomplished at one multiplicity of infection. Cells were sorted for GFP expression with a FACS Melody cell sorter (BD Transduction) 48 h post-transduction.

2.2.2.5 Inhibition of RNA synthesis

For the analysis of RNA stability, 72 h post-transfections cells were treated with 5 μM actinomycin D (ActD) to inhibit RNA transcription for indicated time points. Abundance at different time points was determined by RT-qPCR.

2.2.2.6 Cell number analysis

To analyze cell proliferation, 1×10^4 cells were seeded into a 24-well plate. Cell numbers were determined via flow cytometry (MACSQuant$^{®}$, Miltenyi Biotec) from day 0 on every day. Dead cells were excluded by adding propidium iodide (Thermo Fisher Scientific).

2.2.2.7 Cell cycle analysis

For cell cycle analysis, cells were pelletized upon trypsinization, washed and incubated in cold 70 % EtOH for 1 h on ice. Afterwards, cells were pelletized by centrifugation, washed twice with PBS and incubated in 200 μl RNaseA (Roth) in PBS (100 μg/ml) for 30 min at RT. Again the cells were pelletized and stained in 50 μg/ml propidium iodide. Stained cells were analyzed for DNA content by flow cytometry with a MACSQuant flow cytometer and the MACSQuantify Software (Miltenyi Biotec).

2.2.2.8 Apoptosis assay

To measure apoptosis the relative Caspase3/7 activity was determined by using the Caspase-Glo 3/7 assay (Promega), according to the manufacturer's instructions. Therefore, 24 h post-transfection 1 x 10^4 cells were seeded into a 96-well plate. 72 h post-transfection Caspase 3/7 activity was measured with a Luminometer (Promega) upon incubation with Caspase-Glo 3/7.

2.2.2.9 3D-spheroid growth and invasion assay

For spheroid growth and invasion 1 x 10^4 cells per well (24 h post-transfection) were seeded in an ultra-low attachment round bottom 96-well plate (Corning, 7007) using FBS-containing (10%) DMEM. Spheroid growth was monitored for 3 days by light microscopy (Nikon TE2000-E), and viability was determined by CellTiter-Glo (Promega). Spheroid area was determined by using Fiji Software (http://fiji.sc). Upon spheroid formation (72 h), an invasion matrix (Trevigen; 5 mg/ml) was added to monitor tumor cell infiltration for further 24-48 h using light microscopy, according to the manufacturer's instructions. The relative invasion index was determined by the perimeters of the invasive front normalized to spheroid body perimeter.

2.2.2.10 Anoikis resistance assay

To test for anoikis resistance, 1×10^4 cells were seeded in an ultra-low attachment flat bottom 96-well plate (Corning, 3474) using DMEM containing 0.5% FBS. Cell viability was determined by using CellTiter-Glo after seven days. Formation of cell aggregates was imaged by light microscopy (Nikon TE2000-E).

2.2.2.11 Single cell migration

For single cell migration analyses, 24 h post-transfection 1×10^3 cells were seeded on collagen I pre-coated 8-well chamber slides (IBIDI). Cell spreading was allowed overnight. 60 h post-transfection cells were labeled with CellMask Deep Red live dye (Thermo Fisher Scientific) before migration was monitored over 10 h by time lapse analyses (5 min/frame) using a Leica SP5 X inverse confocal microscope, equipped with a Ludin cube life chamber, 20x dry objective and multi-positioning. Automated cell tracking was performed using the „CellMigrationAnalyzer" tool of the MiToBo (http://mitobo.informatik.uni-halle.de) package for Fiji Software to determine the mean speed [µm/min] of those single cells observed over a time period of a minimum of 2 h. At least 100 cells per condition of three independent experiments were analyzed.

2.2.2.12 Luciferase reporter assay

For the analysis of 3'end-dependent regulation, pmirGLO (Promega) plasmids, comprising the 3'end of AURKB and 3'UTRs of LIMK1 or RRM2 transcripts were used. A reporter containing a minimal vector-encoded 3′UTR (empty) served as normalization control. Cells were transfected with the respective plasmid and Lipofectamine 3000 reagent (see 2.2.2.2). The activities of firefly and renilla luciferases were determined 48 h post-transfection by Dual-Glo (Promega), according to the manufacturer's instructions.

2.2.2.13 Compound testing

To assess cell viability in response to changing compound concentrations 3 x 10^4 (C643 and BHT-101) or 6 x 10^4 (8305C) cells were plated in a 96-well plate. Vehicle (DMSO) or the respective compound (see 2.1.5.5) was added 24 h post-seeding at indicated concentrations. CellTiter-Glo was used 72 h post-treatment, according to the manufacturer's protocol. EC_{50} and E_{max} values were calculated by using GraphPad Prism 7. The combined effect of ABBV-075 and BTYNB was calculated and visualized by using the Highest Single Agent model (δ-synergy score > 0 indicates synergy; < 0 indicates antagonism) by using the R package synergyfinder.

2.2.3 Molecular biology

2.2.3.1 Plasmids and cloning

To generate firefly luciferase plasmids, comprising the 3'end of AURKB or 3'UTRs of LIMK1 and RRM2, the respective DNA was amplified from cDNA of 8305C cells and inserted through restriction enzyme sites EcoRI and XhoI into a pmirGLO vector (Promega) with optimized MCS (multiple cloning site), as previously described (Busch et al., 2016). PLVX plasmids (TakaraBio) for stable expression of GFP-tagged IGF2BP1 wildtype, IGF2BP1 mutant, non-targeting shRNA shC and IGF2BP1-targeting shRNA shI1 were previously generated and derived from (Gutschner et al., 2014; Muller et al., 2018). To target the IGF2BP1 locus for CRISPR/Cas9-mediated knockout, previously generated pSG-RFP plasmids comprising respective guide RNAs and the Cas9-coding pcDNA-Cas9 were used (Muller et al., 2018). To target the METTL3 locus, target sequences derived from the Brunello library were used (Doench et al., 2016). Information on plasmids and oligonucleotides used for polymerase chain reaction (PCR) or oligo annealing are summarized in tables 6, 7 and 8. All cloned constructs were validated by Sanger-sequencing (Eurofins Genomics GmbH).

2.2.3.2 Plasmid digestion

For restriction cloning, 2 μg plasmid DNA was digested with 1 unit of the respective restriction enzyme and its buffer (EcoRI, XhoI, 10x CutSmart buffer; NEB) for 15 min at 37°C.

2.2.3.3 DNA amplification by polymerase-chain reaction

For cloning purposes, DNA amplification by polymerase-chain reaction (PCR) was performed with the Phusion High-Fidelity DNA Polymerase (Thermo Fisher Scientific), according to the manufacturer's instructions. For amplification the following reaction mix was added:

cDNA	5-50 ng
10mM dNTPs	0.5 μl
10μM sense/antisense Oligonucleotide	1 μl each
5xGC Buffer	5 μl
Phusion High Fidelity DNA Polymerase	0.5 μl
Nuclease-free water	add to 25 μl

The mix was vortexed and the amplification was performed with the following program:

Step	Temperature	Time	
Initial Denaturation	98°C	5min	
Denaturation	98°C	10s	
Primer-Annealing	60-65°C	30s	35 cycles
Elongation	72°C	30s-90s	
Final Elongation	72°C	-	

2.2.3.4 Oligonucleotide annealing

For annealing of oligonucleotides, 5 μl sense, 5 μl antisense oligonucleotides (100 μM each) and 5 μl nuclease-free water was mixed. The oligonucleotides were

incubated at decreasing temperatures: 95°C for 5 min, followed by 65°C for 5 min and afterwards cooled down to RT. Annealed oligos were used for ligation into linearized vectors.

2.2.3.5 Agarose gel electrophoresis

Separation of nucleic acids was performed on a 1% TAE agarose gel (with ethidium bromide added) at 120 V. The Quick-load 2-log DNA-ladder (NEB) was used as size marker. The DNA samples were mixed with 6x DNA loading dye. Signals were detected with an UV imager.

2.2.3.6 DNA extraction from agarose gels

DNA extraction from agarose gels was performed with the Wizard® SV Gel and PCR Clean-Up System (Promega), according to the manufacturer's instructions.

2.2.3.7 Ligation

A ligation of linearized DNA fragments and vectors was performed with the following reaction mix:

2x Quick Ligation Buffer (NEB)	5 μl
1 μl T4 Ligase (NEB)	1 μl
Insert / Vector	5 / 1 mol. ratio
Nuclease-free water	add to 10 μl

The reaction mix was incubateed at RT for 15 min.

2.2.3.8 Transformation of *E. coli* TOP10

For the transformation of ligated plasmids, chemo-competent *E. coli* TOP10 bacteria were used. The bacteria were thawed on ice for 10 min. Subsequently, 5 μl of the ligation reaction mix was added to the reaction tube and incubated for another 20 min

on ice. Afterwards, the bacteria were heat shocked at 42°C for 60 sec. Subsequently, the reaction tube was placed on ice for 3 min, followed by adding 500 µl LB medium and an incubation step at 37°C for 60 min. Subsequently, the bacteria were plated on LB-agar plates containing respective antibiotics and were grown over night in an incubator at 37°C.

2.2.3.9 DNA preparation from *E. coli*

For DNA mini and midi preparations bacteria were grown in LB-medium over night at 37°C in an incubator. Extraction of DNA was performed by using the QIAprep Spin Miniprep Kit or the QIAprep Spin Midiprep Kit (Qiagen), according to manufacturer's instructions.

2.2.3.10 Protein extraction

For protein extraction from mammalian cell culture samples, medium was discarded and the cells were washed with PBS. Afterwards, the cells were scraped from the plate and harvested in PBS in a 1.5 ml reaction tube. Subsequently, the cells were pelletized by centrifugation at 2,000 rpm for 3 min. The supernatant was discarded and the pellet was frozen in liquid nitrogen, prior to storage at -80°C.

For protein expression analysis, total protein from cells pellets or tissue samples was extracted in Total Lysis buffer, supplemented with protease and phosphatase inhibitor cocktails (Sigma-Aldrich). The protein concentration was determined by using the DC Protein Assay (BioRad), according to the manufacturer's instructions.

2.2.3.11 SDS-Polyacrylamide gel electrophoresis and Western blot-analysis

For SDS-Polyacrylamide Gel Electrophoresis (SDS-PAGE) samples were boiled at 95°C with NuPage LDS Sample Buffer (containing 0.1 M DTT) and run on NuPage® Novex 4-12% Bis-Tris Protein Gels (Thermo Fisher Scientific). After SDS-PAGE, proteins were transferred by wet blotting onto a nitro-cellulose membrane. Protein

expression and phosphorylation was analyzed upon blocking with milk (5 % (w/v)) and incubation with indicated antibodies by a near-infrared scanner (LICOR).

2.2.3.12 Isolation of total RNA and genomic DNA from tissues and cell lines

Total RNA from human and murine tissues was isolated by using the miRNeasy Kit (Quiagen), according to the manufacturer's instructions.

Total RNA from cell culture samples was isolated using guanidiniumthiocyanat-phenol-chloroform extraction (Chomczyński & Sacchi, 2006). The cells were washed with ice-cold PBS, subsequently lysed in 1 ml TRIzol per 10 cm^2 surface area, scratched from the dish and transferred into an RNase-free 1.5 ml reaction tube. The sample was frozen and stored at -80°C. After thawing the RNA was extracted by adding 200 μl chloroform, shaking the sample for 15 sec, followed by incubation for 3 min at RT. The phases were separated through centrifugation for 15 min at 13,000x g and 4°C. The RNA-containing aqueous phase was transferred into a new 1.5 ml reaction tube, mixed with 1 vol. ice-cold isopropyl alcohol and incubated for 20 min at RT for precipitation. Subsequently, the RNA was pelletized by centrifugation for 10 min at 13,000x g and 4°C. The RNA was washed twice with ice-cold 75 % ethanol and centrifuged for 5 min at 13,000x g and 4°C. After removal of the ethanol by pipetting, the RNA was dried for several minutes at RT and resolved within nuclease-free water. RNA integrity was assessed with a Bioanalyzer 2100 (Agilent). The RNA was stored at -80°C.

Genomic DNA (gDNA) from frozen human tissue and cell lines was extracted with the AllPrep DNA/RNA Kit (Quiagen), according to the manufacturer's instructions. The gDNA was stored at -20°C.

2.2.3.13 Reverse transcription

For the synthesis of complementary DNA (cDNA) a reverse transcription reaction was performed. Therefor, 2 µg isolated total RNA in 14.5 μl water was incubated with 5 μM random-hexamer (R6) oligonucleotides for 5 min at 65°C to obstruct any secondary structures. For reverse transcription the following reaction mix was added:

5x Buffer (Promega)	4 μl
10mM dNTPs	1 μl
M-MLV Reverse Transcriptase (PROMEGA)	0.5 μl

Subsequently, the reaction was performed with a Thermocycler (Eppendorf) and the following program:

Step	Temperature	Time
Denaturation	65°C	5min
Cool Down	4°C	hold
Addition of 5,5 μl reaction mix		
	20°C	5min
R6-Annealing	25°C	5min
	30°C	5min
Reverse Transcription	42°C	60min
Inactivation	72°C	15min
End	4°C	hold

Subsequently, cDNA was stored at -20°C or used directly for RT-qPCR or other applications.

2.2.3.14 Quantitative real-time PCR

To assess the relative abundance of mRNAs, real-time quantitative PCR (RT-qPCR) was performed. RT-qPCR analysis was performed with 2.5 μl diluted (1:10) cDNA, 2.5 μl ORA™ qPCR Green ROX L Mix (highQu) and 0.4 μM of each oligonucleotide, using a LightCycler 480 (Roche). The PCR conditions were as follows:

Step	Temperature	Time	
DNA polymerase activation	95°C	5min	
Denaturation	95°C	10 s	
Primer-Annealing	60°C	10 s	40 cycles
Elongation	72°C	20 s	
Melting curve	65°C-95°C	-	

Cycle threshold (CT)-values were used for calculation of abundance and differential expression of mRNAs to control/house-keeping genes by using the ΔCT- or ΔΔCT method, respectively (Livak and Schmittgen, 2001).

2.2.4.15 Fluorescence-based dNTP quantification assay

Quantification of cellular deoxyribonucleotides (dNTP) was assessed as previously described (Wilson et al., 2011). For extraction of intracellular dNTPs 72 h post-transfection 1×10^7 cells for each condition were harvested by trypsinisation, washed, resuspended in ice-cold 60% methanol, incubated at 95°C for 3 min and subsequently sonicated for 30 s. To remove precipitates the samples were centrifugated at 13,000 rpm. To remove molecules > 3 kDa the supernatant was passed through a centrifugal filter (Millipore) at 4°C, according to the manufacturer's protocol. Upon evaporation with a vacuum centrifuge (Eppendorf) the pellet was resuspended in nuclease-free water for fluorescence-based qPCR analysis of dNTP content. Previously described templates, fluorescent 6-FAM probes (IDT), primer (see tables 8 and 9) and chemicals for AmpliTaq Gold-based (Thermo Fisher Scientific) elongation were used on a LightCycler 480 (Roche). Each 10 μl reaction contained 2.5 μl extract or dNTP standard, 1 mM $MgCl_2$, 1 μl 10x PCR Buffer II, 0.25 units AmpliTaq Gold, 0.1 mM of each dNTP (excluding the one to be analyzed), 0.4 μM primer NDP1, 0.4 μM respective template and 0.4 μM respective 6-FAM probe. The PCR conditions were as follows: 10 min at 95°C (hot start), 30 min at 60°C (extension), every 5 min 6-FAM fluorescence detection. Absolute quantification was carried out by generating a standard curve for detection of each dNTP via the „Absolute Quantification/Fit Points" method, implemented in the LightCycler 480 Software.

2.2.3.16 Chromatin immunoprecipitation

Chromatin immunoprecipitation (ChIP) experiments were performed essentially as described previously (Carey et al., 2009). In detail, 2.5×10^7 cells (C643, 8505C or 8305C) were treated with 1 % formaldehyde for 10 min at RT, quenched with 100 mM Tris (pH 7.2) and harvested in ice-cold PBS. Lysis was accomplished in two

cycles of incubation with ChIP-lysis buffer, supplemented with protease inhibitors. Nuclei were enriched by centrifugation for 10 min at 4000 rpm and 4°C. Afterwards lysis of nuclei was accomplished by incubation in ice-cold nuclei lysis buffer, supplemented with protease inhibitors, for 5 min on ice. Chromatin was sheared with a sonicator to a size range of 200-500 bp. For ChIP, 25 µg of sheared chromatin was incubated with 5 µg anti-IgG (Abcam), anti-H3K4me3 (Abcam) or anti-H3K27me3 (Abcam) antibodies overnight in dilution buffer, supplemented with protease inhibitors. On the next day 20 µl magnetic Dynabeads (Thermo Fischer Scientific) per IP were washed twice in dilution buffer, added to each IP and incubated on a spinning wheel for 2 h at 4°C. The beads were washed twice with low-salt wash buffer, twice with high-salt wash buffer, twice with LiCl wash buffer and once with TE buffer. Each wash step on a spinning wheel lasted 3 min at 4°C. Subsequently, the TE was removed from the magnetic beads, elution buffer (TE supplemented with 1 % SDS) and 20 µg/µl proteinase K was added and cross-linking was reversed overnight at 65°C. DNA was finally eluted using the WIZARD®SV Gel & PCR Clean-Up System (Promega), according to the manufacturer's instructions and analyzed by RT-qPCR.

2.2.3.17 RNA co-immunoprecipitation

For RNA co-immunoprecipitation (RIP), cell extracts (5×10^6 per condition) were prepared for 10 min on ice using RIP buffer. Samples were centrifuged at 13.000 rpm for 5 min at 4°C. The supernatants were incubated with 5 µg anti-GFP antibody (Sigma-Aldrich) and 20 µl pre-washed magnetic Protein G Dynabeads (Thermo Fisher Scientific) for 30 min at RT on a spinning-wheel. After three washing steps with RIP buffer, protein-RNA complexes were eluted with 110 µl RIP buffer, supplemented with 10 % SDS, for 10 min at 65°C. For protein isolation 25 µl were used for Western blotting. 75 µl of eluate was used to analyze co-purified RNA by subsequent extraction by using TRIzol and analysis by RT-qPCR.

2.2.3.18 M6A-RIP

The m6A-RIP protocol was performed essentially as described (Vu et al., 2017). Total RNA was isolated by TRIzol and poly(A)+ RNA was purified by using Oligo-

(dT)25 magnetic Dynabeads (Thermo Fisher Scientific). 5 μg of anti-m6A antibody (Synaptic Systems) or anti-IgG (Abcam) was bound to Protein G magnetic Dynabeads (Thermo Fisher Scientific) in m6A-IP buffer for 1 h at 4°C. Afterwards, 1 μg of poly(A)+ RNA in 400 μl IP buffer was added to the antibody-coupled beads for 2 hours at 4°C. Samples were washed three times in IP buffer and twice with high-salt wash buffer. RNA was eluted from the beads by incubation with 200 μl 0.5 μg/μl N6-methyladenosine 5-monophosphate sodium salt (Sigma-Aldrich) for 1 h at 4°C. Upon ethanol precipitation, input RNA and eluted poly(A)+ RNA was reverse-transcribed with random hexamers. Enrichment of m6A-containing transcripts was determined by RT-qPCR.

2.2.3.19 Quantification of m6A-marked transcripts

Poly(A)+ RNA was isolated using Oligo-(dT)25 magnetic Dynabeads (Thermo Fisher Scientific). N6-methyladenosine-marked poly(A)+ RNA (control or METTL3-KO cells) was quantified by using the EpiQuick m6A RNA Methylation Colorimetric Quantification Kit (EpiGentek, P-9005), according to the manufacturer's instructions.

2.2.3.20 Deep-sequencing and differential gene expression

For total RNA-sequencing (RNA-seq) library preparation and sequencing was performed at the IKFZ (Leipzig, Germany). For total and small RNA-seq low quality read ends as well as remaining parts of sequencing adapters were clipped using Cutadapt (v 1.4.2 or 1.6). Subsequently, reads were aligned to the human genome (UCSC GRCh19) using TopHat (v 2.0.12; (Kim et al., 2013)) or Bowtie2 (V 2.2.4; (Langmead and Salzberg, 2012)), respectively. FeatureCounts (v 1.4.6; (Liao et al., 2014)) was used for summarizing gene-mapped reads. Ensembl (GRCh37.75; (Yates et al., 2016)) was used for annotations.

MRNA-seq and sWGS was performed by Novogene (Hongkong). Processing of mRNA-seq data was performed as described above for total RNA-seq. For sWGS low quality read ends and remaining sequencing adapters were clipped off using Cutadapt (v 1.14). Trimmed reads were aligned to the human genome (UCSC GRCh38) using HiSat2 (v 2.1.0 (Kim et al.)). Sequenced reads were trimmed for

adaptor sequences and low quality sequences using Cutadapt (v 1.14). Trimmed reads were mapped against the human genome (hg38 UCSC) using HiSat2 (v 2.1.0). Copy number variations were analyzed using R package cn.MOPS (v 1.28.0 (Klambauer et al.)) using chromosome normalization (Poisson), excluding sex chromosomes, and compared with control DNA samples (Promega).

2.2.4 Database analysis

2.2.4.1 Kaplan-Meier analysis

Patient survival was analyzed by using the cBioPortal platform (http://cbioportal.org), combining patient data from the TCGA for papillary and follicular thyroid carcinoma and from the MSKCC (Memorial Sloan Kettering Cancer Center) for anaplastic thyroid carcinoma ((Cancer Genome Atlas Research, 2014; Gao et al., 2013; Landa et al., 2016).

2.2.4.2 GSEA-analysis

Gene set enrichment analyses (GSEA) were performed with the GSEA-Software (v 3.0; (Subramanian et al., 2005)) using MSigDB (v 6.1 or 6.2) gene set collections hallmark (H), curated (C2) and oncogenic (C6) for a list of all protein coding genes ranked according to fold changes in „ATC to noATC", upon depletion of IGF2BP1 or JQ1-treatment.

2.2.4.3 IGF2BP1-CLIP and m6A-RIP-seq data analysis

Peak coordinates from publicly available CLIP data and m6A-RIP data (Conway et al., 2016; Hafner et al., 2010; Van Nostrand et al., 2016; Xuan et al., 2018), obtained from ENCODE, NCBI GEO, CLIPdb and RMBase V2.0, were mapped to all annotated genes (RefSeq hg19). For IGF2BP1-binding, the following number of datasets was considered: 2 PAR-CLIP (HEK293), 2 eCLIP (hESCs), 2 eCLIP (HepG2) and 2 eCLIP (K562). For m6A-RIP sites the coordinates of peaks from all available m6A-dependent experiments obtained from RMBase V2.0 were considered.

2.2.5 Statistics

Statistical analysis were performed using GraphPad Prism software (V7.0). Statistical significance was determined by using non-parametric Mann-Whitney test or two-tailed Student's t-test, as indicated. DOR were calculated by using MedCalc (V19.1.3). A principal component analysis was performed by using the R pcaExplorer (http://bioconductor.org/packages/pcaExplorer). Gene expression correlations were tested with Pearson correlation by using the Genomics Analysis and Visualization Platform (http://r2.amc.nl) and GEPIA2 (gepia2.cancer-pku.cn). The number of replicates is stated in the respective figure legend.

3. RESULTS

3.1 IGF2BP1 *de novo* expression in ATC is a useful diagnostic tool

3.1.1 The transcriptional landscape of thyroid carcinoma is severely altered from WDTC to ATC

Accumulated survival data for ATC, PTC and FTC, derived from cBioportal, indicated the dramatic shift of survival probability from patients suffering from WDTC to ATC (Figure 8A) (Cancer Genome Atlas Research et al., 2013; Gao et al., 2013; Landa et al., 2016). The determined survival rate for ATC patients was 8.16 months in median, whereas no rates could be defined for WDTC. To progress understanding of the molecular pathogenesis and to reveal novel markers of the largely fatal malignancy of
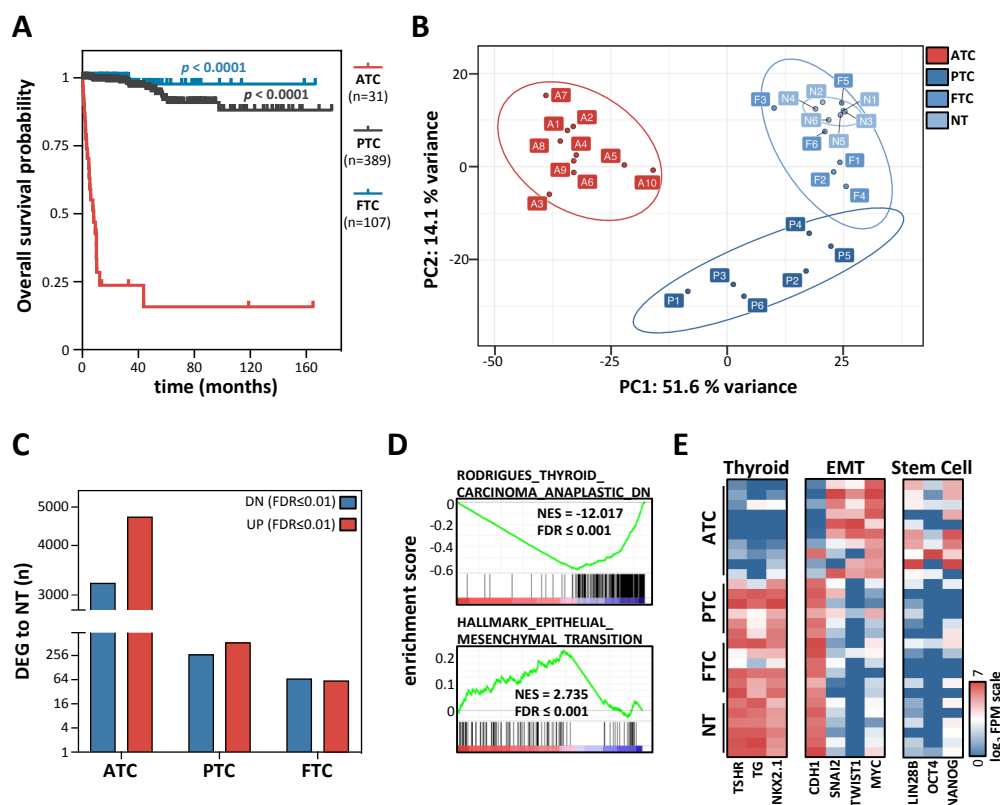
Figure 8. The protein-coding transcriptional landscape is severly altered in ATC. **A)** Kaplan-Meier analysis of overall survival data from PTC (n = 389), FTC (n = 107) and ATC (n = 31) patients, derived from cBIO-portal (TCGA & MSKCC data). **B)** Principle component (PC) analysis on RNA-seq data derived from the test cohort, including 10 ATC, 6 PTC, 6 FTC and 6 NT samples. **C)** Number of differentially expressed (DEG; FDR ≤ 0.01) protein-coding genes (mRNA) for each thyroid carcinoma subtype versus NT, by RNA-seq. **D)** Gene set enrichment analysis (GSEA) plots of genes deregulated in ATC vs noATC, as determined by RNA-seq. NES = normalized enrichment score. **E)** Heatmap presentation of log2 FPM (fragments per million) values determined for indicated genes by RNA-seq, as in B). Statistical significance was determined by Log-rank test (Mantel-Cox) (A).

ATC, RNA-seq in a retrospective study was performed with a test cohort. Molecular and clinical characteristics of the tumor cohort are presented in Table A1, Appendix. The protein-coding transcriptome of ten ATC was compared with six PTC, six FTC and six NT (collectively referred to as "noATC"). A principle component analysis of all samples revealed that primary ATC samples cluster well together and show a clear separation from WDTC and NT in terms of gene expression, independent of their mutational status (Figure 8B). Interestingly, a lower variance between FTC and NT, than between PTC and NT could be observed. In detail, a comparison of numbers on differentially expressed protein-coding genes of each thyroid carcinoma subtype to NT revealed approx. 8000 differentially expressed genes with an FDR ≤ 0.01 for ATC (Figure 8C). For PTC and FTC only approx. 500 or 100 protein-coding genes, respectively, showed differential expression compared to NT. This indicated a severe deregulation of the protein-coding transcriptome in ATC.

Gene set enrichment analyses (GSEA) confirmed the finding of a severely altered expression pattern for ATC, as shown by Rodrigues et al., 2007 via micro-array analysis (Figure 8D) (Rodrigues et al., 2007). Among other pathways, GSEA identified EMT-like dedifferentiation in ATC (HALLMARK_EPITHELIAL_ MESENCHYMAL_TRANSITION). In accordance, pro-mesenchymal dedifferentiation was further supported by the loss of E-cadherin (CDH1) and the upregulation of stemness and EMT-associated markers MYC, SNAI2, TWIST1, OCT3/4 (POU5F1), LIN28B and NANOG (Figure 8E) (Carina et al., 2013; Guo et al., 2014).

3.1.2 IGF2BP1 is an mRNA- and protein marker of ATC

To date, the ATC frequently represents a diagnosis of exclusion due to the lack of robust positive markers. As a timely decision for this lethal malignancy is necessary, the reliable identification even of microscopic foci of ATC within low-grade thyroid cancer would bring a benefit to any patient (Cabanillas et al., 2016). To identify exclusive markers of ATC, differential mRNA expression from samples from the test cohort was further analyzed. For consideration, two criteria were presumed: **1)** *de novo*-expression (mean FPM in noATC samples < 1; fold change in ATC against noATC samples > 50), and **2)** low relative standard deviation (RSD) of expression in

ATC. The top 20 genes identified by this analysis are shown in Table 13 and indicated in red in Figure 9A.

Table 13. Top 20 identified ATC-exclusive markers

Gene name	log2 foldchange (ATC vs noATC)	FDR (ATC vs noATC)	RSD	Cancer testis gene*
IGF2BP1	5.8008	4.8157E-38	0.1409	Yes
MAGEA2B	6.4879	4.3948E-28	0.3512	Yes
MAGEA2	6.3036	2.5740E-28	0.3526	Yes
DUX4L2	6.0914	3.3856E-21	0.3725	No
DUX4L6	5.7370	4.2742E-18	0.3737	No
DUX4L5	5.7618	4.7851E-17	0.3754	No
MAGEA3	7.6799	9.7494E-32	0.3813	Yes
MAGEA6	7.1070	5.0678E-28	0.4091	Yes
MAGEA12	7.7511	7.8765E-28	0.4806	Yes
DUX4	6.0547	1.4599E-18	0.4865	Yes
DUX4L3	5.7640	2.1113E-16	0.5032	No
XAGE1E	5.7851	2.0036E-17	0.6333	Yes
XAGE1B	5.9017	2.0458E-16	0.6573	Yes
XAGE1D	6.1376	1.7237E-16	0.7181	No
CT47A2	5.7574	2.6330E-15	0.7314	Yes
XAGE1A	7.0252	1.9515E-17	0.7458	No
CT47A6	5.9934	4.8163E-14	0.7730	Yes
MAGEC1	5.8336	6.3688E-13	0.8126	Yes
TMEM158	6.1610	6.0203E-15	0.8285	No
MSLN	7.0175	3.9930E-13	0.9407	No

* Information was obtained from the computational analysis by da Silva *et al.*, 2017 (da Silva et al., 2017)

Amongst the top ranked genes, 60 % (12/20) were reported testis antigens of advanced interest in the focus of immunotherapy, as most recently reported for MAGEA3-targeting in a phase-II clinical trial (da Silva et al., 2017; Lu et al., 2017). Nonetheless, we identified IGF2BP1 with the lowest RSD.

The findings from RNA-seq were validated by Western blotting of total protein isolated from ATC-derived cell lines (C643 and 8305C) and individual tumor samples of each subtype from the initial cohort (Figure 9B, C). The analyses confirmed *de novo* expression of IGF2BP1 protein in ATC, as well as the co-expression of MAGEA3 on protein level. Further, the upregulation of MYC and SNAI2, as well as the loss of CDH1 expression was in accordance with previous findings (Carina et al.,

2013). Although the second oncofetal member of the IGF2BP protein family, IGF2BP3, was upregulated in ATC as well, IGF2BP1 showed the most prominent and discriminative enhancement of the IGF2BP family at the mRNA level (Figure 9D).
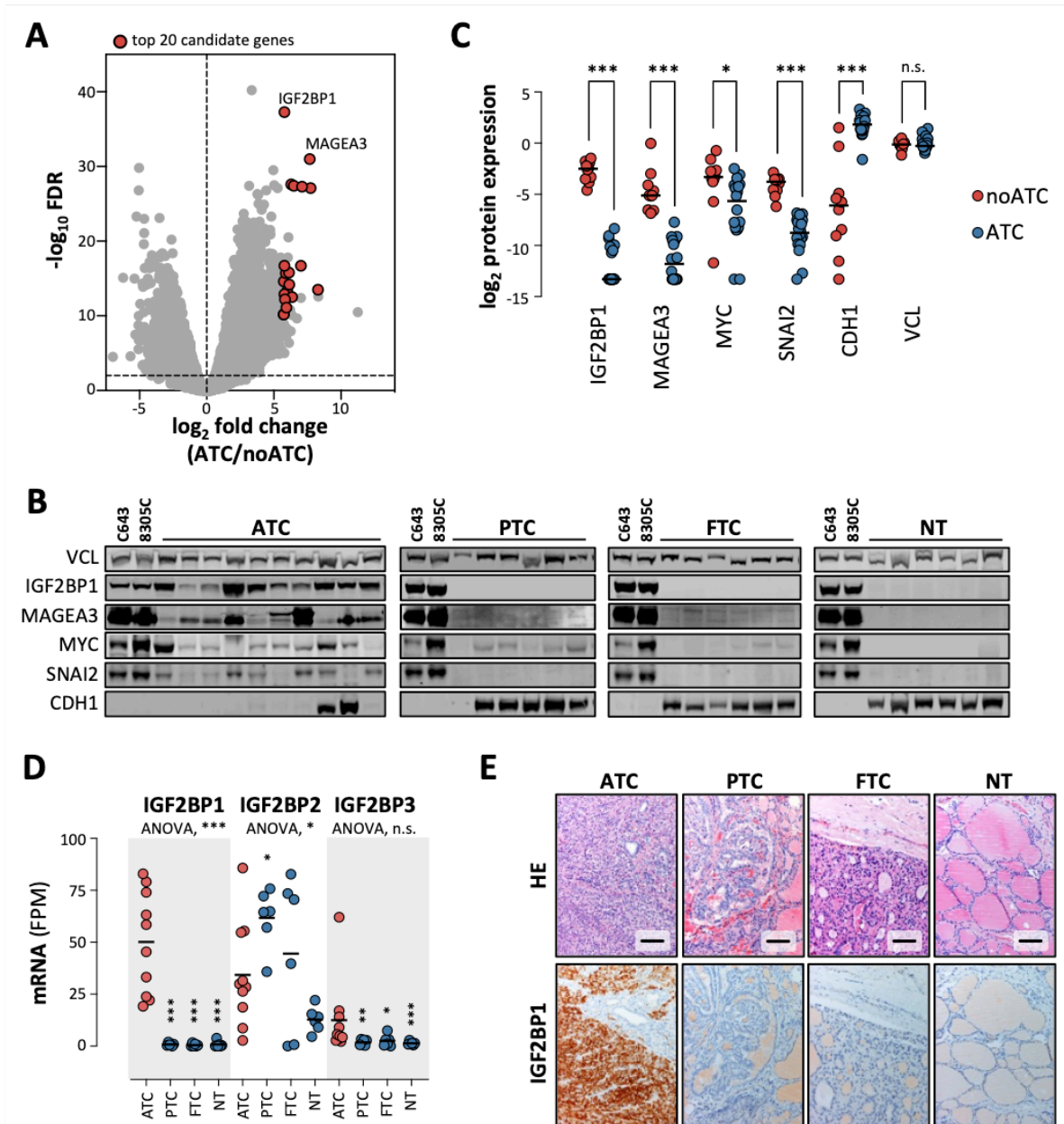
Figure 9. IGF2BP1 is a positive marker for ATC. **A)** Volcano plot of log2 mRNA fold changes plotted against the -log FDR (false discovery rate) for 10 ATCs versus 18 noATCs (6 PTC, 6 FTC and 6 NT samples). Horizontal dashed line indicate threshold (FDR ≤ 0.01) for identification of significantly altered gene expression. Indicated in red are the top twenty ATC-exclusive genes identified by: I) mean FPM in noATC samples < 1; II) fold change in ATC against noATC samples > 50. **B, C)** Representative Western blot analysis and respective quantification of indicated proteins of individual samples, prior used for RNA-seq in Figure 8B. VCL served as loading control. D) IGF2BP1-3 mRNA expression determined in ATC and noATC samples by RNA-seq is shown. **E)** IGF2BP1 expression analyzed by immunohistochemistry in representative samples investigated in (A). HE, hematoxylin eosin staining. Scale bars, 100 μm. Statistical significance was determined by Mann-Whitney-test (C, D) or ANOVA (D) (***p ≤ 0.001; **p ≤ 0.01; *p ≤ 0.05; n.s. p > 0.05).

The consistent *de novo* expression of IGF2BP1, and less striking of MAGEA3, in ATC suggested a robust, positive marker. To evaluate this in further detail, representative tumor samples of the initial cohort were analyzed by IHC after staining with a commercially available antibody. This confirmed the selective *de novo* expression of IGF2BP1 in ATC for the test cohort (brown staining, Figure 9E). No IGF2BP1 expression was observed in FTC, PTC and NT samples.

To further confirm the exclusive expression of IGF2BP1 protein in general within ATC and evaluate its potential use in IHC, we assessed two independent thyroid carcinoma validation cohorts: one tissue microarray provided by the university clinics Halle (TMA I: 20 ATC, 147 tumor samples total) and a commercial tissue microarray (TMA II: 6 ATC, 70 tumor samples total). Molecular and clinical characteristics
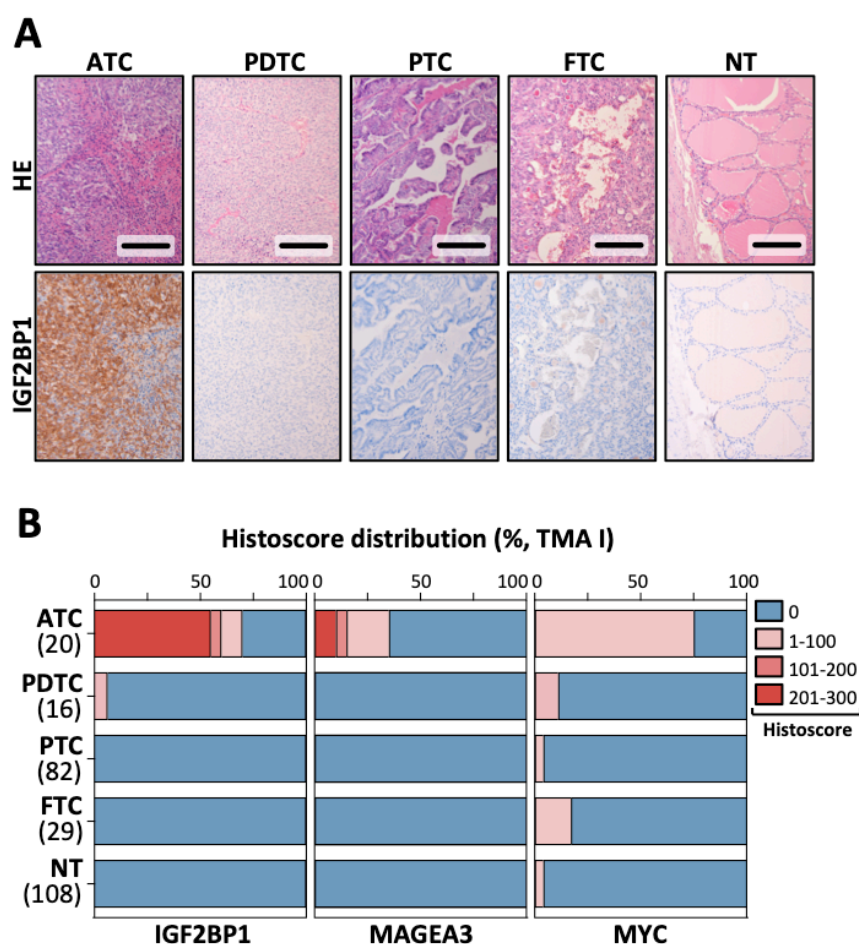
Figure 10. IGF2BP1 is a positive marker for ATC. **A)** IGF2BP1 expression analyzed by immuno-histochemistry in representative samples from an independent tissue microarray (TMA I). HE, hematoxylin eosin staining. Scale bars, 100 *μm.* **B)** Percentage view of IGF2BP1, MAGEA3 and MYC-Histoscores for TMA I. Sample numbers are indicated. ATC, anaplastic thyroid carcinoma; PDTC, poorly-differentiated thyroid carcinoma; PTC, papillary thyroid carcinoma; FTC, follicular thyroid carcinoma; NT, normal thyroid.

of the tumor cohorts are presented in Table A1, Appendix.

Stainings were performed with commercially available antibodies and the respective expression was objectively determined by Histoscore. IGF2BP1 protein was detectable in 70 % (14/20) of analyzed ATC samples in TMA I (Figure 10A, B) and in 50 % (3/6) of the samples in the TMA II (Table A1, Appendix). Importantly, protein expression could not be observed in any other tested tissues, except for one PDTC sample. MAGEA3 could also be detected exclusively in ATC tissues, but weaker and to a much lesser extent. MYC expression was observed for all sample types. In spite of this, the majority of ATC samples were positive, whereas only few PDTC, PTC, FTC and NT samples could show a signal for MYC expression.

Among all samples tested for protein expression via Western blotting and IHC, 75 % (27/36) ATC samples expressed IGF2BP1 protein, whereas only 0.5 % (1/203) of any other less aggressive thyroid carcinoma samples and 0 % (0/124) of non-malignant thyroid tissues were tested positive (see Table A1, Appendix). This suggests IGF2BP1 to be a discriminative marker for ATC detectable via RNA and protein. Diagnostic accuracy for thyroid carcinoma was resolved by determining a respective overall diagnostic odds ratio (DOR). The DOR is a single indicator for test performance upon binary classification (ATC vs. no ATC or disease vs. no disease). It represents the ratio of the odds of positive test results if patients present with an ATC, relative to the odds of the test being positive for patients with no ATC. A DOR can range from 0 to ∞, but > 1 indicates a correct discrimination and the higher the value, the better the performance (Glas et al., 2003). For IGF2BP1 a ratio of 612
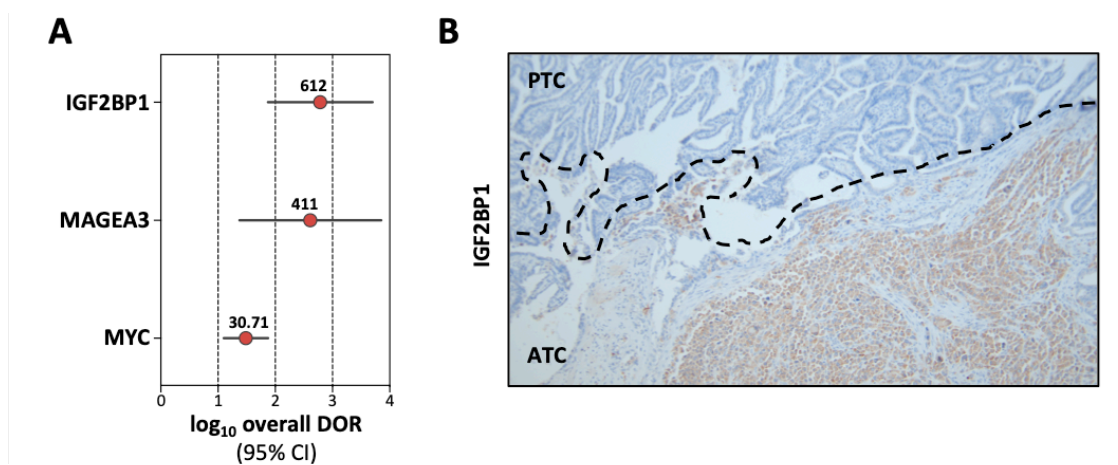
Figure 11. IGF2BP1 detection is of high value for diagnosis. **A)** Plot of $\log_2$ DOR values for ATC diagnosis determined for indicated proteins by including all patient samples analyzed in this study. Error bars indicate 95 % confidence intervals (95 % CI). **B)** IHC analysis of IGF2BP1 in a patient-derived sample with ATC- and PTC content.

(95 % CI: 74.6 to 5021) and for MAGEA3 a ratio of 411 (95 % CI: 24 to 7099) was determined (Figure 11A). Following this, the tissues of patients being positively stained for IGF2BP1 or MAGEA3 definitely harbor ATC portions. MYC is also an indicator of ATC, but the rate of false-positives can be substantially higher. In support of the ATC-selective expression of IGF2BP1, *de novo* expression was observed in a patient-derived ATC sample with PTC content (Figure 11B). IGF2BP1 protein expression was exclusively observed in the ATC area. In conclusion, this indicated the potential use of IGF2BP1 expression for discriminating ATC from other thyroid malignancies, even within a single patient sample.

3.2 IGF2BP1 expression is epigenetically and transcriptionally regulated in ATC-derived cells and harbors oncogenic potential

3.2.1 IGF2BP1 *de novo* expression is unlikely a consequence of chromosomal aberrations in ATC

The *IGF2BP1* locus is located on the long arm of chromosome 17 (17q21.32). Recently, this region was found to be commonly gained in breast cancer and neuroblastoma (Bell et al., 2015; Doyle et al., 2000). The event of chromosomal gain could be linked to lowered survival probabilities of patients suffering from these diseases. To further elucidate, whether alterations in copy numbers could be associated with *de novo* expression of IGF2BP1, shallow whole genome sequencing (sWGS) of the ATC samples from the initial test cohort was performed. However, copy numbers of the IGF2BP1 gene locus remained unchanged in 90 % (9/10) of ATC (Figure 12; Table A1, Appendix). In one sample a breakpoint was detected in the first intron of the *IGF2BP1* locus (sample #5). Whether or not this would contribute to IGF2BP1 expression requires further investigation. Following this observation, IGF2BP1 *de novo* expression in ATC is unlikely due to genomic alterations and must be the consequence of other mechanisms.
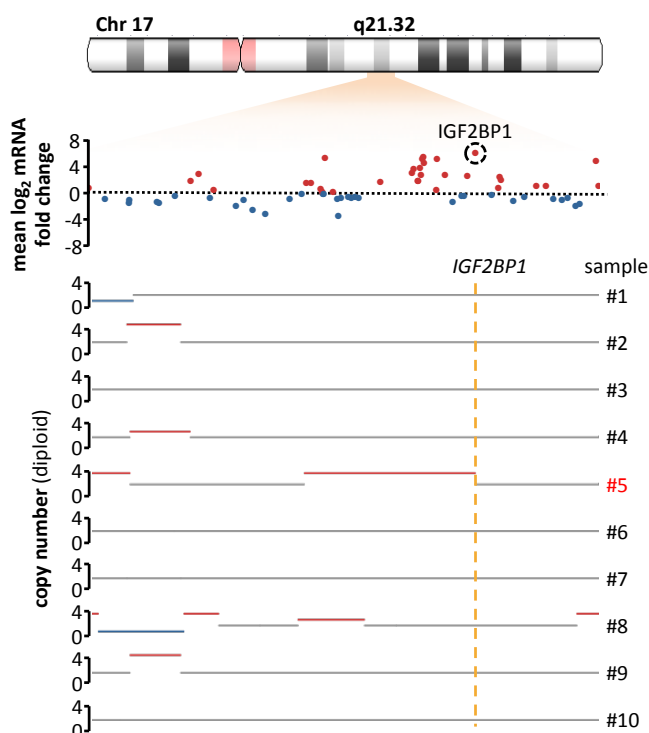
Figure 12. IGF2BP1 *de novo* expression in ATC occurs unlikely due to genomic alterations. Genomic deletion or amplification events were determined by shallow Whole Genome Sequencing (sWGS) of ATC samples from the test cohort. (Upper panel) Mean $\log_2$ mRNA fold changes and (lower panel) gene copy numbers of analyzed ATC samples are shown within the indicated region of chromosome 17. Blue lines indicate regions of copy number loss, red lines indicate regions of copy number gain. The position of the *IGF2BP1* (17q21.32, dashed line) locus is highlighted.

3.2.2 IGF2BP1 *de novo* expression depends on epigenetic activation and the MYC transcription factor in ATC

The lack of genetic abberations of the *IGF2BP1* locus in the majority of analyzed samples implied the likeliness of epigenetic reprogramming as a major determinant of IGF2BP1 *de novo* expression in ATC. Transcriptome and ChIP-seq studies in embryonic stem (ESC) and neuroal progenitor cells (NPC) suggested that the silencing of IGF2BP1 synthesis is associated with reduced H3K4 and increased H3K27 tri-methylation (me3) at the *IGF2BP1* promoter (Figure 13A, B; (Consortium, 2012; Meissner et al., 2008)). It is assumed, that in general H3K4m3 is an abundant histone modification at promoters of active transcription, whereas H3K27m3 represents a hallmark of transcriptional repression (Hyun et al., 2017). In support of this, GSEA indicated that the vast majority of silenced genes with repressive H3K27me3 marks in mouse brains, including *Igf2bp1*, are upregulated in ATC (Meissner et al., 2008) (Figure 13C). Furthermore, this finding implied that dedifferentiation in ATC is associated with the upregulation of embryonal stem cell expression signatures. To evaluate the association of histone methylation with IGF2BP1 synthesis, H3K4me3- and H3K27me3-ChIP studies were performed in three ATC-derived cell lines, which either showed (C643, 8305C) or lacked (8505C) IGF2BP1 protein and RNA expression (Figure 13D). H3K4me3/H3K27me3 ChIP-ratios determined for the GAPDH promoter were found essentially unchanged, supporting barely altered expression (Figure 13E). In contrast, ratios assessed at the *IGF2BP1* promoter were significantly decreased in 8505C cells that essentially lack IGF2BP1 expression. The dynamic methylation/demethylation of H3K4 is primarily facilitated by the trithorax group (TrxG) proteins (Schuettengruber et al., 2011). Amongst the major H3K4-directed tri-methyltransferases (26), only SETD1A/B showed a striking upregulation in ATC and significantly associated expression with IGF2BP1 ($R_{SETD1A} = 0.2525$; $R_{SETD1B} = 0.4316$; Figure 13F). Accordingly, IGF2BP1 synthesis was analyzed upon SETD1A/B co-depletion in ATC-derived 8305C cells. Decreased expression of both tri-methyltransferases led to reduced IGF2BP1 protein and mRNA levels (Figure 13G). This suggested that the *de novo* expression of IGF2BP1 in ATC essentially involves enhanced H3K4 tri-methylation at the IGF2BP1 promoter by SETD1A/B.
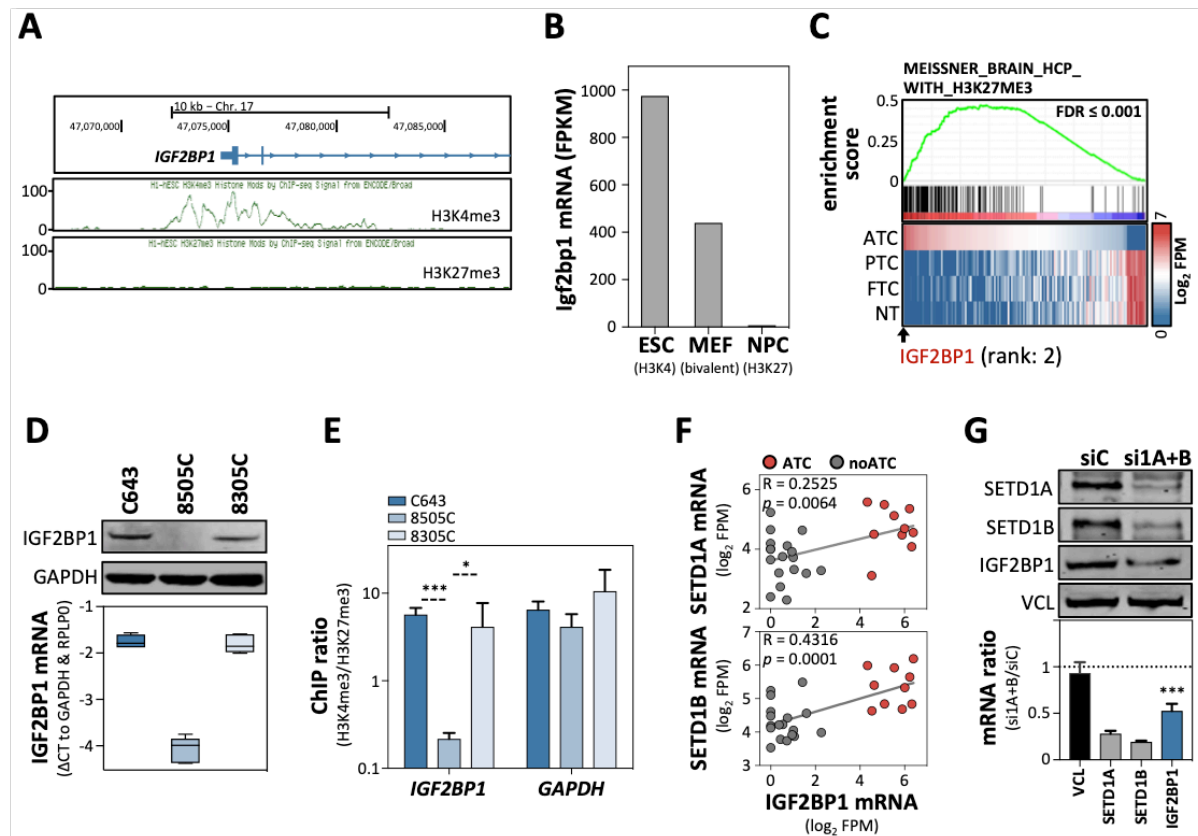
Figure 13. IGF2BP1 expression relies on activating histone marks at its promoter. **A)** H3K4me3 and H3K27me3 ChIP-Seq data of the *IGF2BP1* promoter region in human embryonic stem cells are shown along with a reported CpG island and MYC-binding sites determined by ChIP-Seq. Data were derived from ENCODE database. **B)** Igf2bp1 mRNA expression (FPKM) in mouse embryonic stem cells (ESC; predominantly H3K4me3 marks), mouse embryonic fibroblasts (MEFs; bivalent H3K4me3 and H3K27me3 marks) and mouse neural progenitor cells (NPC; predominantly H3K27me3 marks) is shown by a bar diagram. Data derived from (Meissner et al., 2008). **C)** GSEA (upper panel) enrichment plot of genes silenced by H3K27me3 in differentiated brain mouse tissue and upregulated in ATC. The heatmap (lower panel) shows the average log2 FPM of genes comprised in the gene set for indicated samples from the test cohort. **D)** Western blot (upper panel) and RT-qPCR analyses (lower panel; ΔCT-values are shown by box plots) of IGF2BP1 expression in indicated ATC-derived cell lines. GAPDH and RPLP0 served as loading and normalization controls. **E)** Ratios of H3K4me3 versus H3K27me3 marks at the *IGF2BP1* and *GAPDH* promoters determined by ChIP-RT-qPCR. **F)** SETD1A and SETD1B mRNA abundances were plotted over IGF2BP1 mRNA levels (log$_2$ FPM), prior determined by RNA-seq in ATC (red) and noATC (grey) samples from the test cohort. Association of expression was analyzed by Pearson correlation studies. Correlation coefficient (R), significance (*p*) and the regression line are shown. **G)** Western blot (upper panel) and RT-qPCR (lower panel) analyses of IGF2BP1, SETD1A and SETD1B expression in 8305C cells transfected with control (siC) or SETD1A/B-directed siRNA pools. VCL served as loading (upper panel) and negative (lower panel) control. Statistical significance was determined by two-tailed Student's t-test (*** *p* ≤ 0.001; * *p* ≤ 0.05).

Permissive chromatine structures at promoters, marked as "active", enable the association of specific transcription factors (Klemm et al., 2019). Previous studies in cancer cell lines indicated, that the synthesis of IGF2BP1 can be enhanced by MYC family transcription factor (MYC and MYCN) binding to a CpG island region (Figure

14A) within the *IGF2BP1* promoter region (Bell et al., 2015; Consortium, 2012; Noubissi et al., 2010). However, in the 33 cancer transcriptomes provided by the TCGA, no significant association of MYC and IGF2BP1 expression could be observed (Figure 14B). In sharp contrast, IGF2BP1 and MYC showed a significant co-upregulation in ATC of the test cohort ($R_{MYC} = 0.7432$; Figure 14C). This suggested MYC as a major transcription factor for IGF2BP1 expression in ATC. In agreement, the depletion of MYC significantly impaired IGF2BP1 protein and mRNA abundance (Figure 14D). Intriguingly, a MYC-depletion negatively affected the viability of 8305C cells in a 3D-tumor cell spheroid growth assay, delineating the
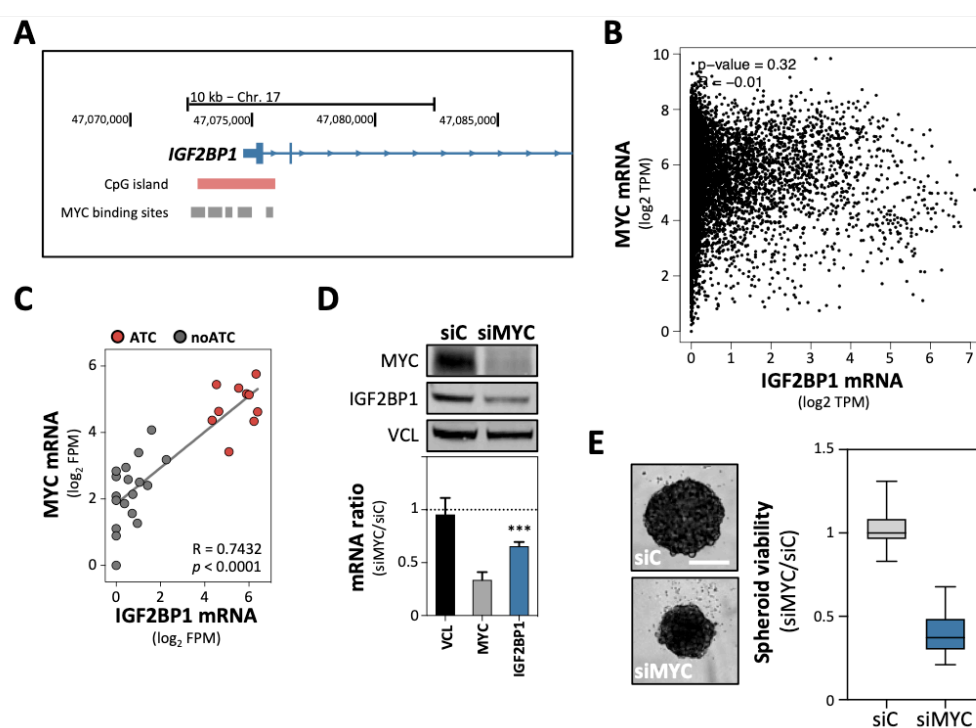
Figure 14. IGF2BP1 transcription is supported by MYC. **A)** *IGF2BP1* promoter region in human embryonic stem cells are shown along with a reported CpG island and MYC-binding sites determined by ChIP-Seq. Data were derived from ENCODE database. **B)** Levels (log$_2$ TPM) of MYC mRNA levels were plotted over IGF2BP1 mRNA levels from a TCGA pan-cancer analysis (including 33 cohorts) by using GEPIA2. **C)** MYC mRNA abundances were plotted over IGF2BP1 mRNA levels (log$_2$ FPM) for ATC (red) and noATC (grey) samples from the test cohort. Association of expression was analyzed by Pearson correlation studies. Correlation coefficient (R), significance (*p*) and the regression line are shown. **D)** Western blot (upper panel) and RT-qPCR (lower panel) analyses of MYC and IGF2BP1 expression in 8305C cells transfected with control (siC) or MYC-directed (siMYC) siRNA pools. VCL served as loading (upper panel) and negative (lower panel) control. **E)** Viability of 8305C-derived spheroids (n = 12 per condition), 72 h post-transfection. Left panel, representative images of spheroids. Scale bar, 200 *µ*m. Box plots (right panel) show spheroid viability determined by CellTiter-GLO, normalized to the median viability of siC-transfected control (set to one). Error bars indicate standard deviation. Statistical significance was determined by two-tailed Student's t-test (*** p ≤ 0.001).

oncogenic role of MYC (Figure 14E). In sum, these findings suggested that the *de novo* expression of IGF2BP1 is induced by SETD1A/B-directed epigenetic re-programming and driven by MYC-dependent transcription. Further, this implied a function in cancer progression.

3.2.3 IGF2BP1 conveys an oncogenic potential *in cellulo* and *in vivo*

IGF2BP1 *de novo* expression in ATC and previous studies in other cancer-derived cells suggested oncogenic roles also in ATC-derived cells (Bell et al., 2013). This was studied in the more proliferative C643 cells stably depleted for IGF2BP1 by a previously reported shRNA (Gutschner et al., 2014). To monitor how the knockdown of IGF2BP1 interferes with tumor growth *in vivo*, C643 cells stably transduced with vectors expressing control or IGF2BP1-directed shRNAs and iRFP (near-infrared fluorescent protein) were injected subcutaneously into the left flank of nude mice, as previously described in other cancer cell models (Figure 15A (Gutschner et al., 2014)). Tumor growth was monitored by non-invasive near-infrared imaging using iRFP as a tracer. The quantitative assessment of tumor volume demonstrated that the depletion of IGF2BP1 severely impaired the tumor growth of C643 cells (Figure 15A). These findings suggested IGF2BP1 as a potent enhancer of tumor growth in ATC. This was analyzed in further detail by overexpression of GFP (control) or GFP-tagged IGF2BP1 in 8305C cells. The quantitative assessment of tumor growth indicated that the overexpression of IGF2BP1 substantially increased tumor volume upon a lack phase, as evidenced by non-invasive near-infrared imaging (Figure 15B). The pre-clinical significance of these findings was further evaluated via transient depletion of IGF2BP1. In agreement with studies in other cancer cell lines (Kobel et al., 2007), the depletion of IGF2BP1 via siRNAs resulted in reduced MYC expression in 8305C and C643 (Figure 15C). Consistent with the *in vivo* findings, growth effects were confirmed by significantly reduced cell numbers of both cell lines upon IGF2BP1 depletion over indicated timepoints (Figure 15D). Suggesting a growth promoting effect by IGF2BP1, cell cycle progression was analyzed by flow cytometry upon IGF2BP1-knockdown. This revealed a substantial (8305C) and moderate but significant (C643) impairment of G1/S progression (Figure 15E). Previous reports
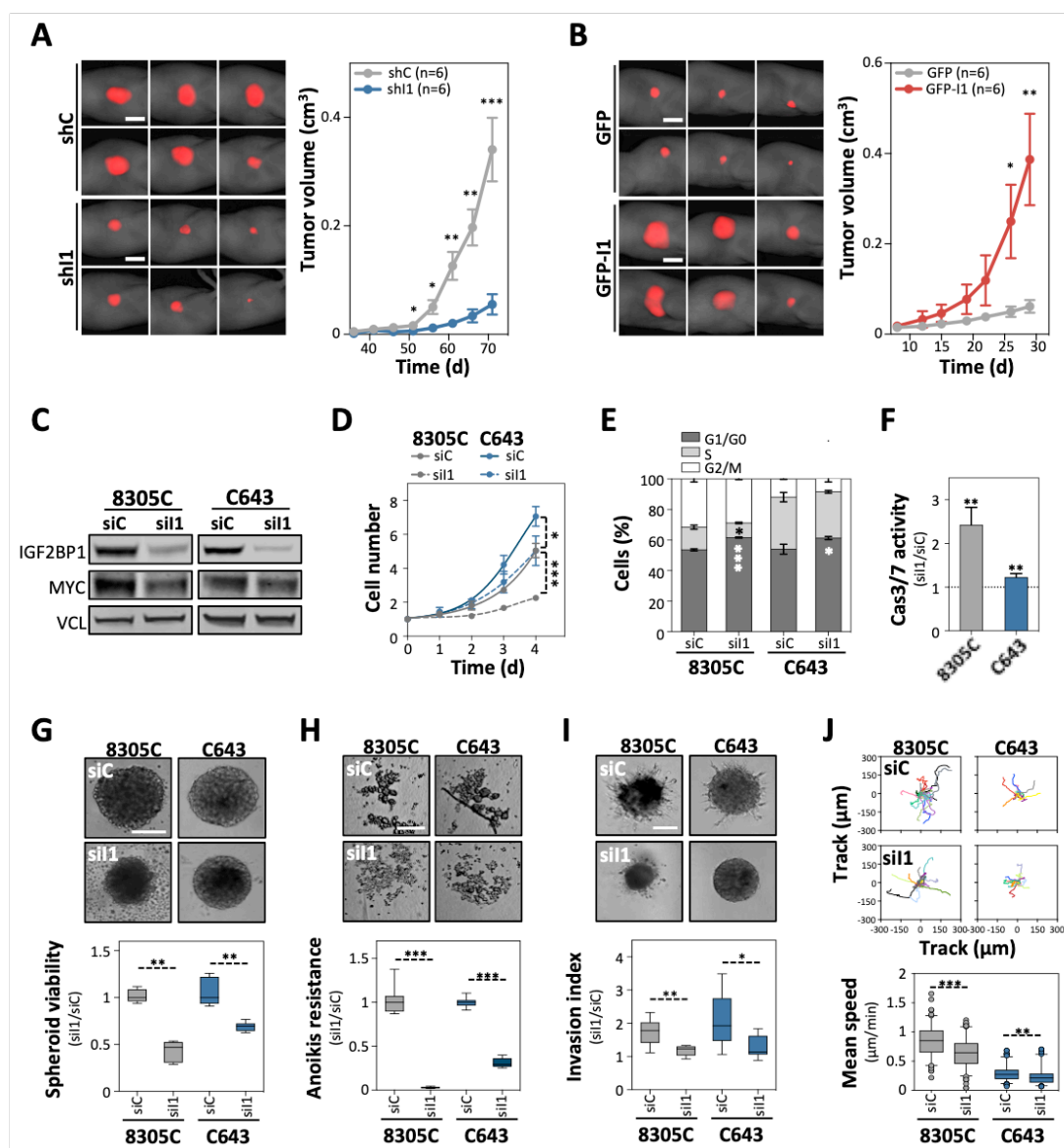
Figure 15. IGF2BP1 harbours oncogenic potential. **A, B)** C643 cells (A) stably expressing iRFP and a control (shC), or IGF2BP1-directed shRNA (shI1) and 8305C cells (B) stably expressing iRFP and GFP, or GFP-IGF2BP1 (GFP-I1) were subcutaneously injected (n = 6, each condition) in nude mice. Near-infrared (iRFP), overlayed with bright field images of tumor-bearing mice at 71 (A) or 29 (B) days post-injection are shown in left panels. Scale bars, 1 cm. Tumor volumes were measured at indicated time points post-injection (right panels). Error bars indicate standard error of mean (SEM). **C)** Representative Western blot analysis of IGF2BP1 and MYC-protein expression in C643 and 8305C cells upon IGF2BP1 depletion using siRNA pools (siI1) compared to controls (siC). VCL served as loading control. **D)** 2D cell proliferation of 8305C and C643 upon IGF2BP1 depletion at indicated time points post-transfection. **E)** Percentage of 8305C and C643 cells transfected as in (C) in indicated cell cycle phases as determined by flow cytometry. **F)** Ratio of Caspase3/7 activities, determined by Caspase-Glo, in 8305C and C643 cells transfected as in (C) **G)** Viability of 8305C- and C643-derived spheroids (n = 12 per condition), determined by CellTiter-GLO, 72 h post-transfection as in (C). Upper panel, representative images of spheroids; scale bar, 200 μm. Box plots (lower panel) show spheroid viability normalized to the median viability of siC-transfected controls (set to one). **H)** Anoikis-resistance of 8305C and C643 cells (n = 12 per condition) 7 days post-transfection as in (C). Upper panel, representative images of cell aggregates; scale bar, 300 μm. Box plots (lower panel) show cell viability as determined in (G) **I)** Spheroid invasion of 8305C and C643 spheroids (n = 12 per condition) in matrigel 6 d post-transfection as in (C). Upper panel, representative images of spheroids; scale bar,

200 μm. Box plots (lower panel) indicate the determined invasion index. **J)** The mean speed of 2D single cell migration on collagen I was determined in 8305C and C643 cells transfected as in (C). Cell tracks were monitored for 10 h starting ~60 h post-transfection. Upper panel, centroid cell tracks. Box plots (lower panel) indicate the mean speed of n = 100 cells monitored per condition.

also described an anti-apoptotic function for IGF2BP1 in liver cancer (Gutschner et al., 2014). This was supported, as Caspase-3/7 activity was substantially (8305C) or modestly (C643) increased upon depletion (Figure 15F). Thus, IGF2BP1 promotes cell cycle progression and interferes with apoptosis in a variable but conserved manner in ATC-derived cells. Furthermore, IGF2BP1 impaired tumor cell spheroid growth. Under permissive growth conditions (10% FBS), the depletion of IGF2BP1 impaired spheroid growth in both ATC cell lines as evidenced by significantly reduced viability and size of spheroids (Figure 15G). Under non-permissive growth conditions (0.5% FBS), the depletion severely affected non-adhesive growth suggesting a role of IGF2BP1 in promoting anoikis resistance of ATC-derived cells (Figure 15H). Anoikis is a form of programmed cell death upon detachment from an appropriate extra-cellular matrix. It represents a physiologically relevant process for tissue homeostasis and development, but can be deregulated in cancers, called anoikis resistance. It is a prerequisite for invasion/metastasis (Kim et al., 2012). Surrounded by solid tissue, an anoikis resistant mesenchymal-like/non epithelial-like cancer cell must possess the ability to invade and migrate. The invasive potential of 8305C- as well as C643-derived spheroids was tested in Matrigel matrices. The depletion of IGF2BP1 severely diminished the invasive potential (Figure 15I). The analysis of 2D cell motility upon IGF2BP1 knockdown showed that the mean speed of single cell migration was significantly reduced in 8305C as well as C643 cells (Figure 15J). Collectively, these findings revealed that IGF2BP1 promotes the growth, migratory as well as the invasive potential of ATC-derived cells *in vitro* and *in vivo* suggesting it as a post-transcriptional enhancer of ATC progression.

3.3 IGF2BP1 is an m6A-dependent post-transcriptional enhancer of MYC-driven gene expression

3.3.1 IGF2BP1 enhances an oncogenic MYC-driven gene expression signature

Previous *in cellulo* studies indicated that IGF2BP1's oncogenic role in cancer cells largely relies on the stabilization of mRNAs resulting in the enhanced expression of oncogenes like MYC or LIN28B (Busch et al., 2016; Huang et al., 2018a). Consistently, the depletion of IGF2BP1 in three ATC-derived cell lines was associated with reduced MYC expression due to impaired MYC mRNA stability (Fgure 16A, B). The findings implied that IGF2BP1 post-transcriptionally enhances MYC-driven gene expression in ATC. This was evaluated by a GSEA-meta examination of gene sets correlated with IGF2BP1 or MYC expression in the test cohort, prior analyzed by RNA-seq (Figure 16C). A significant correlation of MYC- and IGF2BP1-associated gene expression was revealed. Notably, among genes associated with both, gene sets comprising MYC target transcripts and genes upregulated in thyroid cancer with adverse prognosis were significantly enriched (positive ES). Gene sets downregulated in ATC were substantially decreased among genes with MYC/IGF2BP1-associated expression (negative ES). These studies raised the hypothesis, that IGF2BP1 not only forms a positive feedback loop with MYC in ATC but may also influence MYC-driven transcripts directly. The latter was further supported by two findings: I) Among genes associated with MYC expression in ATC, transcripts downregulated by IGF2BP1 depletion in 8305C cells showed elevated probability of conserved IGF2BP1-binding, as indicated by CLIP studies (Figure 16D). II) GSEA revealed downregulation of the HALLMARK_MYC_ TARGETS_V1 gene set upon IGF2BP1 depletion in ATC-derived cells (Figure 16E). To identify MYC-driven genes potentially enhanced by IGF2BP1 post transcription in ATC, genes had to fit three criteria (Figure 16F): I) significant association with MYC in ATC (MYC R+); II) significant association with IGF2BP1 in ATC (IGF2BP1 R+); III) significant downregulation upon IGF2BP1 depletion in ATC-derived 8305C cells (I1- KD DN). These analyses identified 956 genes fulfilling all three criteria. Most of these
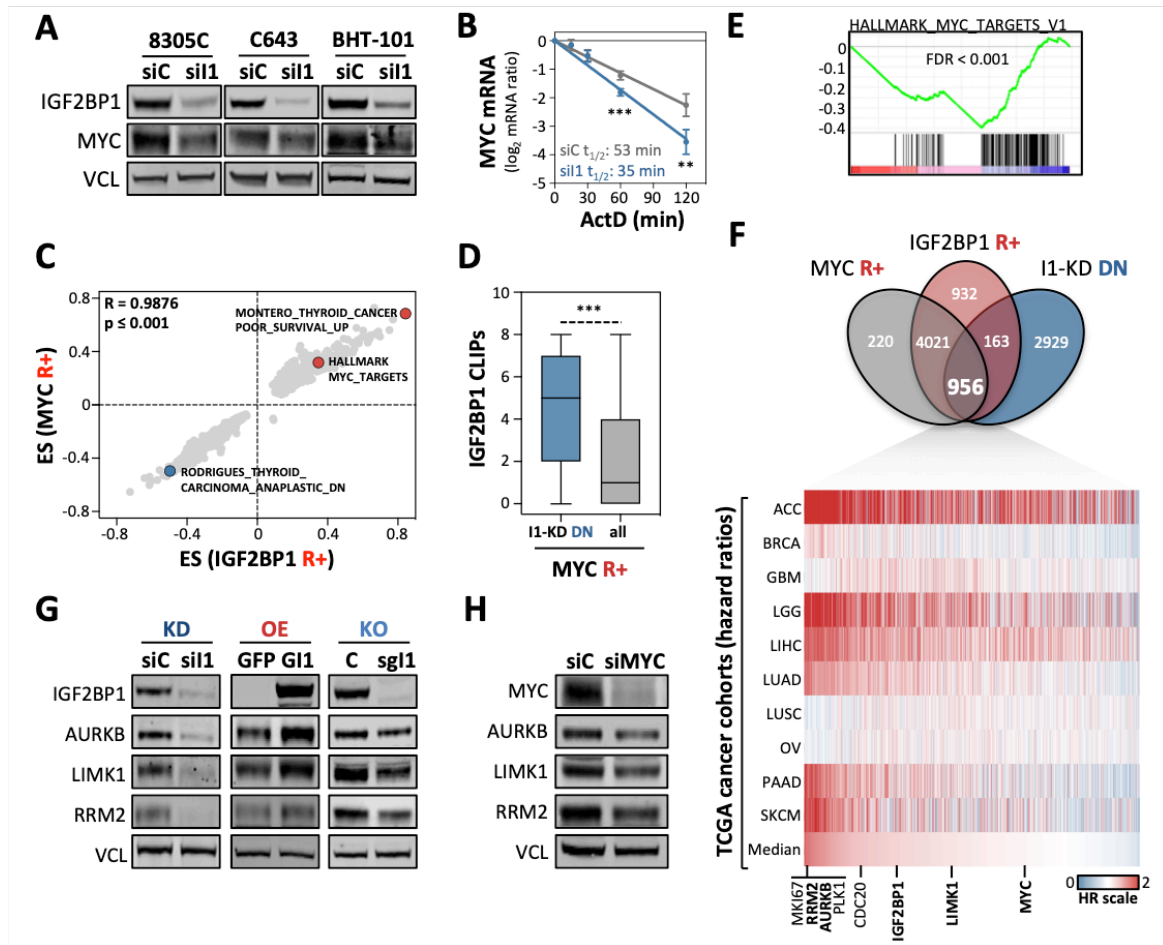
Figure 16. IGF2BP1 enhances an oncogenic MYC-driven gene expression signature. **A)** Western blot analysis of IGF2BP1 and MYC expression in indicated ATC-derived cell lines transfected with control (siC) or IGF2BP1-directed (siI1) siRNA pools. VCL served as loading control. **B)** RT-qPCR analyses of MYC mRNA decay in 8305C cells transfected with control (siC) or IGF2BP1-directed (siI1) siRNA pools. RNA synthesis was inhibited by actinomycin D (ActD; 5 µM) for indicated times. Transcript abundance was normalized to input level. $t_{1/2}$, mRNA half-life. **C)** GSEA analyses were performed on MYC (MYC R+) as well as IGF2BP1 associated (IGF2BP1 R+) gene expression as determined by Pearson correlation analyses in patient tissue samples, prior used for RNA seq. The enrichment scores (ES) of gene sets significantly (FDR ≤ 0.05) associated with both, MYC- and IGF2BP1-correlated gene expression were plotted. **D)** Depicted is the conservation of IGF2BP1 binding (IGF2BP1 CLIPs out of eight experiments) with all genes being positively associated with MYC expression (MYC R+; all) or significantly (FDR ≤ 0.01) downregulated genes identified upon IGF2BP1-depletion (I1-KD DN) in 8305C cells by mRNA-seq. **E)** GSEA enrichment plot of genes observed to be downregulated by RNA-seq upon IGF2BP1-depletion in 8305C cells and being reported for the indicated hallmark pathway. **F)** Venn diagram (upper panel) depicting the number of genes positively associated with MYC (MYC R+) and IGF2BP1 (IGF2BP1 R+) expression from samples prior used for RNA-seq, as well as significantly (FDR≤0.01) downregulated (DN) genes identified upon IGF2BP1 depletion in 8305C cells by mRNA-seq. Hazard ratios (HR) for intersecting genes are shown (lower panel) for selected indicated TCGA cancer cohorts. Indicated are the median hazard ratios for transcripts as mentioned in the text. **G)** Western blot analyses of indicated proteins upon IGF2BP1 knockdown (KD, dark blue) and overexpression (OE, red) in 8305C cells as well as IGF2BP1-deletion (KO, light blue) in C643 cells. VCL served as loading control. **H)** Western blot analyses of indicated proteins upon MYC knockdown in 8305C cells. Statistical significance was determined by two-tailed Student's t-test (B) and Mann-Whitney test (D) (*** p ≤ 0.001; ** p ≥ 0.01; * p ≥ 0.05).

genes showed conserved association with poor prognosis in a panel of ten cancers derived from TCGA, indicated by hazard ratios (HR) greater 1. This supported the view that despite a direct regulation of MYC mRNA turnover, IGF2BP1 is a conserved, post-transcriptional enhancer of MYC target transcripts. Amongst and next to IGF2BP1 and MYC, the described IGF2BP1 target MKI67 and other pro-proliferative transcripts (including CDC20 or PLK1) were identified (Gutschner et al., 2014; Jia et al., 2016). Further, three mRNAs encoding proteins with distinct, but conserved oncogenic roles were evaluated. Two of these, AURKB and RRM2, encode essential regulators of cell cycle progression (Aye et al., 2015; Tang et al., 2017). The third, LIMK1, is a crucial regulator of actin dynamics and consequently tumor cell migration and invasion (Prunier et al., 2017). To validate IGF2BP1-dependent regulation of the three candidate target mRNAs, steady state protein abundances were monitored upon IGF2BP1 knockdown (KD) and overexpression (OE) in 8305C cells, or in CRISPR/Cas9-mediated IGF2BP1 deletion (KO) in C643 cells, respectivly (Figure 16G). The expression of all three factors was significantly reduced by IGF2BP1-KD/KO in all tested cell lines and elevated by IGF2BP1 overexpression in 8305C cells on protein and mRNA (mRNA data not shown). This indicated conserved regulation by IGF2BP1 in ATC-derived cell lines. If the expression is also controlled by MYC was analyzed in 8305C. Upon siRNA-mediated depletion of MYC, protein and mRNA abundance (mRNA data not shown) was significantly downregulated, indicating AURKB, RRM2 and LIMK1 as effectors of MYC/IGF2BP1-driven gene expression in ATC (Figure 16H).

3.3.2 IGF2BP1 target mRNAs convey oncogenic potential

The findings on enhancement of a MYC-dependent gene expression signature implied an oncogenic potential for IGF2BP1. To address whether IGF2BP1 modulates ATC phenotypes by promoting effector expression, tumor cell properties observed upon IGF2BP1 depletion and effector knockdown in ATC-derived cells were compared. Note, AURKB, RRM2 and LIMK1 showed a conserved association with IGF2BP1 expression and came along with an unfavorable prognosis in a pan-cancer analysis, including all 33 TCGA cancer cohorts (Figure 17A, B).
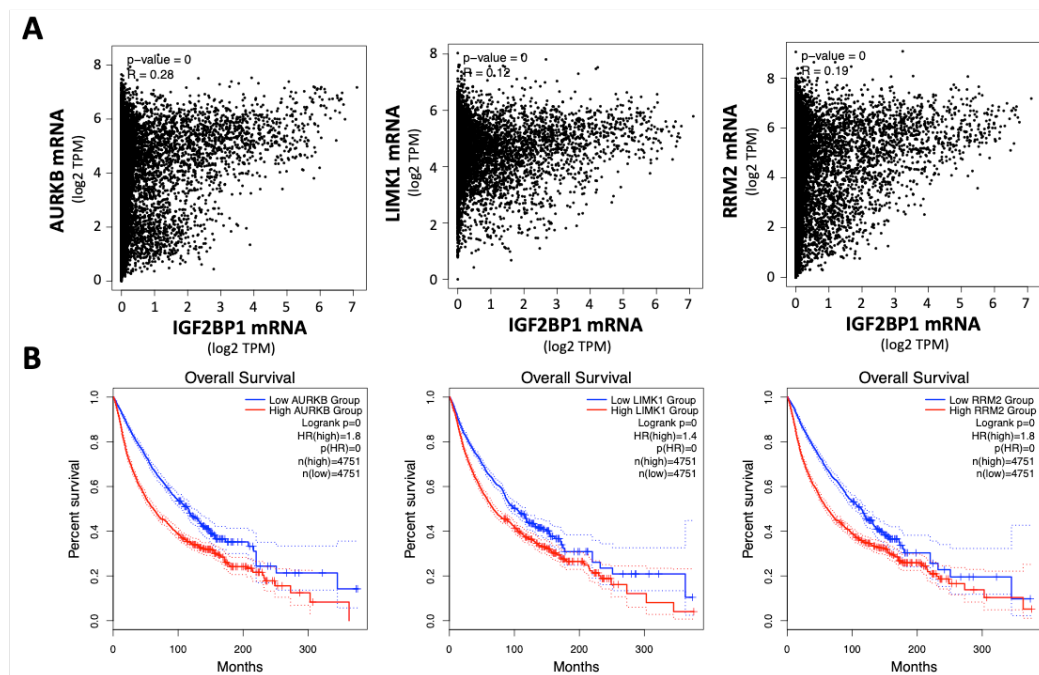
Figure 17. The novel IGF2BP1 effector mRNAs have a prognostic value. **A)** Levels (log$_2$ TPM) of indicated mRNAs were plotted over IGF2BP1 mRNA levels from a TCGA pan-cancer analysis by using GEPIA2. **B)** Kaplan Meier analyses of AURKB, RRM2 and LIMK1 from the TCGA pan-cancer dataset were performed using GEPIA2. The overall survival probabilities along with HR and p-values determined by GEPIA2 are shown.

AURKB is a crucial protein kinase modulating chromosomal segregation by facilitating the phosphorylation of substrates including serine 10 of histone-H3 (H3-S10) during mitosis (Tang et al., 2017). In agreement, AURKB depletion was associated with essentially abolished phosphorylation at H3-S10 (Figure 18A; pH3(Ser10)). Associated with reduced AURKB abundance, reduced phosphorylation at H3-S10 was also observed upon IGF2BP1 depletion. These findings suggested that IGF2BP1 promotes AURKB-driven phosphorylation by enhancing AURKB expression. The ribonucleotide-diphosphate reductase subunit M2 (RRM2) is essential for ensuring sufficient dNTP supply required for replication (Aye et al., 2015). To test, whether an IGF2BP1-dependent downregulation of RRM2 affects the cellular availability of dNTPs, was tested by a fluorescent PCR-based assay (Figure 18B) (Wilson et al., 2011). Consistently, the levels of all four dNTPs were substantially reduced upon RRM2 and IGF2BP1 depletion, in ATC-derived cells. This suggested that IGF2BP1 modulates NTP/dNTP homeostasis by controlling RRM2 expression and thereby promotes cell cycle progression. The LIM domain kinase 1 (LIMK1) is an essential regulator of the actin cytoskeleton influencing actin dynamics mainly by phosphorylating cofilin 1 (CFL1) at serine 3 (CFL1-S3) (Prunier et al.,

2017). In support of this, LIMK1 knockdown resulted in essentially abolished phosphorylation of CFL1-S3 (Figure 18C; pCFL1(Ser3)). Likewise, the downregulation of LIMK1 in response to IGF2BP1 depletion was associated with substantially reduced phosphorylation at CFL1-S3. These findings provide further evidence supporting IGF2BP1 as a post-transcriptional regulator of the actin cytoskeleton controlling actin dynamics by regulating LIMK1 abundance. If the observed regulation of its effectors also translates into the regulation of oncogenic cell phenotypes was determined by monitoring spheroid growth, invasion and anoikis resistance of ATC-derived cells upon effector depletion. The knockdown of each of
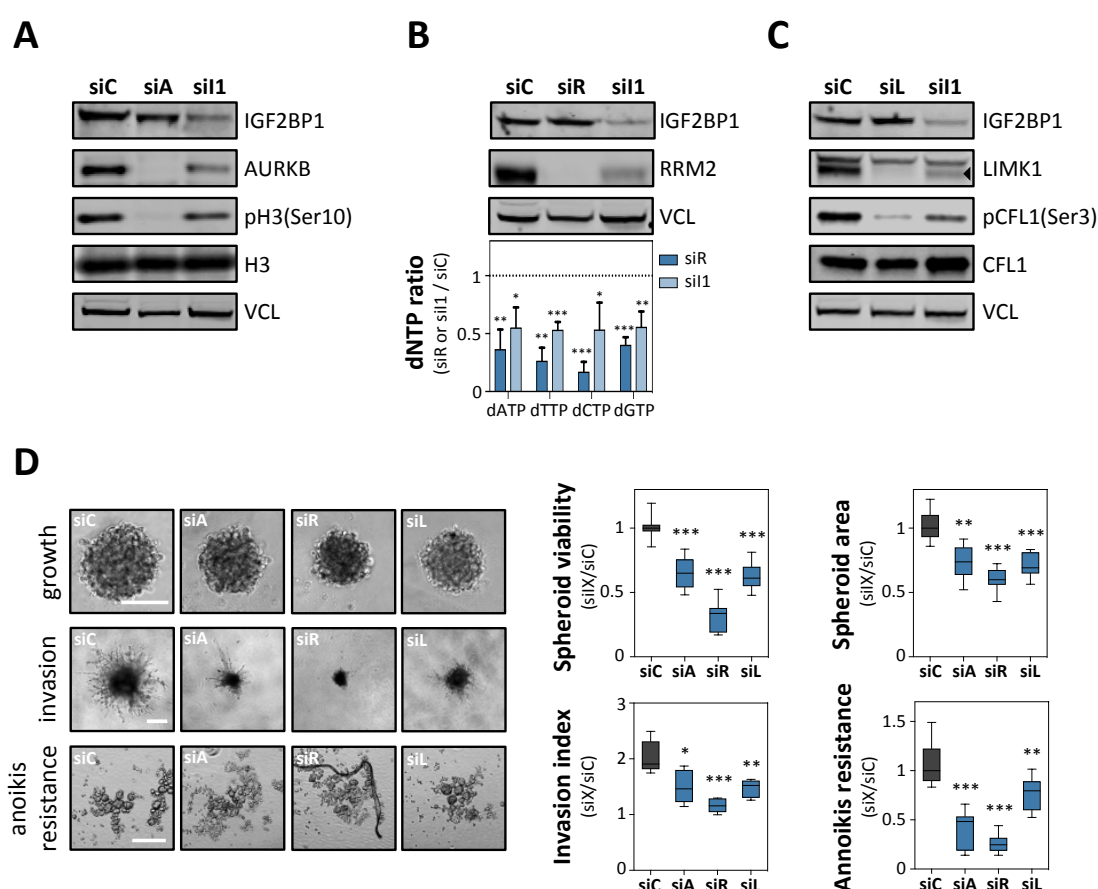
Figure 18. IGF2BP1 target mRNAs convey oncogenic potential. **A-C)** Western blot analysis of indicated proteins and post-translational modifications in 8305C cells transfected with control (siC), AURKB- (siA), RRM2- (siR), LIMK1- (siL) or IGF2BP1-directed (siI1) siRNA pools. VCL served as loading control. The level of dNTPs (shown as ratio, lower panel) upon RRM2 and IGF2BP1 depletion was determined relative to siC-transfected controls. **D)** Analysis of spheroid viability, invasion, as well as anoikis-resistance with 8305C cells. Scale bars, 200 μm (spheroid viability, invasion) or 300 μm (anoikis resistance). Representative images of spheroids and cell aggregates are shown in left panels. Box plots (right panel) show determined spheroid viability, area, invasion and anoikis-resistance (n = 12 per condition) normalized to the median of siC-transfected controls (set to one). Statistical significance was determined by two-tailed Student's t-test from three independent experiments (*** $p \leq 0.001$; ** $p \geq 0.01$; * $p \geq 0.05$).

the three IGF2BP1 target mRNAs significantly impaired the analyzed cell phenotypes (Figure 18D). Although these findings may be biased by a partial interdependence of the analyzed cell properties, they provide strong evidence that IGF2BP1 promotes an aggressive tumor cell phenotype by promoting the expression of the three novel effectors AURKB, RRM2 and LIMK1 at the post-transcriptional level.

3.3.3 IGF2BP1 stabilizes MYC-driven mRNAs in a 3'end- and m6A-dependent manner

Recent studies indicated that IGF2BP1's main and conserved role in cancer cells is the 3'end-dependent (referring to the last exon including the 3'UTR) impairment of target mRNA turnover (Muller et al., 2018). In agreement, CLIP studies in HEK293, ESCs, HepG2 and K562 cells (Conway et al., 2016; Hafner et al., 2010; Van Nostrand et al., 2016) indicated conserved IGF2BP1-binding at the 3'-end of all three MYC/IGF2BP1-driven effector transcripts (Figure 19A). Further, IGF2BP-specifcity for distinct transcripts is facilitated by the occurrence of N^6-methyladenosines (m6A), mainly within 3'UTRs or near the stop codons (Huang et al., 2018a). Intriguingly, a partial overlap of IGF2BP1 binding sites with m6A-modified nucleotides, as reported by m6A-RIP-seq studies, was observed (Xuan et al., 2018). The 3'end-dependency was further validated by RIP (RNA co-immunoprecipitation) in ATC-derived cells. Compared to control cells, expressing either GFP or RNA-binding deficient IGF2BP1 (mut), the previously reported RNA-dependent recruitment of ELAVL1 (HuR) protein and the MYC mRNA (positive controls) were severely enhanced for wild type GFP-IGF2BP1 (Figure 19B). In contrast to the HISTH2AC mRNA (negative control), selective association with GFP-IGF2BP1 was also determined for AURKB, RRM2 and LIMK1 mRNAs indicating these again as novel, conserved target mRNAs of IGF2BP1. If regulation by IGF2BP1 is in fact 3'end-dependent was analyzed by monitoring the activity of luciferase reporters comprising the 3'ends of the respective mRNAs. The activity of control reporters (EV) remained essentially unchanged by IGF2BP1 overexpression (OE, red) in 8305C cells or its deletion (KO, blue) in C643 cells (Figure 19C). In contrast, the activity of reporters containing the last exon of AURKB, or 3'UTRs of RRM2 or LIMK1 were significantly enhanced by IGF2BP1 overexpression and decreased by its deletion. This suggested that IGF2BP1 impairs

the turnover of the respective mRNAs in a 3'end-dependent manner. In agreement, upon Actinomycin D treatment the half-life of all three MYC/IGF2BP1-driven effector mRNAs was significantly reduced by IGF2BP1 depletion in 8305C cells (Figure 19D-F).
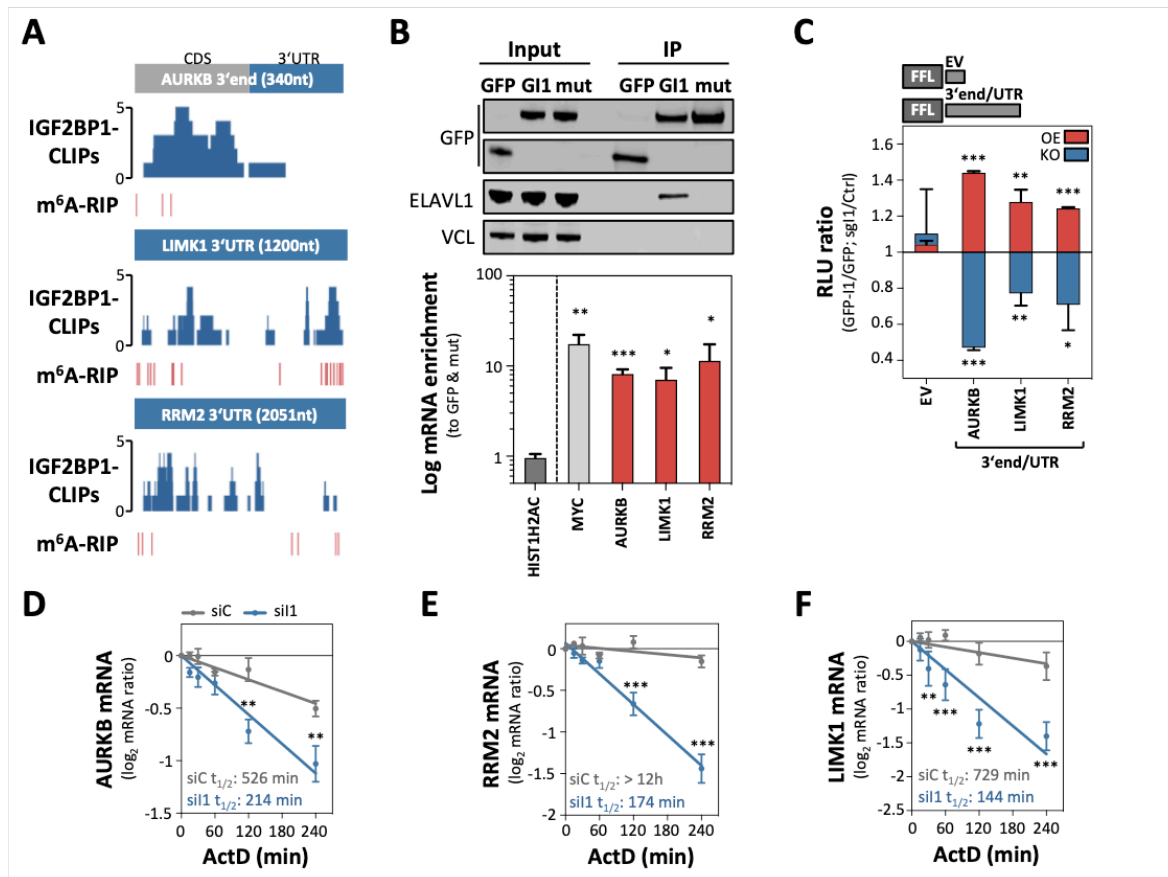

Figure 19. IGF2BP1 stabilizes effector mRNAs. **A)** Graphs indicate IGF2BP1 CLIP- and m6A-site distribution in the last exon (including the 3'UTR) of indicated genes. Eight independent, publicly available CLIP analyses performed in cancer-derived cells and m6A-RIP studies were considered **B)** RT-qPCR analyses of mRNAs co-purified with GFP, GFP-IGF2BP1 (GI1) or RNA-binding deficient GFP-IGF2BP1 (mut) by immunoprecipitation. The $\log_{10}$ enrichment of indicated mRNAs with GFP-IGF2BP1 was determined relative to their co-purification with GFP and mut upon input normalization. HISTH2AC served as negative control. **C)** Activity ratios of luciferase reporters comprising the last exon of AURKB, LIMK1 or RRM2 (depicted on top) were determined in 8305C cells expressing GFP or GFP-IGF2BP1 (GFP-I1; OE, red) and parental (Ctrl) or IGF2BP1-deleted (sgI1; KO, blue) C643 cells. A reporter comprising the vector-encoded 3'UTR (EV) served as control. **D-F)** RT-qPCR analyses of AURKB, RRM2 and LIMK1 mRNA decay in 8305C cells transfected with control (siC) or IGF2BP1-directed (siI1) siRNA pools. RNA synthesis was inhibited by actinomycin D (ActD; 5 µM) for indicated time. Transcript abundance was normalized to input levels. $t_{1/2}$, mRNA half-life. Error bars indicate standard deviation. Statistical significance was determined by two-tailed Student's t-test from three independent experiments (*** $p \leq 0.001$; ** $p \geq 0.01$; * $p \geq 0.05$).

Recently, it was shown that for some IGF2BP1 target transcripts, the 3'end-dependent impairment of target mRNA turnover is furthermore controlled by m6A modification of the regulated mRNAs, resulting in enhanced mRNA binding of

IGF2BPs (Huang et al., 2018a). To elucidate *cis*-element specificity of IGF2BP1 to the identified target mRNAs via m6A-modified nucleotides, observed sites reported by m6A-RIP-seq studies were compared to IGF2BP1-CLIPs, showing a partial overlap (Figure 19A) (Xuan et al., 2018). Aiming to address if the expression of the three IGF2BP1 target mRNAs is also m6A-dependent in ATC-derived cells, the m6A-methyltransferase METTL3 was deleted in C643 cells via CRISPR/Cas9 (Figure 20A). METTL3 is the enzymatic subunit of the m6A-modifying complex with major importance in developmental processes and several cancers (Lan et al., 2019). The deletion of METTL3 was associated with severely reduced m6A levels in poly(A)+ RNAs, accompanied by reduced protein and mRNA levels of the IGF2BP1 effectors AURKB, LIMK1, RRM2 and the positive control MYC (Figure 20A-C). Further, a decrease of spheroid size and viability could be observed (Figure 20D). It is important to note, that IGF2BP1 abundance remained essentially unchanged. The observation that IGF2BP1 and VCL expression remained essentially unaffected whereas the m6A-modification of all analyzed target mRNAs was significantly reduced by the loss of METTL3, as analyzed by m6A-RIP-qPCR, suggested that IGF2BP1 modulates the expression of its effectors in a 3'end- and m6A-dependent manner upstream of the m6A pathway (Figure 20E). In support of this notion, the activity of luciferase reporters harboring the 3'end of AURKB and 3'UTRs of LIMK1 or RRM2 was significantly reduced by METTL3-deletion (Figure 20F). To address if IGF2BP1- and m6A-dependent regulation as well as mRNA association are conserved in ATC-derived cells, the latter was probed by IGF2BP1-RIP in 8305C cells depleted for METTL3 by siRNA pools (Figure 20G, H). Although the expression and immunoprecipitation of GFP (control) and GFP-IGF2BP1 remained unchanged by the knockdown of METTL3, the co-purification of all three novel IGF2BP1 target mRNAs and the MYC mRNA as postive control was significantly reduced (Figure 20G, H). In summary, these findings indicated that IGF2BP1 promotes the expression of oncogenic effectors in a conserved, 3'end and m6A-dependent manner by impairing mRNA decay.
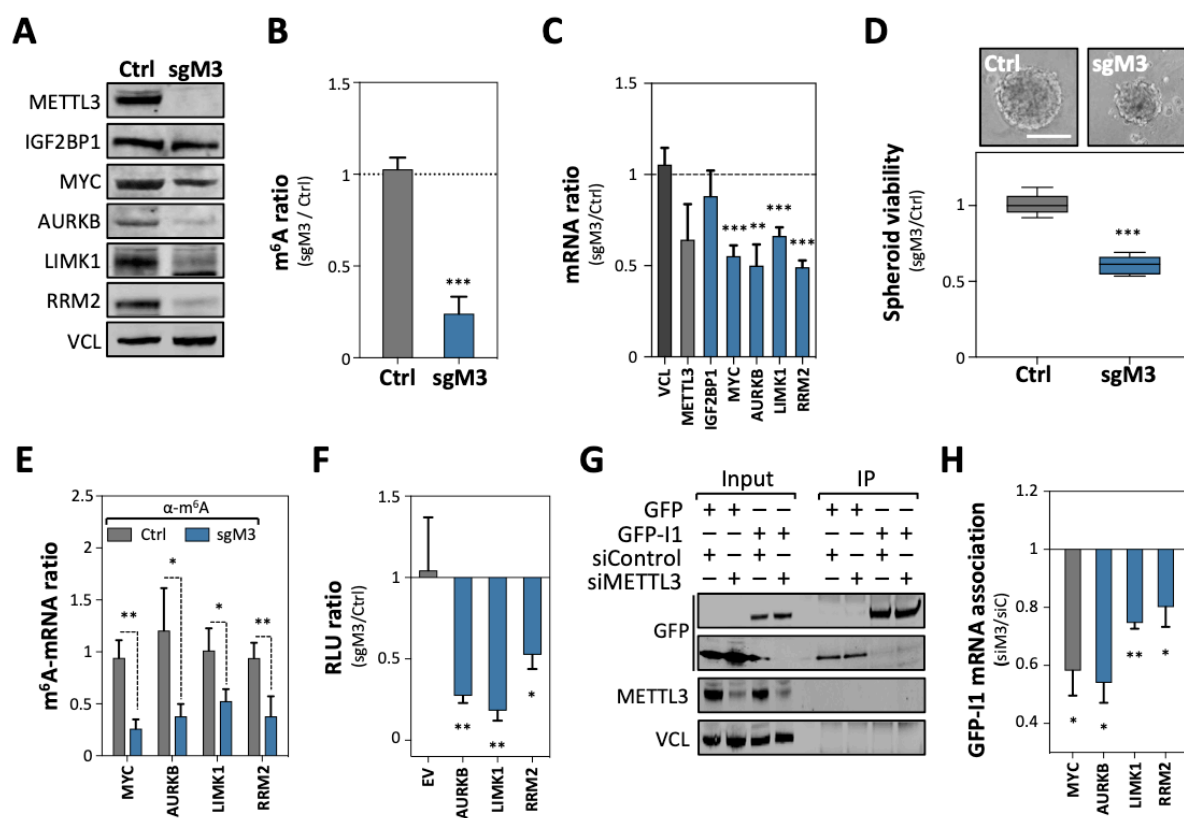
Figure 20. IGF2BP1 promotes AURKB, LIMK1 and RRM2 expression in an m6A-dependent manner. **A)** Western blot analyses of indicated proteins in C643 cells transfected with Cas9 only (Ctrl) or deleted for METTL3 (sgM3). VCL served as loading control. **B)** M6A levels in poly(A)+ RNA were determined in C643 cells transfected with Cas9 only (Ctrl) or deleted for METTL3 (D, lower panel). Median m6A level (dashed line) determined in controls (Ctrl) served for calculating m6A ratios. **C)** RT-qPCR analyses of indicated mRNAs in C643 Ctrl or sgM3 cells, as in (A). VCL served as negative control. **D)** Analysis of spheroid viability in Ctrl and sgM3 cells. Representative images of spheroids are shown in the upper panel. Scale bar, 200 μm. Box plots (lower panel) show determined spheroid viability (n = 12 per condition) normalized to the median of Ctrl cells (set to one). **E)** M6A-RIP-qPCR analysis of indicated mRNAs in poly(A)+ RNA isolated from C643 cells analyzed in (A). M6A-mRNA ratio of depicted mRNAs was calculated relative to the median m6A-mRNA level determined in Ctrl samples. MYC served as positive control. **F)** Activity ratios of luciferase reporters comprising the last exon of AURKB and 3'UTRs of LIMK1 or RRM2 were determined from C643 Ctrl and sgM3 cells. A reporter comprising the vector-encoded 3'UTR (EV) served as control. **G, H)** Western blot (G) and RT-qPCR (H) analyses of indicated proteins and mRNAs co-purified with GFP or GFP-IGF2BP1 (GFP-I1) by immunoprecipitation (IP) from 8305C cells transfected with control (siC) or METTL3-directed (siM3) siRNA pools. VCL served as loading (Input) and negative (IP) control. The GFP-I1 mRNA association ratio was determined by mRNA enrichments (normalized to GFP) determined in siM3- versus siC-transfected cells. Error bars indicate standard deviation of at least three analyses. Statistical significance was determined by Student's t-test (*** $p \leq 0.001$; ** $p \leq 0.01$; * $p \leq 0.05$).

3.4. The MYC/IGF2BP1-driven gene expression signature is targetable by BETi and BTYNB in synergy

At present, there is no clinically evaluated and FDA-approved direct therapeutic inhibition of MYC or IGF2BP1. However, indirect MYC-inhibition by BET (bromodomain and extra-terminal motif) inhibitors (BETi) (pan-)targeting bromodomain proteins (BRDs) has been demonstrated in various cancer models, including ATC xenografts (Chen et al., 2018; Enomoto et al., 2017; Zhu et al., 2017). Further, the therapeutic value is currently evaluated in accordance with FDA-guidelines for several solid and hematological malignancies (Alqahtani et al., 2019). RNA-seq of thyroid cancer samples indicated upregulated expression of three BRDs, BRD3, BRD4 and BRDT, and downregulation of BRD2 (Figure 21).
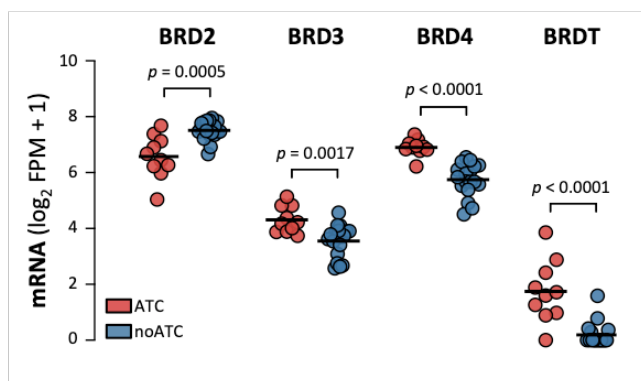
Figure 21. Expression of BRDs is upregulated in ATC. Scatter dot plot presentation of mRNA expression (log2 (FPM + 1)) for indicated transcripts in ATC vs noATC samples, as determined by RNA-seq from the test cohort (see Figure 8). Statistical significance was determined by Mann-Whitney test.

This suggested that BRDi might provide an effective first-line treatment option inhibiting invasive growth in ATC by impairing MYC/IGF2BP1-driven transcription. To test this, BETis (ABBV-075, CPI-203, CPI-0610, PLX51107, OTX015) currently evaluate in clinical trials for other malignancies, widely studied JQ1 and PROTAC-based BET degraders (BETd; ARV-825 and ARV-771) were analyzed in three ATC-derived cell lines (Figure 22) (Stathis and Bertoni, 2018). The determined half-effective concentrations (EC_{50}), required to impair tumor cell viability, were in the nM-range for all tested compounds. Drug efficacies (E_{max}) were all beyond 0.5. ABBV-075 (Mivebresib), a recently developed BRDi (McDaniel et al., 2017), stood out in these studies with an average EC_{50} of ~20 nM and average E_{max} of ~0.1 over all three tested cell lines.

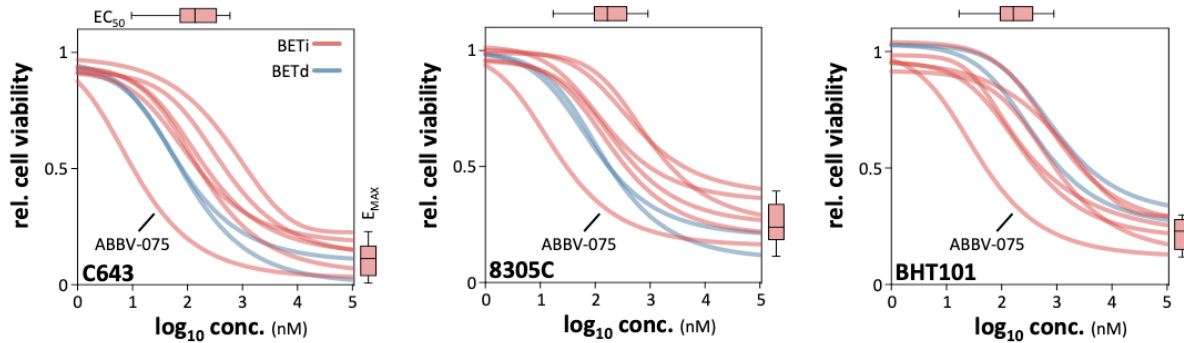**Figure 22.** BETi and BETd show superior efficacy in ATC-derived cells. Cell viability ratios (to DMSO) of C643, 8305C and BHT-101 cells exposed to eight different BET-targeting compounds at different concentrations have been determined after 72h. Shown are response curves for treatments with BET-inhibitors (BETi; red) and BET-degraders (BETd; blue). Box plots indicate the distribution of EC_{50}-doses or E_{MAX} for all eight compounds.

To test if BRDi/d are suitable to impair MYC/IGF2BP1-driven gene expression, C643 cells were exposed to JQ1 at its determined EC_{50} concentration (Fig. 23A). The analysis of the protein-coding transcriptome via mRNA-seq revealed 398 of previously identified 956 MYC/IGF2BP1-dependent transcripts to be significantly downregulated amongst differentially expressed genes and 142 transcripts were found to be upregulated. Intriguingly, AURKB, RRM2 and LIMK1 expression was impaired by the treatment, next to MKI67 and other pro-proliferative transcripts. Subsequently, changes in protein expression were confirmed by Western blotting (Fig. 23B). To evaluate effect conservation for any BETi/d, ATC-derived cell lines were exposed to EC_{50} concentrations of indicated compounds and gene expression was monitored by RT-qPCR (Fig. 23C). The use of any compound consistently decreased the expression of MYC and IGF2BP1 expression in all three tested ATC-derived cell lines. Substantial downregulation was also observed for AURKB, LIMK1 and RRM2 in the three tested cell lines, indicating BETi/d as a promising therapeutic strategy to impair MYC/IGF2BP1-driven gene expression in ATC and its growth. This study suggested a battery of BETi/d compounds, ahead of all ABBV-075, which proved promising with superior efficacy in recent trials in other malignancies (Sarina Anne et al., 2018; Stathis and Bertoni, 2018).
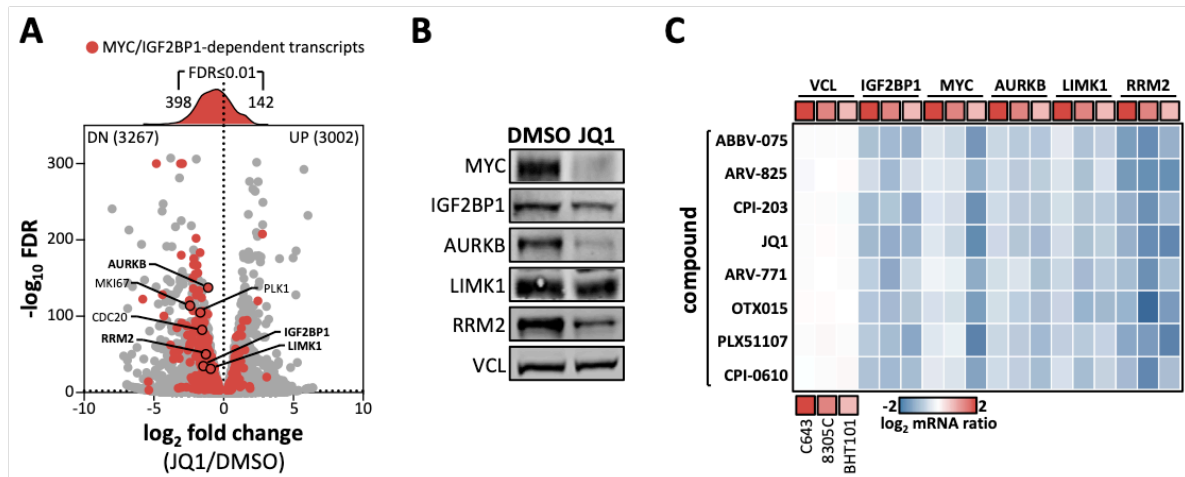
Figure 23. BETi/d-treatment reduces the expression MYC/IGF2BP1-dependent genes. **A)** Volcano plot of $\log_2$ mRNA fold changes plotted against the $-\log_{10}$ FDR for JQ1 treatment versus DMSO in C643 cells. Indicated in red are the MYC/IGF2BP1-dependent genes, as determined in Figure 16F. The histogram on top of the volcano plot indicates the distribution of the MYC/IGF2BP1-dependent genes among down- and upregulated genes. **B)** Western blot analyses of indicated proteins upon JQ1 treatment of C643 cells, as in (A) **C)** Heatmap presentation of $\log_2$ mRNA ratios determined by RT-qPCR for indicated transcripts upon treatment with indicated compounds at EC_{50} concentration compared to DMSO-treated controls in indicated cells lines.

In cell culture models BET inhibitors proved even more efficient in combinatorial therapy approaches (Bui et al., 2017). To test a progressive treatment strategy the targeted inhibition of IGF2BP1 was included. Therefore, ABBV-075 was combined with BTYNB, an inhibitor of IGF2BP1 function without any clinical evaluation so far (Mahapatra et al., 2017). Half-effective impairment of growth (EC_{50}) for C643, 8305C and BHT101 cells was achieved with concentrations of ~7 μM (Figure 24A). At EC_{50} concentrations the expression of downstream effectors, as shown by RT-qPCR for three ATC-derived cell lines and by Western Blot for C643 cells was decreased (Figure 24B, C). To evaluate a potential synergy of ABBV-075 and BTYNB, cell viability was monitored upon applying varying concentrations of combined compounds (Figure 24D, E). In C643 cells, synergistic inhibition of cell viability was indicated by synergy δ-scores determined by the HSA-model (Ianevski et al., 2017). This provided further evidence for the synergy of MYC-driven transcription and post-transcriptional super-enhancement by IGF2BP1, suggesting combinatorial treatment by ABBV-075 and BTYNB as a promising avenue in ATC therapy.
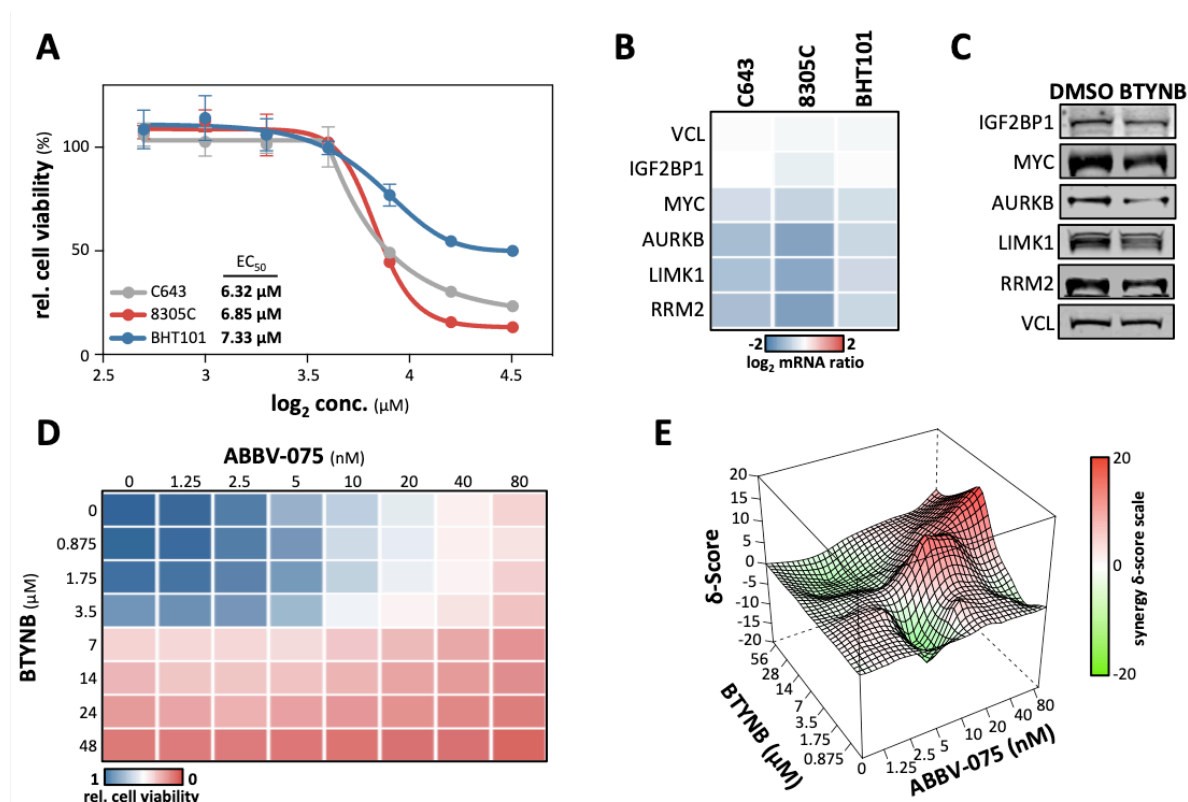
Figure 24. ATC-derived cells are vulnerable to a synergistic combination of BET- and IGF2BP1 inhibition. **A)** Cell viability ratios (to DMSO) of C643, 8305C and BHT-101 cells exposed to IGF2BP1 targeting BTYNB at different concentrations for 72h. Response curves and EC_{50} values are shown. **B)** Heatmap presentation of $\log_2$ mRNA ratios determined by RT-qPCR for indicated transcripts upon treatment with BTYNB (to DMSO) at EC_{50} concentration in indicated cells lines. **C)** Representative Western blot analyses of indicated proteins in C643 cells exposed to BTYNB at EC_{50} concentration and DMSO controls. **D)** Heatmap presentation of relative C643 cell viability (to DMSO), 72 h upon exposure to serial dilutions of ABBV-075 (1.25 nM - 80 nM) in combination with BTYNB (0.875 μM - 48 μM). J) Synergy δ-scores determined in **E)** are depicted by a 3D presentation. δ-scores > 0 indicate drug synergy. δ-scores < 0 indicate drug antagonism.

3.5 PRELIMINARY DATA – The expression of human IGF2BP1 induces ATC-like malignancies in a murine two-hit model

The findings, presented in this work, suggested an oncogenic potential for IGF2BP1. However, at present *in vivo* data on IGF2BP1 function are rare (Bell et al., 2013; Degrauwe et al., 2016). Tessier *et al.* identified IGF2BP1 to be pro-oncogenic in mammary epithelial cells of adult female mice upon induction of expression (Tessier et al., 2004). Nonetheless, in mean it took 53 weeks until the animals developed tumors, not resembling rapid growth of highly aggressive cancers. This suggests that IGF2BP1 alone is not sufficient to induce fast growing tumors, which might depend on at least a second genetic hit. It was shown that IGF2BP1 enhances lung tumor growth in synergy with a mutated $Kras^{G12D}$, constitutively being active (Rosenfeld et al., 2019). In consequence, in the here presented study a transgenic mouse model was used to investigate, whether the human IGF2BP1 is able to induce ATC in synergy with a major genetic event of thyroid cancer progression.

Mice were generated harbouring a Tamoxifen-inducible Cre recombinase ($TgCreER^{T2}$) under the control of the thyroglobulin promoter (Undeutsch et al., 2014), as well as a loxP-silenced transgene coding for the human IGF2BP1 and an iRFP for tracing (*LSL-IGF2BP1*). Upon application of Tamoxifen, the Cre/lox-P system specifically facilitates the genetic deletion of an inactivating element within the promoter upstream of the IGF2BP1-coding gene, exclusively in follicular cells of the thyroid (Figure 25A). In a preliminary experiment, three months upon induction (+ Tamoxifen) mice showed a distinct detectable iRFP signal, indicated by the typical butterfly-shape of the thyroid (Figure 25B). Control mice, only receiving vehicle (– Tamoxifen), hardly showed any detectable signal. To further elucidate specificity, thyroid and skeletal muscle-tissue were used for Western blotting. 8305C cell lysate was used as positive control for IGF2BP1 expression (Figure 25C). Upon induction, IGF2BP1 protein expression was only detectable in thyroid tissue lysate. In terms of survival, none of the animals died or revealed a tumor burden so far (Figure 25D). Please note, that the experiment is still in progress.
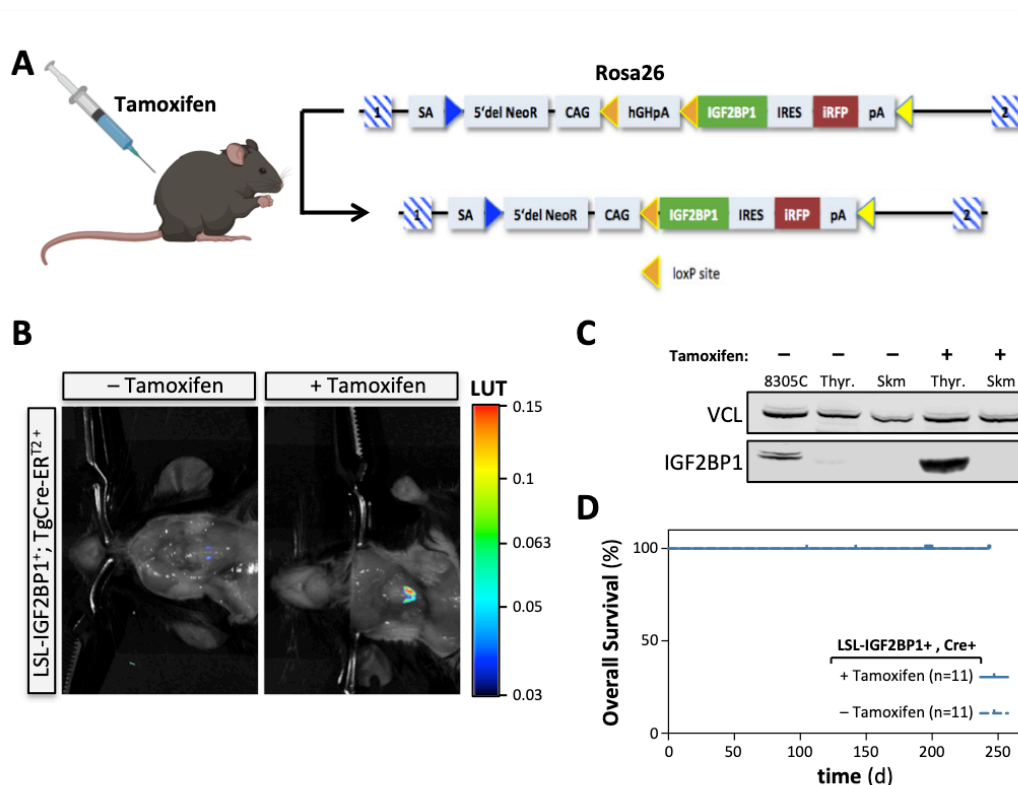
Figure 25. IGF2BP1 expression in transgenic mice is not sufficient for ATC development. **A)** Schematic of the LSL-strategy for co-expressing IGF2BP1 with iRFP. The transgene inserted in the *Rosa26* locus before (upper panel) and after (lower panel) stop cassette (hGHpA) removal by Cre-loxP is indicated with the IGF2BP1 CDS (green), IRES and the iRFP CDS (red). **B)** Near-infrared (iRFP), overlayed with bright field images of mice injected either with vehicle or Tamoxifen (–/+ Tamoxifen, respectively) three months post-induction are shown with identical look up tables (LUT). **C)** Western blot analyses of IGF2BP1 protein in 8305C cells and thyroid or skeletal muscle tissues from mice with or without Tamoxifen injection, as in (B). VCL served as loading control. **D)** Kaplan-Meier survival curves of mice with indicated genotype with or without induction (+/– Tamoxifen).

Intriguingly and in accordance with previous findings (Rosenfeld et al., 2019), the inclusion of a mutated, endogenous and Cre-dependent *Kras* allel (*LSL-Kras^{G12D}*) for thyroid specific co-expression together with IGF2BP1 revealed the development of an ATC-like neoplasia. In median the animals survived for 65 days post-induction, whereas in two of six animals local metastasis could be observed (white arrows; Figure 26A-C). Control mice did not show any tumor burden. A control experiment with mice only harbouring a mutant *Kras* allel, but no IGF2BP1, is in preparation. Nonetheless, previous mouse models, including a mutated *Kras* gene, revealed that this alone never induced an ATC (Kirschner et al., 2016). Next to the comparable clinical presentation of an ATC, RT-qPCR approved molecular characteristics, including the strong decrease of thyroid-specific marker mRNAs Tg, Slc5a5 and

Foxe1 (Figure 26D). The preliminary outcome of the *in vivo* experiments suggested a substantial role of IGF2BP1 in ATC development, dedifferentiation, rapid growth as well as spread into the head-neck region *in vivo*.
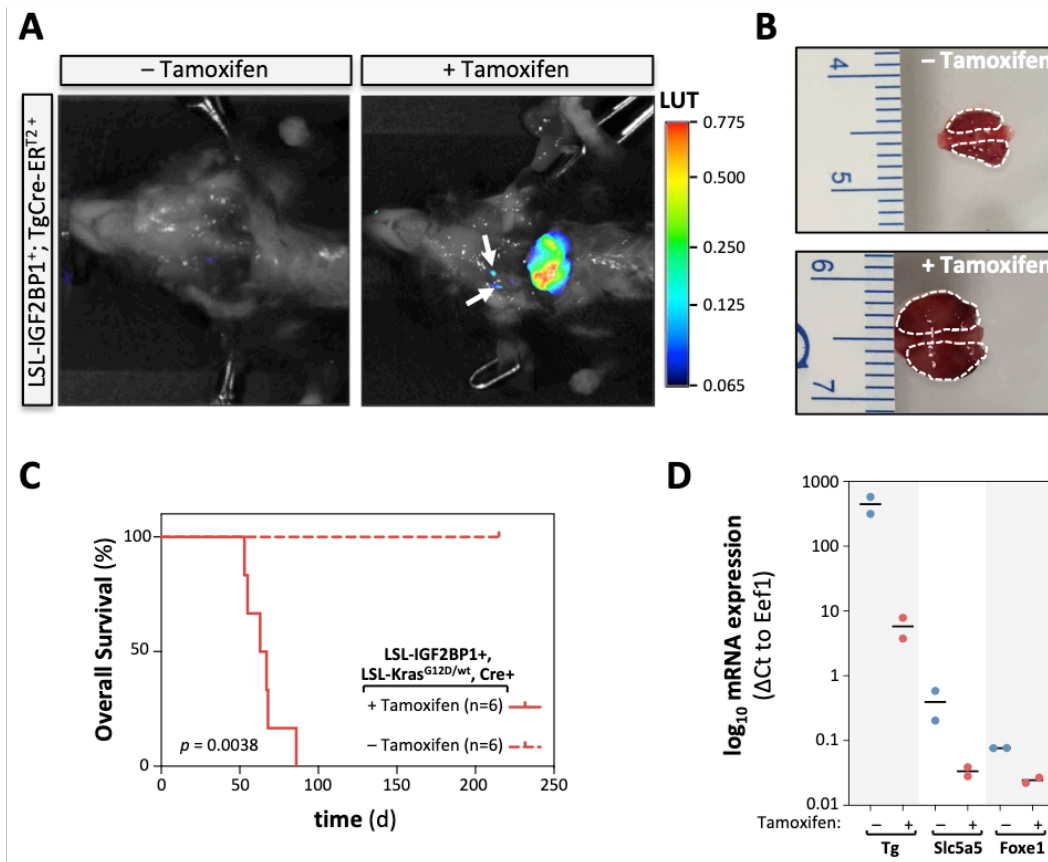
Figure 26. IGF2BP1 expression and Kras^{G12D} induce rapid ATC development in synergy. **A)** Near-infrared (iRFP), overlayed with bright field images of mice injected either with vehicle or Tamoxifen (–/+ Tamoxifen, respectively) are shown with LUTs. White arrows point at sites of local metastasis. **B)** Resected thyroids from mice injected either with vehicle or Tamoxifen (–/+ Tamoxifen, respectively) are shown. Scaling, mm. Dotted lines indicate thyroid lobes. **C)** Kaplan-Meier survival curves of mice with indicated genotype with or without induction (+/– Tamoxifen, respectively). **D)** RT-qPCR analyses of indicated mRNAs in tissues (n = 2 per condition). Statistical significance was determined by log-rank test (C).

4. DISCUSSION

RBPs are essential regulators of RNA metabolism in cancer, hence attracted increasing attention over recent years, including the entire family of IGF2BPs (Bisogno and Keene, 2018; Hattori et al., 2016; Hong, 2017; Pereira et al., 2017; Wurth and Gebauer, 2015). This study investigated the usefulness of the highly selective expression and its role of the oncofetal RBP IGF2BP1 in ATC – from diagnostic value over regulation, impact on pro-oncogenic genes to its potential value in clinical chemotherapy practice.

ATC is the most lethal malignancy of the thyroid, frequently diagnosed solely by exclusion due to the lack of robust positive markers. In contrast to WDTC, ATC are characterized by rapid invasive growth, early metastasis and severe therapy resistance. Therefore, surgery in a limited stage is often the only potentially curative option. Although the majority of patients suffering from ATC are 50 years or older, cohorts from this study included ATC samples from patients at the age of 30 years (Molinaro et al., 2017; Viola et al., 2016). It further stresses the importance of investigating diseases of which usually elder people (like ATC) are affected by.

Aiming at a specific marker-driven approach to improve early ATC diagnosis and reveal novel therapeutic avenues in ATC treatment, comparative RNA-seq analysis of distinct thyroid carcinomas of follicular origin was combined with sWGS and IHC. This revealed robust and exclusive *de novo* expression of the oncofetal RBP IGF2BP1, providing the first positive marker of this malignancy suitable for diagnosis on the mRNA and protein level. In ATC, IGF2BP1 synergizes with upregulated expression of MYC in driving an aggressive tumor cell phenotype, suggesting IGF2BP1 as an m6A-dependent post-transcriptional enhancer of MYC-driven transcription in ATC. This finding provided a rationale for a combinatorial treatment option, further highlighting the need to rapidly investigate the potency of BRDi and IGF2BP1 inhibition as first-line treatments of ATC in clinical settings.

4.1 IGF2BP1 detection is a potentially useful diagnostic tool

ATC is characterized by a severe EMT-like dedifferentiation resulting in a largely therapy resistant malignancy rapidly invading the head-neck region (Kondo et al.,

2006; Smallridge et al., 2012; Tiedje et al., 2017). The comparative analysis of the ATC transcriptome identified a severe epigenetic, transcriptional and post-transcriptional deregulation underlying this disease progression. An observed hallmark of this is the *de novo* expression of testis antigens, including multiple MAGEA family members (see Table 13). These genes are of advanced interest in the focus of immunotherapy and further support the dedifferentiation and gain of stem-like properties observed in ATC. Amongst these genes is MAGEA3 (melanoma-associated antigen 3), which is induced in a variety of metastatic cancers and has been targeted most recently in a phase-II clinical trial (Lu et al., 2017). However, it failed in an extensive phase-III clinical trial in immunotherapy, but could remain as a promising candidate for novel targeted treatment opportunities of ATC (Dreno et al., 2018).

Amongst identified candidate transcripts, the by far smallest variation of expression (rank #1) in ATC was observed for the oncofetal RBP IGF2BP1 suggesting it as an outstanding, potent and robust RNA- as well as protein biomarker distinguishing ATC from NT as well as WDTC. Of note, various oncofetal and stemness-promoting RBPs like IGF2BP3 (but not the paralog IGF2BP2), LIN28B and MSI1 were exclusively upregulated in ATC vs noATC (Hattori et al., 2016). The role of IGF2BP3 essentially remains to be elucidated in continuative analysis. Within the test cohort 100 % of ATC expressed IGF2BP1, detectable at the RNA and protein level, with negligible expression in WDTC or NT. Further, in two independent TMAs IHC analyses demonstrated that the majority of ATC samples were IGF2BP1 positive. This rate likely will be improved by optimizing the sensitivity of immunostaining, since IGF2BP1 mRNA expression was observed in all ATC analyzed by RNA-seq. Some tumors might express only low levels of IGF2BP1, not detectable by automated IHC. However, at present not a single marker of comparable specificity for ATC diagnosis is known in literature. IGF2BP1 also performed well against MAGEA3 and MYC, for which less pronounced intensities were observed in fewer ATC and also some WDTC samples, respectively (Table A1, Appendix; Figure 10). Nonetheless, the protein detection of IGF2BP1, MAGEA3 and MYC appeared to be suitable for the diagnosis of ATC with outstanding DOR. Still, IGF2BP1 revealed by far the strongest consistency.

IGF2BP1-positive ATC samples identified in TMA I showed foci of WDTC/PDTC- or exclusively ATC-content (Table A2, Appendix). Thus, dependency on the disease origin can largely be excluded for IGF2BP1 expression in ATC. Unexpectedly, in TMA I (Figure 10B) a single out of 16 PDTC cores (5.5 %) showing low IGF2BP1 expression was identified, a finding requiring further analyses on extended cohorts. Nevertheless, this study stresses that IGF2BP1 IHC has the potential to help not only defining a diagnosis but also to identify early dedifferentiation in areas of solid histoarchitecture to prevent underestimation of tumor severity. Importantly, because IGF2BP1 is a putative RNA marker in other advance stage cancer subtypes, the here presented detection of protein is significant outside thyroid cancer diagnosis. IGF2BP1 mRNA expression could have a diagnostic and prognostic value in a variety of solid cancers. Accordingly, the here presented validation of the stunning diagnostic value of IGF2BP1 protein expression determined by IHC, provides valuable information beyond the classification of thyroid malignancies.

4.2 IGF2BP1 expression is regulated on the epigenetic and transcriptional level in ATC

Here, sWGS was applied on samples from the test cohort to identify alterations on *IGF2BP1* copy numbers, which was previously observed in other tumors as a central feature of high-grade malignancies (Bell et al., 2015; Doyle et al., 2000). Since costs for sequencing dropped, sWGS has grown into a rising practice for many laboratories to easily monitor gains or losses of genetic regions. This technique likely will replace the almost-outdated array comparative genomic hybridization (aCGH) method due to unrivaled accuracy (Raman et al., 2019). Even though, a samples genome usually is just coverd approx. 0.4-fold times with this technique, the gained information is sufficient to perform robust copy number profiling.

In the here presented study, sWGS demonstrated that the *de novo* expression of IGF2BP1 in ATC cannot be explained by gene gain, as previously observed in other tumors (Bell et al., 2015). Copy numbers of *IGF2BP1* gene locus remained unchanged in 90 % (9/10) amongst ATC samples (Figure 12). Surprisingly, the genetic locus of the MYC oncogene (Chr.8q24.27), showing upregulated mRNA and protein expression in ATC, was also not gained (data not shown), although gain or

amplification of MYC family members is highly correlated with increasing disease severity in other malignancies like neuroblastoma or colorectal cancers (Bell et al., 2015; Lee et al., 2015). But the here presented observation fits previous reports on copy number alterations in ATC (Pozdeyev et al., 2018; Woodward et al., 2017; Yoo et al., 2019). Of note, in one tumor a breakpoint between exon two and three within the *IGF2BP1* locus was detected (Figure 12, sample #5). Whether or not this would be recurrent in other tumors and contributing to IGF2BP1 expression requires further investigation.

Instead of significant copy number alterations, the here presented study strongly suggests that the *de novo* expression of IGF2BP1 could be a consequence of dedifferentiation, associated with a severe epigenetic rearrangement. This essentially involves the upregulation of SETD1A/B, promoting H3K4me3 at various gene *loci*, including *IGF2BP1*. SETD1A/B have barely been reported as oncogenic drivers in cancer unlike other members of the COMPASS family (Joshua and Ali, 2017). This may be due to only few reported mutations in cancer, although mutations of histone methyltransferases in general have been shown in ~25% of ATC (Fagin and Wells, 2016). Even though huge efforts are being made on establishing epigenetic therapy options, no clinically evaluated options for STED1A/B inhibition are available, so far. Current clinical trials for solid and hematologic malignancies commonly rely on inhibiting DNA-methyltransferase activity or the polycomb-repressive complex 2 (in particular EZH2 inhibition). More progressive approaches in terms of epigenetic therapies are currently being tested in pre-clinical settings, including CRISPR/Cas9-mediated suppression of activating histone marks at specific loci or large stretches of chromatin, potentially helping in the near future. But transitioning to the clinics will require considerable innovation (Michalak et al., 2019). Interestingly, via RNAseq of the test cohort samples a third histone methyltransferase, namely DOT1L (data not shown), facilitating H3K79me1, 2, 3, has been identified as significantly upregulated. DOT1L expression strongly correlates with advanced disease, shown for breast cancer and AML. Recent studies led to promising phaseI/II clinical trials (Michalak et al., 2019; Nassa et al., 2019). It was surprising, that direct inhibition with several direct DOT1L-targeting small molecules, as well as siRNA-mediated depletions did

not affect viability or H3K79 methylation of ATC-derived cells (data not shown), requiring further investigation.

The here presented study demonstrated that an interplay of epigenetic dependency of promoter accessibility, together with MYC upregulation as an hallmark of ATC, likely drives IGF2BP1 synthesis. In this respect, MYC is able to specifically bind within a comparably long CpG island region of approx. 3 kb in length to drive transcription (Figure 14A) (Consortium, 2012). According to Mikkelsen et al. and Meissner et al., promoters with high CpG content are more likely to be relevant for early developmental stages and therefore must be controlled in a tighter fashion (Meissner et al., 2008; Mikkelsen et al., 2007). The dependency on a stem cell-like epigenetic environment and a comparably long CpG island that facilitates specificity for one of the major oncogenes, namely MYC, further supports the hypothesis of IGF2BP1 as an oncofetal RBP (Bell et al., 2013).

4.3 IGF2BP1 is an enhancer of an oncogene-driven gene expression signature

In ATC, IGF2BP1 and MYC expression strongly correlate, further suggesting a feedback-loop mechanism leading to a pro-oncogenic synergy of MYC-dependent transcription and post-transcriptional enhancement by IGF2BP1 in an m6A-dependent manner. Of note, across all TCGA-cancer cohorts no conservation of associated MYC and IGF2BP1 expression was observed, but for ATC, making this malignancy a paragon for MYC/IGF2BP1-driven tumorigenesis.

A synergy was evidenced by the conserved association of MYC/IGF2BP1-driven genes with poor prognosis in solid cancers, including three novel MYC-driven target transcripts of IGF2BP1: AURKB, RRM2 and LIMK1. Noteworthy, they are reported miRNA targets, suggesting that IGF2BP1 interferes with AURKB, RRM2 and LIMK1 mRNA degradation in a miRNA-dependent manner, a main and conserved role of this protein in cancer cells (Chang et al., 2018; Chen et al., 2014; Maki-Jouppila et al., 2015; Muller et al., 2018). Nonetheless, investigation on miRNA-dependency was not part of this study. Interestingly, the enhancement of the novel IGF2BP1 downstream targets is supported by the conserved occurrence of m6A, a major

observation of this study. This contributes to the mechanistic understanding of the rather controversial, but general pro-oncogenic role of the METTL3/14/WTAP complex in human cancers, as the observed decrease of cell viability in ATC-derived cells deleted for METTL3 supports an "oncogenic" role (Lan et al., 2019). In agreement with recent studies, IGF2BP1 modulates a transcripts fate as m6A-reading protein (Huang et al., 2018a). Importantly, upon METTL3 deletion in C643 cells, IGF2BP1 expression essentially remained unchanged. This indicated a role of IGF2BP1 as active reader, which is unaffected by the mechanism itself. Choosing to target the m6A-writing complex, upstream of IGF2BPs, represents a seemingly legit rationale for therapy options. Efforts are being made on developing writer-specific inhibitors, in particular against METTL3 for clinical practice to treat several solid and hematologic malignancies (Cully, 2019). Nonetheless, m6A should not be seen as an oncofetal occurrence like IGF2BP1/3, HuR or LIN28A/B expression (Hattori et al., 2016; Pereira et al., 2017). M6A maintains an equilibrium between pluripotency and differentiation and thus, its depletion will most likely not only impact on growth-promoting factors, but could also affect hematopoiesis or adult neurogenesis (Zhao and He, 2015). Thus, targeted inhibition of m6A readers should be the preferred tool of choice.

Only as tip of the iceberg, AURKB, RRM2 and LIMK1 exemplify the impact of IGF2BP1 on the hallmarks of cancer (Hanahan and Weinberg, 2011). Importantly, AURKB and RRM2 were considered candidate targets in clinical trial studies already, as both represent essential factors for molecular pathways a cancer cell heavily relies on. In particular, aurora-kinase targeting has been intensified during the last decade for several malignancies. However, not a single compound exceeded clinical trial phase 2 (Tang et al., 2017). In recent years, research on RRM2 has been intensified for a good reason: Like AURKB, its expression in cancers strongly correlates with very poor prognosis (Cancer Genome Atlas Research et al., 2013). Surprisingly, in the here presented study siRNA-mediated depletion of RRM2, compared to AURKB or LIMK1, revealed the most severe effects on analysed phenotypes (Figure 18). Hence, a cancer cell is probably more likely able to deal with inaccurate cell division (due to a loss of AURKB or LIMK1), rather than with replicative stress due to an imbalance between ribonucleotide- and

desoxyribonucleotide availability. Thus, a clinical trial study on RRM2 targeting with the specific inhibitor COH29 in several solid malignancies started in 2016 (NCT02112565). Further studies showed promising results in recent preclinical studies on other entities like prostate cancer, with excellent efficacy for COH29 (Mazzu et al., 2019). The third downstream effector, LIMK1, is a centrally positioned regulator of actin cytoskeleton dynamics, thus required for invasion. Next to its influence on the generation of actin microfilaments it also affects microtubule formation. Thus, it is not only implicated in cell migration and shaping, but also in cell cycle progression, potentially explaining observed effects in cell viability assays upon LIMK1 depletion in this study. Although multiple LIMK1/2 targeting inhibitors have been developed, studies on the impact of these compounds on cancer cell phenotypes remain sparse and are exclusively pre-clinical (Scott et al., 2010).

In agreement, combining the impaired regulation of AURKB, RRM2, LIMK1 and many additional pro-oncogenic transcripts by IGF2BP1 or MYC depletion, suggests a novel therapy option hitting multiple hallmarks of cancer at once, like a bare "Achilles' heel". This could be either achieved by single compound treatments targeting MYC or IGF2BP1, but also in combination. This study provides a rational for a unique treatment of ATC. Importantly, this option would be completely independent of the mutational landscape and thus, could contribute to the necessity of timely decisions.

4.4 The IGF2BP1/MYC-interplay represents an exploitable "Achille's heel"

Despite many efforts, only very few chemotherapeutic agents affecting ATC growth have yet produced clinically significant results (Molinaro et al., 2017). Recently, the FDA approved the combined appliance of BRAF^{V600E}-targeting dabrafenib, a tyrosine kinase inhibitor, and MEK1/2-targeting trametinib for advanced BRAF^{V600E}-positive ATC. Although response was comparably high, the overall survival was not significantly improved (Subbiah et al., 2018). Unfortunately, this treatment option excludes a substantial number of patients, being BRAF^{V600E}-negative, although BRAF mutations are detected in approx. 47 % of ATC cases (Molinaro et al., 2017). To date, tyrosine kinase inhibitors, including dabrafenib, are promising objects of ongoing research and clinical trials. Thus, still novel treatment modalities have to be

found. An emerging field to overcome this is called pharmacotranscriptomics, as the RNA-phenotype, bridging genotype and phenotype, raised awareness over recent years (Barrie et al., 2012). The here presented study is one of the very few ones using ATC transcriptome information to assess therapy options.

The pivotal role of MYC-driven gene expression, accompanied by the substantial upregulation of BRD3/4/T could be detected via RNA-seq. BRDs are co-activators of MYC, emphasizing to consider BRDi as potent first-line inhibitors of rapid invasive growth of ATC (Delmore et al., 2011). Besides the currently investigated tyrosine kinase inhibitors, BRDis are amongst novel therapy options being investigated for ATC at present (Enomoto et al., 2017; Zhu et al., 2019). Here, highly selective BETi, other than JQ1 not being suitable for patient application (Trabucco et al., 2015), and PROTAC-based BETd have been found to effectively target a MYC/IGF2BP1-driven gene expression in a conserved manner in ATC-derived cell lines (Figures 21-23). Interestingly, all tested compounds revealed EC_{50} exclusively within the nM-range and efficacies beyond 0.5 in three different ATC-derived cell lines. This indicated a general applicability across the tested compounds and a high vulnerability to these.

Importantly, IGF2BP1 was suggested as a key effector of the BRDi JQ1 and implicated in modulating resistance to BETi (Rathert et al., 2015). Upon testing a combinatorial approach of the highly effective and potent BETi ABBV-075 with the, so far not clinically evaluated, IGF2BP1-inhibitor BTYNB proofed the synergy between MYC and IGF2BP1 and likewise unveiled an "Achilles' Heel". Thus, the pivotal role of MYC/IGF2BP1-driven gene expression in ATC suggested a progressive option as promising and rapidly translatable adjuvant first line treatment for effective impairment of tumor growth. This could provide the required gain of time to successfully implement other targeted therapies, in particular MAGEA3-directed T-cell receptor targeting immunotherapies. Such strategies were recently evaluated in a phase-II clinical trial (Lu et al., 2017). The findings indicate ATC as a prime disease for further evaluation of MAGEA3-directed immunotherapies. Notably, beyond first-line treatment options, BETi could prove beneficial for immunotherapies due to enhanced T-cell persistence and validated efficacy in other combinatorial immunotherapy approaches (Joshi and Durden, 2019; Lai et al., 2018). Finally, in view of its sharp upregulation and oncogenic potential in ATC, the here presented

study strongly suggests expediting the clinical evaluation and improvement of IGF2BP1-directed inhibitors in cancer therapy.

4.5 IGF2BP1 is capable of inducing ATC-like malignancies in a two-hit model

The role of IGF2BP1 in cancer progression, metastasis/invasion and proliferation has been frequently investigated (Degrauwe et al., 2016). Nonetheless, *in vivo* analyses remain sparse. In agreement with the here presented data and previous *in vitro*- and xenograft studies (Muller et al., 2018), the few transgenic mouse models for IGF2BPs only present evidence for IGF2BP1 to induce cancers. Thus, the expression of the human IGF2BP1 led to primary breast cancer lesions as well as metastasis in mice after approx. one year (Tessier et al., 2004). In contrast, a loss of Igf2bp1 is proposed to support carcinogenesis of the intestine *in vivo* (Chatterji et al., 2018). The IGF2BP1-homolog IGF2BP3 did not induce tumor formation in pancreas upon overexpression, but may drive a post-transcriptional program active during pancreas development, but also during hematopoiesis (Palanichamy et al., 2016; Wagner et al., 2003). Consistently, a transient depletion of IGF2BP3 in ATC-derived cells did not negatively alter proliferation or anoikis resistance (data not shown), although it is significantly upregulated in this malignancy. This is supported by *in vitro* studies of other cancer entities (Muller et al., 2018). Interestingly, recently it was shown that IGF2BP2-KO mice seem to be protected from carcinogenesis to a certain degree, but yet IGF2BP2 is not described as pro-oncogenic in mice with transgenic overexpression and the protein is rather implicated in adipogenesis (Dai et al., 2015). Although *in vivo* versus *in vitro* evidence for all three IGF2BP family members can be seen as rather conflicting, depending on the cancer type being investigated, a very recent finding on IGF2BP1-dependent severity of lung adenocarcinoma was shown in synergy with the common $Kras^{G12D}$ mutation (Rosenfeld et al., 2019). As Raf/Ras-mutations are frequently observed cancer inducing events in thyroid follicular cells, it emphasized to further investigate the role of the human IGF2BP1 in ATC in a two-hit model with $Kras^{G12D}$ *in vivo* (Fagin and Wells, 2016). Please note, that only preliminary data is presented in this study.

The transgene activation was highly specific for the thyroid, indicated by a localized detectable iRFP signal (Figure 25). Further, a comparison of thyroid tissue with skeletal muscle tissue upon vehicle or Tamoxifen application proved the observation of specific and high IGF2BP1 expression. Of note: Thyroid tissue from –Tamoxifen mice essentially remained IGF2BP1-negative, but a completely silenced transgene could not be excluded from the Western blotting analysis. Irrespectively, none of the +Tamoxifen animals showed significant phenotypic changes to –Tamoxifen animals. The here presented findings were expected, as it was previously reported that in mean approx. after one year tumors will be developed upon IGF2BP1 overexpression in mammary tissues (Tessier et al., 2004). At present, the experiments for the here presented *in vivo* data are not completed and experiments with *Kras*^{G12D}-only mice are in preparation. It is likely, that these animals will not develop tumors, as previously reported (Kirschner et al., 2016).

However, the inclusion of a mutated *Kras* allel, together with IGF2BP1 expression, revealed a dramatic shift in phenotype, confirming the previously reported findings in lung adenocarcinoma (Rosenfeld et al., 2019). Kras^{G12D} represents a constitutively active small GTPase and thus, sustains MAP-kinase signaling and other pathways. These cascades promote several hallmarks of cancer (Schubbert et al., 2007). Interestingly, the observed phenotype presented here was clearly ATC-like, including rapid growth, spread to the head-neck region and a typical gene expression pattern. Nonetheless, histological and whole-transcriptome anaylsis remain to be performed.

The finding raised at least three questions for speculation in terms of thyroid carcinoma progression and IGF2BP1: **1)** *Is IGF2BP1 the consequence of the accumulated mutational burden?* The ATC is exclusively driven by at least two genetic hits and most likely derives from WDTC/PDTC (Molinaro et al., 2017). As it was previously shown that Kras^{G12D} in a single-hit model is not capable of inducing any ATC *in vivo*, it likely suggests that IGF2BP1 *de novo* expression is exclusively a consequence of the second (or later) hit. This could be supported by the fact, that a Kras^{G12D}/P53-KO model in turn develops ATC, but also WDTC (Kirschner et al., 2016). Thus, it would be of great interest if a P53-KO with IGF2BP1 overexpression could drive ATC induction. **2)** *Does the Kras^{G12D}/IGF2BP1 model develop WDTC-independent ATC?* The rapid progression to an ATC-like malignancy in the here presented study is comparably fast. The minimal time from induction to a fully-grown

ATC in any other thyroid carcinoma mouse model described lasted at least three months (Kirschner et al., 2016). This could potentially indicate that this mouse model represents a WDTC/PDTC-independent development of ATC. **3)** *Is IGF2BP1 an oncogene?* The here presented data could finally suggest IGF2BP1 as an oncogenic driver if future efforts prove that IGF2BP1 can substitute a P53-KO from a previous double-hit mouse model.

Lastly, if an ATC-like histology is proven, this mouse model will be of great interest for the first *in vivo* study on direct IGF2BP1 inhibition *in vivo*. This could represent a turning point for one of the most fatal malignancies, the ATC.

5. SUMMARY

The anaplastic thyroid carcinoma (ATC) is by far the most lethal malignancy of the thyroid. No robust positive markers are available, leaving ATC difficult to distinguish from other malignancies of the thyroid without any appropriate treatment so far.

The here presented findings provide IGF2BP1 as the first positive marker for ATC diagnosis by combining comparative RNA-seq, shallow Whole Genome-seq and immunohistochemistry. Among all samples from three independent cohorts, 75% ATC samples expressed IGF2BP1 protein, whereas only one of > 200 less aggressive thyroid carcinoma samples and no non-malignant thyroid tissues were tested positive.

Here, a novel mechanism got presented: the post-transcriptional enhancement of a MYC-driven gene expression signature by IGF2BP1, comprising approx. 1,000 mRNAs, including AURKB, RRM2 and LIMK1. They contribute to a proliferative and invasive ATC tumor cell phenotype *in vivo* and *in vitro*. Likewise, they unveil an "Achille's heel" for a combinatorial therapy approach of BET/IGF2BP1-targeting, improving impairment of cell proliferation in synergy. The study provides the first evidence for superior efficacy of the BET-inhibitor ABBV-075 and the IGF2BP1-directed inhibitor BTYNB in ATC-derived cells. This approach with superior effectiveness could prove as first-line treatment, independent of any mutational status, to gain time for immunotherapies. Lastly, preliminary data suggests IGF2BP1 to have oncogenic potential *in vivo*, and raises several novel hypotheses to test in future.

The here presented findings will improve on current techniques for ATC diagnosis and could be adopted for general cancer pathology routine. Furthermore, this study provides a rationale for a novel first-line treatment option of this therapy-resistant malignancy, applicable for other solid and hematologic malignancies.

6. REFERENCES

Alqahtani, A., Choucair, K., Ashraf, M., Hammouda, D. M., Alloghbi, A., Khan, T., Senzer, N., and Nemunaitis, J. (2019). Bromodomain and extra-terminal motif inhibitors: a review of preclinical and clinical advances in cancer therapy. Future Sci OA *5*, FSO372.

Are, C., and Shaha, A. R. (2006). Anaplastic thyroid carcinoma: biology, pathogenesis, prognostic factors, and treatment approaches. Ann Surg Oncol *13*, 453-464.

Audic, Y., and Hartley, R. S. (2004). Post-transcriptional regulation in cancer. Biol Cell *96*, 479-498.

Aye, Y., Li, M., Long, M. J., and Weiss, R. S. (2015). Ribonucleotide reductase and cancer: biological mechanisms and targeted therapies. Oncogene *34*, 2011-2021.

Bakheet, T., Hitti, E., Al-Saif, M., Moghrabi, W. N., and Khabar, K. S. A. (2018). The AU-rich element landscape across human transcriptome reveals a large proportion in introns and regulation by ELAVL1/HuR. Biochim Biophys Acta Gene Regul Mech *1861*, 167-177.

Barrie, E. S., Smith, R. M., Sanford, J. C., and Sadee, W. (2012). mRNA transcript diversity creates new opportunities for pharmacological intervention. Mol Pharmacol *81*, 620-630.

Beachy, S. H., Onozawa, M., Chung, Y. J., Slape, C., Bilke, S., Francis, P., Pineda, M., Walker, R. L., Meltzer, P., and Aplan, P. D. (2012). Enforced expression of Lin28b leads to impaired T-cell development, release of inflammatory cytokines, and peripheral T-cell lymphoma. Blood *120*, 1048-1059.

Bell, J. L., Turlapati, R., Liu, T., Schulte, J. H., and Huttelmaier, S. (2015). IGF2BP1 harbors prognostic significance by gene gain and diverse expression in neuroblastoma. J Clin Oncol *33*, 1285-1293.

Bell, J. L., Wachter, K., Muhleck, B., Pazaitis, N., Kohn, M., Lederer, M., and Huttelmaier, S. (2013). Insulin-like growth factor 2 mRNA-binding proteins (IGF2BPs): post-transcriptional drivers of cancer progression? Cell Mol Life Sci *70*, 2657-2675.

Bhagwat, A. S., and Vakoc, C. R. (2015). Targeting Transcription Factors in Cancer. Trends Cancer *1*, 53-65.

Bisogno, L. S., and Keene, J. D. (2018). RNA regulons in cancer and inflammation. Curr Opin Genet Dev *48*, 97-103.

Boron, W. F., and Boulpaep, E. L. (2012). Medical physiology : a cellular and molecular approach, Updated second edition. edn (Philadelphia, PA: Saunders/Elsevier).

Boylan, K. L., Mische, S., Li, M., Marques, G., Morin, X., Chia, W., and Hays, T. S. (2008). Motility screen identifies Drosophila IGF-II mRNA-binding protein--zipcode-binding protein acting in oogenesis and synaptogenesis. PLoS Genet *4*, e36.

Bradner, J. E., Hnisz, D., and Young, R. A. (2017). Transcriptional Addiction in Cancer. Cell *168*, 629-643.

Braun, J., Hoang-Vu, C., Dralle, H., and Huttelmaier, S. (2010). Downregulation of microRNAs directs the EMT and invasive potential of anaplastic thyroid carcinomas. Oncogene *29*, 4237-4244.

Bui, M. H., Lin, X., Albert, D. H., Li, L., Lam, L. T., Faivre, E. J., Warder, S. E., Huang, X., Wilcox, D., Donawho, C. K., *et al.* (2017). Preclinical Characterization of BET Family Bromodomain Inhibitor ABBV-075 Suggests Combination Therapeutic Strategies. Cancer Res *77*, 2976-2989.

Burman, K. D. (2014). Is poorly differentiated thyroid cancer poorly characterized? J Clin Endocrinol Metab *99*, 1167-1169.

Busch, B., Bley, N., Muller, S., Glass, M., Misiak, D., Lederer, M., Vetter, M., Strauss, H. G., Thomssen, C., and Huttelmaier, S. (2016). The oncogenic triangle of HMGA2, LIN28B and IGF2BP1 antagonizes tumor-suppressive actions of the let-7 family. Nucleic Acids Res *44*, 3845-3864.

Cabanillas, M. E., Zafereo, M., Gunn, G. B., and Ferrarotto, R. (2016). Anaplastic Thyroid Carcinoma: Treatment in the Age of Molecular Targeted Therapy. J Oncol Pract *12*, 511-518.

Cancer Genome Atlas Research, N. (2014). Integrated genomic characterization of papillary thyroid carcinoma. Cell *159*, 676-690.

Cancer Genome Atlas Research, N., Weinstein, J. N., Collisson, E. A., Mills, G. B., Shaw, K. R., Ozenberger, B. A., Ellrott, K., Shmulevich, I., Sander, C., and Stuart, J. M. (2013). The Cancer Genome Atlas Pan-Cancer analysis project. Nat Genet *45*, 1113-1120.

Cao, J., Mu, Q., and Huang, H. (2018). The Roles of Insulin-Like Growth Factor 2 mRNA-Binding Protein 2 in Cancer and Cancer Stem Cells. Stem Cells Int *2018*, 4217259.

Cardis, E., Kesminiene, A., Ivanov, V., Malakhova, I., Shibata, Y., Khrouch, V., Drozdovitch, V., Maceika, E., Zvonova, I., Vlassov, O., *et al.* (2005). Risk of thyroid cancer after exposure to 131I in childhood. J Natl Cancer Inst *97*, 724-732.

Carey, M. F., Peterson, C. L., and Smale, S. T. (2009). Chromatin immunoprecipitation (ChIP). Cold Spring Harb Protoc *2009*, pdb prot5279.

Carina, V., Zito, G., Pizzolanti, G., Richiusa, P., Criscimanna, A., Rodolico, V., Tomasello, L., Pitrone, M., Arancio, W., and Giordano, C. (2013). Multiple pluripotent stem cell markers in human anaplastic thyroid cancer: the putative upstream role of SOX2. Thyroid *23*, 829-837.

Chang, C. C., Lin, C. C., Wang, C. H., Huang, C. C., Ke, T. W., Wei, P. L., Yeh, K. T., Hsu, K. C., Hsu, N. Y., and Cheng, Y. W. (2018). miR-211 regulates the expression of RRM2 in tumoral metastasis and recurrence in colorectal cancer patients with a k-ras gene mutation. Oncol Lett *15*, 8107-8117.

Chao, J. A., Patskovsky, Y., Patel, V., Levy, M., Almo, S. C., and Singer, R. H. (2010). ZBP1 recognition of beta-actin zipcode induces RNA looping. Genes Dev *24*, 148-158.

Chatterji, P., Hamilton, K. E., Liang, S., Andres, S. F., Wijeratne, H. R. S., Mizuno, R., Simon, L. A., Hicks, P. D., Foley, S. W., Pitarresi, J. R., *et al.* (2018). The LIN28B-IMP1 post-transcriptional regulon has opposing effects on oncogenic signaling in the intestine. Genes Dev *32*, 1020-1034.

Chen, H., Liu, H., and Qing, G. (2018). Targeting oncogenic Myc as a strategy for cancer treatment. Signal Transduct Target Ther *3*, 5.

Chen, P., Zeng, M., Zhao, Y., and Fang, X. (2014). Upregulation of Limk1 caused by microRNA-138 loss aggravates the metastasis of ovarian cancer by activation of Limk1/cofilin signaling. Oncol Rep *32*, 2070-2076.

Consortium, E. P. (2012). An integrated encyclopedia of DNA elements in the human genome. Nature *489*, 57-74.

Conway, A. E., Van Nostrand, E. L., Pratt, G. A., Aigner, S., Wilbert, M. L., Sundararaman, B., Freese, P., Lambert, N. J., Sathe, S., Liang, T. Y.*, et al.* (2016). Enhanced CLIP Uncovers IMP Protein-RNA Targets in Human Pluripotent Stem Cells Important for Cell Adhesion and Survival. Cell Rep *15*, 666-679.

Cully, M. (2019). Chemical inhibitors make their RNA epigenetic mark. Nat Rev Drug Discov *18*, 892-894.

da Silva, V. L., Fonseca, A. F., Fonseca, M., da Silva, T. E., Coelho, A. C., Kroll, J. E., de Souza, J. E. S., Stransky, B., de Souza, G. A., and de Souza, S. J. (2017). Genome-wide identification of cancer/testis genes and their association with prognosis in a pan-cancer analysis. Oncotarget *8*, 92966-92977.

Dai, N., Christiansen, J., Nielsen, F. C., and Avruch, J. (2013). mTOR complex 2 phosphorylates IMP1 cotranslationally to promote IGF2 production and the proliferation of mouse embryonic fibroblasts. Genes Dev *27*, 301-312.

Dai, N., Zhao, L., Wrighting, D., Kramer, D., Majithia, A., Wang, Y., Cracan, V., Borges-Rivera, D., Mootha, V. K., Nahrendorf, M.*, et al.* (2015). IGF2BP2/IMP2-Deficient mice resist obesity through enhanced translation of Ucp1 mRNA and Other mRNAs encoding mitochondrial proteins. Cell Metab *21*, 609-621.

Dani, C., Blanchard, J. M., Piechaczyk, M., El Sabouty, S., Marty, L., and Jeanteur, P. (1984). Extreme instability of myc mRNA in normal and transformed human cells. Proc Natl Acad Sci U S A *81*, 7046-7050.

Degrauwe, N., Suva, M. L., Janiszewska, M., Riggi, N., and Stamenkovic, I. (2016). IMPs: an RNA-binding protein family that provides a link between stem cell maintenance in normal development and cancer. Genes Dev *30*, 2459-2474.

Delmore, J. E., Issa, G. C., Lemieux, M. E., Rahl, P. B., Shi, J., Jacobs, H. M., Kastritis, E., Gilpatrick, T., Paranal, R. M., Qi, J.*, et al.* (2011). BET bromodomain inhibition as a therapeutic strategy to target c-Myc. Cell *146*, 904-917.

Dettmer, M., Schmitt, A., Steinert, H., Haldemann, A., Meili, A., Moch, H., Komminoth, P., and Perren, A. (2011). Poorly differentiated thyroid carcinomas: how much poorly differentiated is needed? Am J Surg Pathol *35*, 1866-1872.

Disney, M. D., Dwyer, B. G., and Childs-Disney, J. L. (2018). Drugging the RNA World. Cold Spring Harb Perspect Biol *10*.

Doyle, G. A., Bourdeau-Heller, J. M., Coulthard, S., Meisner, L. F., and Ross, J. (2000). Amplification in human breast cancer of a gene encoding a c-myc mRNA-binding protein. Cancer Res *60*, 2756-2759.

Dreno, B., Thompson, J. F., Smithers, B. M., Santinami, M., Jouary, T., Gutzmer, R., Levchenko, E., Rutkowski, P., Grob, J. J., Korovin, S.*, et al.* (2018). MAGE-A3 immunotherapeutic as adjuvant therapy for patients with resected, MAGE-A3-positive, stage III melanoma (DERMA): a double-blind, randomised, placebo-controlled, phase 3 trial. Lancet Oncol *19*, 916-929.

Enomoto, K., Zhu, X., Park, S., Zhao, L., Zhu, Y. J., Willingham, M. C., Qi, J., Copland, J. A., Meltzer, P., and Cheng, S. Y. (2017). Targeting MYC as a Therapeutic Intervention for Anaplastic Thyroid Cancer. J Clin Endocrinol Metab *102*, 2268-2280.

Eom, T., Antar, L. N., Singer, R. H., and Bassell, G. J. (2003). Localization of a beta-actin messenger ribonucleoprotein complex with zipcode-binding protein

modulates the density of dendritic filopodia and filopodial synapses. J Neurosci *23*, 10433-10444.

Esteller, M. (2002). CpG island hypermethylation and tumor suppressor genes: a booming present, a brighter future. Oncogene *21*, 5427-5440.

Fagin, J. A., and Wells, S. A., Jr. (2016). Biologic and Clinical Perspectives on Thyroid Cancer. N Engl J Med *375*, 1054-1067.

Fakhraldeen, S. A., Clark, R. J., Roopra, A., Chin, E. N., Huang, W., Castorino, J., Wisinski, K. B., Kim, T., Spiegelman, V. S., and Alexander, C. M. (2015). Two Isoforms of the RNA Binding Protein, Coding Region Determinant-binding Protein (CRD-BP/IGF2BP1), Are Expressed in Breast Epithelium and Support Clonogenic Growth of Breast Tumor Cells. J Biol Chem *290*, 13386-13400.

Farina, K. L., Huttelmaier, S., Musunuru, K., Darnell, R., and Singer, R. H. (2003). Two ZBP1 KH domains facilitate beta-actin mRNA localization, granule formation, and cytoskeletal attachment. J Cell Biol *160*, 77-87.

Ferlay, J., Colombet, M., Soerjomataram, I., Mathers, C., Parkin, D. M., Pineros, M., Znaor, A., and Bray, F. (2019). Estimating the global cancer incidence and mortality in 2018: GLOBOCAN sources and methods. Int J Cancer *144*, 1941-1953.

Fortis, S. P., Anastasopoulou, E. A., Voutsas, I. F., Baxevanis, C. N., Perez, S. A., and Mahaira, L. G. (2017). Potential Prognostic Molecular Signatures in a Preclinical Model of Melanoma. Anticancer Res *37*, 143-148.

Fox, R. G., Park, F. D., Koechlein, C. S., Kritzik, M., and Reya, T. (2015). Musashi signaling in stem cells and cancer. Annu Rev Cell Dev Biol *31*, 249-267.

Furukawa, K., Preston, D., Funamoto, S., Yonehara, S., Ito, M., Tokuoka, S., Sugiyama, H., Soda, M., Ozasa, K., and Mabuchi, K. (2013). Long-term trend of thyroid cancer risk among Japanese atomic-bomb survivors: 60 years after exposure. Int J Cancer *132*, 1222-1226.

Gangolli, S. D., van den Brandt, P. A., Feron, V. J., Janzowsky, C., Koeman, J. H., Speijers, G. J., Spiegelhalder, B., Walker, R., and Wisnok, J. S. (1994). Nitrate, nitrite and N-nitroso compounds. Eur J Pharmacol *292*, 1-38.

Gao, J., Aksoy, B. A., Dogrusoz, U., Dresdner, G., Gross, B., Sumer, S. O., Sun, Y., Jacobsen, A., Sinha, R., Larsson, E.*, et al.* (2013). Integrative analysis of complex cancer genomics and clinical profiles using the cBioPortal. Sci Signal *6*, pl1.

Garneau, N. L., Wilusz, J., and Wilusz, C. J. (2007). The highways and byways of mRNA decay. Nat Rev Mol Cell Biol *8*, 113-126.

Gehring, N. H., Wahle, E., and Fischer, U. (2017). Deciphering the mRNP Code: RNA-Bound Determinants of Post-Transcriptional Gene Regulation. Trends Biochem Sci *42*, 369-382.

Gerstberger, S., Hafner, M., and Tuschl, T. (2014). A census of human RNA-binding proteins. Nat Rev Genet *15*, 829-845.

Glas, A. S., Lijmer, J. G., Prins, M. H., Bonsel, G. J., and Bossuyt, P. M. (2003). The diagnostic odds ratio: a single indicator of test performance. J Clin Epidemiol *56*, 1129-1135.

Gress, T. M., Muller-Pillasch, F., Geng, M., Zimmerhackl, F., Zehetner, G., Friess, H., Buchler, M., Adler, G., and Lehrach, H. (1996). A pancreatic cancer-specific expression profile. Oncogene *13*, 1819-1830.

Gu, W., Wells, A. L., Pan, F., and Singer, R. H. (2008). Feedback regulation between zipcode binding protein 1 and beta-catenin mRNAs in breast cancer cells. Mol Cell Biol *28*, 4963-4974.

Guo, Z., Hardin, H., and Lloyd, R. V. (2014). Cancer stem-like cells and thyroid cancer. Endocr Relat Cancer *21*, T285-300.

Gutschner, T., Hammerle, M., Pazaitis, N., Bley, N., Fiskin, E., Uckelmann, H., Heim, A., Grobeta, M., Hofmann, N., Geffers, R.*, et al.* (2014). Insulin-like growth factor 2 mRNA-binding protein 1 (IGF2BP1) is an important protumorigenic factor in hepatocellular carcinoma. Hepatology *59*, 1900-1911.

Hafner, M., Landthaler, M., Burger, L., Khorshid, M., Hausser, J., Berninger, P., Rothballer, A., Ascano, M., Jr., Jungkamp, A. C., Munschauer, M.*, et al.* (2010). Transcriptome-wide identification of RNA-binding protein and microRNA target sites by PAR-CLIP. Cell *141*, 129-141.

Hammerle, M., Gutschner, T., Uckelmann, H., Ozgur, S., Fiskin, E., Gross, M., Skawran, B., Geffers, R., Longerich, T., Breuhahn, K.*, et al.* (2013). Posttranscriptional destabilization of the liver-specific long noncoding RNA HULC by the IGF2 mRNA-binding protein 1 (IGF2BP1). Hepatology *58*, 1703-1712.

Hanahan, D., and Weinberg, R. A. (2000). The hallmarks of cancer. Cell *100*, 57-70.

Hanahan, D., and Weinberg, R. A. (2011). Hallmarks of cancer: the next generation. Cell *144*, 646-674.

Hansen, T. V., Hammer, N. A., Nielsen, J., Madsen, M., Dalbaeck, C., Wewer, U. M., Christiansen, J., and Nielsen, F. C. (2004). Dwarfism and impaired gut development in insulin-like growth factor II mRNA-binding protein 1-deficient mice. Mol Cell Biol *24*, 4448-4464.

Harris, T. J., and McCormick, F. (2010). The molecular pathology of cancer. Nat Rev Clin Oncol *7*, 251-265.

Hattori, A., Buac, K., and Ito, T. (2016). Regulation of Stem Cell Self-Renewal and Oncogenesis by RNA-Binding Proteins. Adv Exp Med Biol *907*, 153-188.

Haugen, B. R., Alexander, E. K., Bible, K. C., Doherty, G. M., Mandel, S. J., Nikiforov, Y. E., Pacini, F., Randolph, G. W., Sawka, A. M., Schlumberger, M.*, et al.* (2016). 2015 American Thyroid Association Management Guidelines for Adult Patients with Thyroid Nodules and Differentiated Thyroid Cancer: The American Thyroid Association Guidelines Task Force on Thyroid Nodules and Differentiated Thyroid Cancer. Thyroid *26*, 1-133.

Hentze, M. W., Castello, A., Schwarzl, T., and Preiss, T. (2018). A brave new world of RNA-binding proteins. Nat Rev Mol Cell Biol *19*, 327-341.

Hermann, T. (2002). Rational ligand design for RNA: the role of static structure and conformational flexibility in target recognition. Biochimie *84*, 869-875.

Hirsch, F. R., Varella-Garcia, M., Bunn, P. A., Jr., Di Maria, M. V., Veve, R., Bremmes, R. M., Baron, A. E., Zeng, C., and Franklin, W. A. (2003). Epidermal growth factor receptor in non-small-cell lung carcinomas: correlation between gene copy number and protein expression and impact on prognosis. J Clin Oncol *21*, 3798-3807.

Hitti, E., Bakheet, T., Al-Souhibani, N., Moghrabi, W., Al-Yahya, S., Al-Ghamdi, M., Al-Saif, M., Shoukri, M. M., Lanczky, A., Grepin, R.*, et al.* (2016). Systematic Analysis of AU-Rich Element Expression in Cancer Reveals Common Functional Clusters Regulated by Key RNA-Binding Proteins. Cancer Res *76*, 4068-4080.

Hong, S. (2017). RNA Binding Protein as an Emerging Therapeutic Target for Cancer Prevention and Treatment. J Cancer Prev *22*, 203-210.

Huang, H., Weng, H., Sun, W., Qin, X., Shi, H., Wu, H., Zhao, B. S., Mesquita, A., Liu, C., Yuan, C. L., *et al.* (2018a). Recognition of RNA N(6)-methyladenosine by IGF2BP proteins enhances mRNA stability and translation. Nat Cell Biol *20*, 285-295.

Huang, X., Zhang, H., Guo, X., Zhu, Z., Cai, H., and Kong, X. (2018b). Insulin-like growth factor 2 mRNA-binding protein 1 (IGF2BP1) in cancer. J Hematol Oncol *11*, 88.

Huttelmaier, S., Zenklusen, D., Lederer, M., Dictenberg, J., Lorenz, M., Meng, X., Bassell, G. J., Condeelis, J., and Singer, R. H. (2005). Spatial regulation of beta-actin translation by Src-dependent phosphorylation of ZBP1. Nature *438*, 512-515.

Hyun, K., Jeon, J., Park, K., and Kim, J. (2017). Writing, erasing and reading histone lysine methylations. Exp Mol Med *49*, e324.

Ianevski, A., He, L., Aittokallio, T., and Tang, J. (2017). SynergyFinder: a web application for analyzing drug combination dose-response matrix data. Bioinformatics *33*, 2413-2415.

Ito, T., Seyama, T., Hayashi, Y., Hayashi, T., Dohi, K., Mizuno, T., Iwamoto, K., Tsuyama, N., Nakamura, N., and Akiyama, M. (1994). Establishment of 2 human thyroid-carcinoma cell-lines (8305c, 8505c) bearing p53 gene-mutations. Int J Oncol *4*, 583-586.

Jackson, R. J., Hellen, C. U., and Pestova, T. V. (2010). The mechanism of eukaryotic translation initiation and principles of its regulation. Nat Rev Mol Cell Biol *11*, 113-127.

Jeng, Y. M., Chang, C. C., Hu, F. C., Chou, H. Y., Kao, H. L., Wang, T. H., and Hsu, H. C. (2008). RNA-binding protein insulin-like growth factor II mRNA-binding protein 3 expression promotes tumor invasion and predicts early recurrence and poor prognosis in hepatocellular carcinoma. Hepatology *48*, 1118-1127.

Jia, L., Li, B., and Yu, H. (2016). The Bub1-Plk1 kinase complex promotes spindle checkpoint signalling through Cdc20 phosphorylation. Nat Commun *7*, 10818.

Jonson, L., Christiansen, J., Hansen, T. V. O., Vikesa, J., Yamamoto, Y., and Nielsen, F. C. (2014). IMP3 RNP safe houses prevent miRNA-directed HMGA2 mRNA decay in cancer and development. Cell Rep *7*, 539-551.

Joshi, S., and Durden, D. L. (2019). Combinatorial Approach to Improve Cancer Immunotherapy: Rational Drug Design Strategy to Simultaneously Hit Multiple Targets to Kill Tumor Cells and to Activate the Immune System. J Oncol *2019*, 5245034.

Joshua, J. M., and Ali, S. (2017). Multiple Roles for the MLL/COMPASS Family in the Epigenetic Regulation of Gene Expression and in Cancer. Annual Review of Cancer Biology *1*, 425-446.

Jung, C. W., Han, K. H., Seol, H., Park, S., Koh, J. S., Lee, S. S., Kim, M. J., Choi, I. J., and Myung, J. K. (2015). Expression of cancer stem cell markers and epithelial-mesenchymal transition-related factors in anaplastic thyroid carcinoma. Int J Clin Exp Pathol *8*, 560-568.

Kato, T., Hayama, S., Yamabuki, T., Ishikawa, N., Miyamoto, M., Ito, T., Tsuchiya, E., Kondo, S., Nakamura, Y., and Daigo, Y. (2007). Increased expression of insulin-like growth factor-II messenger RNA-binding protein 1 is associated with tumor progression in patients with lung cancer. Clin Cancer Res *13*, 434-442.

Kechavarzi, B., and Janga, S. C. (2014). Dissecting the expression landscape of RNA-binding proteins in human cancers. Genome Biol *15*, R14.

Kim, D., Langmead, B., and Salzberg, S. L. (2015). HISAT: a fast spliced aligner with low memory requirements. Nat Methods *12*, 357-360.

Kim, D., Pertea, G., Trapnell, C., Pimentel, H., Kelley, R., and Salzberg, S. L. (2013). TopHat2: accurate alignment of transcriptomes in the presence of insertions, deletions and gene fusions. Genome Biol *14*, R36.

Kim, Y. N., Koo, K. H., Sung, J. Y., Yun, U. J., and Kim, H. (2012). Anoikis resistance: an essential prerequisite for tumor metastasis. Int J Cell Biol *2012*, 306879.

Kirschner, L. S., Qamri, Z., Kari, S., and Ashtekar, A. (2016). Mouse models of thyroid cancer: A 2015 update. Mol Cell Endocrinol *421*, 18-27.

Kitahara, C. M., Linet, M. S., Beane Freeman, L. E., Check, D. P., Church, T. R., Park, Y., Purdue, M. P., Schairer, C., and Berrington de Gonzalez, A. (2012). Cigarette smoking, alcohol intake, and thyroid cancer risk: a pooled analysis of five prospective studies in the United States. Cancer Causes Control *23*, 1615-1624.

Klambauer, G., Schwarzbauer, K., Mayr, A., Clevert, D. A., Mitterecker, A., Bodenhofer, U., and Hochreiter, S. (2012). cn.MOPS: mixture of Poissons for discovering copy number variations in next-generation sequencing data with a low false discovery rate. Nucleic Acids Res *40*, e69.

Klemm, S. L., Shipony, Z., and Greenleaf, W. J. (2019). Chromatin accessibility and the regulatory epigenome. Nat Rev Genet *20*, 207-220.

Kobel, M., Weidensdorfer, D., Reinke, C., Lederer, M., Schmitt, W. D., Zeng, K., Thomssen, C., Hauptmann, S., and Huttelmaier, S. (2007). Expression of the RNA-binding protein IMP1 correlates with poor prognosis in ovarian carcinoma. Oncogene *26*, 7584-7589.

Kondo, T., Ezzat, S., and Asa, S. L. (2006). Pathogenetic mechanisms in thyroid follicular-cell neoplasia. Nat Rev Cancer *6*, 292-306.

Kudinov, A. E., Karanicolas, J., Golemis, E. A., and Boumber, Y. (2017). Musashi RNA-Binding Proteins as Cancer Drivers and Novel Therapeutic Targets. Clin Cancer Res *23*, 2143-2153.

La Perle, K. M. D., and Jordan, C. D. (2012). Endocrine System. 211-227.

Lai, X., Stiff, A., Duggan, M., Wesolowski, R., Carson, W. E., 3rd, and Friedman, A. (2018). Modeling combination therapy for breast cancer with BET and immune checkpoint inhibitors. Proc Natl Acad Sci U S A *115*, 5534-5539.

Lan, Q., Liu, P. Y., Haase, J., Bell, J. L., Huttelmaier, S., and Liu, T. (2019). The Critical Role of RNA m(6)A Methylation in Cancer. Cancer Res *79*, 1285-1292.

Landa, I., Ibrahimpasic, T., Boucai, L., Sinha, R., Knauf, J. A., Shah, R. H., Dogan, S., Ricarte-Filho, J. C., Krishnamoorthy, G. P., Xu, B.*, et al.* (2016). Genomic and transcriptomic hallmarks of poorly differentiated and anaplastic thyroid cancers. J Clin Invest *126*, 1052-1066.

Langmead, B., and Salzberg, S. L. (2012). Fast gapped-read alignment with Bowtie 2. Nat Methods *9*, 357-359.

Le, H. T., Sorrell, A. M., and Siddle, K. (2012). Two isoforms of the mRNA binding protein IGF2BP2 are generated by alternative translational initiation. PLoS One *7*, e33140.

Lee, K. S., Kwak, Y., Nam, K. H., Kim, D. W., Kang, S. B., Choe, G., Kim, W. H., and Lee, H. S. (2015). c-MYC Copy-Number Gain Is an Independent Prognostic Factor in Patients with Colorectal Cancer. PLoS One *10*, e0139727.

References

Leung, K. M., van Horck, F. P., Lin, A. C., Allison, R., Standart, N., and Holt, C. E. (2006). Asymmetrical beta-actin mRNA translation in growth cones mediates attractive turning to netrin-1. Nat Neurosci *9*, 1247-1256.

Levine, A. J. (1997). p53, the cellular gatekeeper for growth and division. Cell *88*, 323-331.

Levy, M., Lin, F., Xu, H., Dhall, D., Spaulding, B. O., and Wang, H. L. (2010). S100P, von Hippel-Lindau gene product, and IMP3 serve as a useful immunohistochemical panel in the diagnosis of adenocarcinoma on endoscopic bile duct biopsy. Hum Pathol *41*, 1210-1219.

Liao, Y., Smyth, G. K., and Shi, W. (2014). featureCounts: an efficient general purpose program for assigning sequence reads to genomic features. Bioinformatics *30*, 923-930.

Lin, C., and Miles, W. O. (2019). Beyond CLIP: advances and opportunities to measure RBP-RNA and RNA-RNA interactions. Nucleic Acids Res *47*, 5490-5501.

Lin, E. C. (2010). Radiation risk from medical imaging. Mayo Clin Proc *85*, 1142-1146; quiz 1146.

Livak, K. J., and Schmittgen, T. D. (2001). Analysis of relative gene expression data using real-time quantitative PCR and the 2(-Delta Delta C(T)) Method. Methods *25*, 402-408.

Lu, Y. C., Parker, L. L., Lu, T., Zheng, Z., Toomey, M. A., White, D. E., Yao, X., Li, Y. F., Robbins, P. F., Feldman, S. A.*, et al.* (2017). Treatment of Patients With Metastatic Cancer Using a Major Histocompatibility Complex Class II-Restricted T-Cell Receptor Targeting the Cancer Germline Antigen MAGE-A3. J Clin Oncol *35*, 3322-3329.

Mahaira, L. G., Katsara, O., Pappou, E., Iliopoulou, E. G., Fortis, S., Antsaklis, A., Fotinopoulos, P., Baxevanis, C. N., Papamichail, M., and Perez, S. A. (2014). IGF2BP1 expression in human mesenchymal stem cells significantly affects their proliferation and is under the epigenetic control of TET1/2 demethylases. Stem Cells Dev *23*, 2501-2512.

Mahapatra, L., Andruska, N., Mao, C., Le, J., and Shapiro, D. J. (2017). A Novel IMP1 Inhibitor, BTYNB, Targets c-Myc and Inhibits Melanoma and Ovarian Cancer Cell Proliferation. Transl Oncol *10*, 818-827.

Maki-Jouppila, J. H., Pruikkonen, S., Tambe, M. B., Aure, M. R., Halonen, T., Salmela, A. L., Laine, L., Borresen-Dale, A. L., and Kallio, M. J. (2015). MicroRNA let-7b regulates genomic balance by targeting Aurora B kinase. Mol Oncol *9*, 1056-1070.

Manieri, N. A., Drylewicz, M. R., Miyoshi, H., and Stappenbeck, T. S. (2012). Igf2bp1 is required for full induction of Ptgs2 mRNA in colonic mesenchymal stem cells in mice. Gastroenterology *143*, 110-121 e110.

Mark, J., Ekedahl, C., Dahlenfors, R., and Westermark, B. (1987). Cytogenetical observations in five human anaplastic thyroid carcinomas. Hereditas *107*, 163-174.

Mauer, J., Luo, X., Blanjoie, A., Jiao, X., Grozhik, A. V., Patil, D. P., Linder, B., Pickering, B. F., Vasseur, J. J., Chen, Q.*, et al.* (2017). Reversible methylation of m(6)Am in the 5' cap controls mRNA stability. Nature *541*, 371-375.

Mayr, C., and Bartel, D. P. (2009). Widespread shortening of 3'UTRs by alternative cleavage and polyadenylation activates oncogenes in cancer cells. Cell *138*, 673-684.

Mazzu, Y. Z., Armenia, J., Chakraborty, G., Yoshikawa, Y., Coggins, S. A., Nandakumar, S., Gerke, T. A., Pomerantz, M. M., Qiu, X., Zhao, H.*, et al.* (2019). A Novel Mechanism Driving Poor-Prognosis Prostate Cancer: Overexpression of the DNA Repair Gene, Ribonucleotide Reductase Small Subunit M2 (RRM2). Clin Cancer Res *25*, 4480-4492.

McDaniel, K. F., Wang, L., Soltwedel, T., Fidanze, S. D., Hasvold, L. A., Liu, D., Mantei, R. A., Pratt, J. K., Sheppard, G. S., Bui, M. H.*, et al.* (2017). Discovery of N-(4-(2,4-Difluorophenoxy)-3-(6-methyl-7-oxo-6,7-dihydro-1H-pyrrolo[2,3-c]pyridin -4-yl)phenyl)ethanesulfonamide (ABBV-075/Mivebresib), a Potent and Orally Available Bromodomain and Extraterminal Domain (BET) Family Bromodomain Inhibitor. J Med Chem *60*, 8369-8384.

McTiernan, A., Ulrich, C., Slate, S., and Potter, J. (1998). Physical activity and cancer etiology: associations and mechanisms. Cancer Causes Control *9*, 487-509.

Meissner, A., Mikkelsen, T. S., Gu, H., Wernig, M., Hanna, J., Sivachenko, A., Zhang, X., Bernstein, B. E., Nusbaum, C., Jaffe, D. B.*, et al.* (2008). Genome-scale DNA methylation maps of pluripotent and differentiated cells. Nature *454*, 766-770.

Michalak, E. M., Burr, M. L., Bannister, A. J., and Dawson, M. A. (2019). The roles of DNA, RNA and histone methylation in ageing and cancer. Nat Rev Mol Cell Biol *20*, 573-589.

Mikkelsen, T. S., Ku, M., Jaffe, D. B., Issac, B., Lieberman, E., Giannoukos, G., Alvarez, P., Brockman, W., Kim, T. K., Koche, R. P.*, et al.* (2007). Genome-wide maps of chromatin state in pluripotent and lineage-committed cells. Nature *448*, 553-560.

Mills, A. A. (2010). Throwing the cancer switch: reciprocal roles of polycomb and trithorax proteins. Nat Rev Cancer *10*, 669-682.

Minuesa, G., Albanese, S. K., Xie, W., Kazansky, Y., Worroll, D., Chow, A., Schurer, A., Park, S. M., Rotsides, C. Z., Taggart, J.*, et al.* (2019). Small-molecule targeting of MUSASHI RNA-binding activity in acute myeloid leukemia. Nat Commun *10*, 2691.

Mitchell, S. F., and Parker, R. (2014). Principles and properties of eukaryotic mRNPs. Mol Cell *54*, 547-558.

Molenaar, J. J., Domingo-Fernandez, R., Ebus, M. E., Lindner, S., Koster, J., Drabek, K., Mestdagh, P., van Sluis, P., Valentijn, L. J., van Nes, J.*, et al.* (2012). LIN28B induces neuroblastoma and enhances MYCN levels via let-7 suppression. Nat Genet *44*, 1199-1206.

Molinaro, E., Romei, C., Biagini, A., Sabini, E., Agate, L., Mazzeo, S., Materazzi, G., Sellari-Franceschini, S., Ribechini, A., Torregrossa, L.*, et al.* (2017). Anaplastic thyroid carcinoma: from clinicopathology to genetics and advanced therapies. Nat Rev Endocrinol *13*, 644-660.

Monaco, F. (2003). Classification of thyroid diseases: suggestions for a revision. J Clin Endocrinol Metab *88*, 1428-1432.

Mueller-Pillasch, F., Pohl, B., Wilda, M., Lacher, U., Beil, M., Wallrapp, C., Hameister, H., Knochel, W., Adler, G., and Gress, T. M. (1999). Expression of the highly conserved RNA binding protein KOC in embryogenesis. Mech Dev *88*, 95-99.

Muller, S., Bley, N., Glass, M., Busch, B., Rousseau, V., Misiak, D., Fuchs, T., Lederer, M., and Huttelmaier, S. (2018). IGF2BP1 enhances an aggressive tumor cell phenotype by impairing miRNA-directed downregulation of oncogenic factors. Nucleic Acids Res *46*, 6285-6303.

References

Muller, S., Glass, M., Singh, A. K., Haase, J., Bley, N., Fuchs, T., Lederer, M., Dahl, A., Huang, H., Chen, J.*, et al.* (2019). IGF2BP1 promotes SRF-dependent transcription in cancer in a m6A- and miRNA-dependent manner. Nucleic Acids Res *47*, 375-390.

Muller-McNicoll, M., and Neugebauer, K. M. (2013). How cells get the message: dynamic assembly and function of mRNA-protein complexes. Nat Rev Genet *14*, 275-287.

Musselman, C. A., Lalonde, M. E., Cote, J., and Kutateladze, T. G. (2012). Perceiving the epigenetic landscape through histone readers. Nat Struct Mol Biol *19*, 1218-1227.

Nassa, G., Salvati, A., Tarallo, R., Gigantino, V., Alexandrova, E., Memoli, D., Sellitto, A., Rizzo, F., Malanga, D., Mirante, T.*, et al.* (2019). Inhibition of histone methyltransferase DOT1L silences ERalpha gene and blocks proliferation of antiestrogen-resistant breast cancer cells. Sci Adv *5*, eaav5590.

Neelamraju, Y., Hashemikhabir, S., and Janga, S. C. (2015). The human RBPome: from genes and proteins to human disease. J Proteomics *127*, 61-70.

Nguyen, L. H., Robinton, D. A., Seligson, M. T., Wu, L., Li, L., Rakheja, D., Comerford, S. A., Ramezani, S., Sun, X., Parikh, M. S.*, et al.* (2014). Lin28b is sufficient to drive liver cancer and necessary for its maintenance in murine models. Cancer Cell *26*, 248-261.

Nguyen, Q. T., Lee, E. J., Huang, M. G., Park, Y. I., Khullar, A., and Plodkowski, R. A. (2015). Diagnosis and treatment of patients with thyroid cancer. Am Health Drug Benefits *8*, 30-40.

Nicastro, G., Candel, A. M., Uhl, M., Oregioni, A., Hollingworth, D., Backofen, R., Martin, S. R., and Ramos, A. (2017). Mechanism of beta-actin mRNA Recognition by ZBP1. Cell Rep *18*, 1187-1199.

Nielsen, F. C., Nielsen, J., and Christiansen, J. (2001). A family of IGF-II mRNA binding proteins (IMP) involved in RNA trafficking. Scand J Clin Lab Invest Suppl *234*, 93-99.

Nielsen, J., Cilius Nielsen, F., Kragh Jakobsen, R., and Christiansen, J. (2000). The biphasic expression of IMP/Vg1-RBP is conserved between vertebrates and Drosophila. Mech Dev *96*, 129-132.

Nielsen, J., Kristensen, M. A., Willemoes, M., Nielsen, F. C., and Christiansen, J. (2004). Sequential dimerization of human zipcode-binding protein IMP1 on RNA: a cooperative mechanism providing RNP stability. Nucleic Acids Res *32*, 4368-4376.

Nikiforova, M. N., Lynch, R. A., Biddinger, P. W., Alexander, E. K., Dorn, G. W., 2nd, Tallini, G., Kroll, T. G., and Nikiforov, Y. E. (2003). RAS point mutations and PAX8-PPAR gamma rearrangement in thyroid tumors: evidence for distinct molecular pathways in thyroid follicular carcinoma. J Clin Endocrinol Metab *88*, 2318-2326.

Nishino, J., Kim, S., Zhu, Y., Zhu, H., and Morrison, S. J. (2013). A network of heterochronic genes including Imp1 regulates temporal changes in stem cell properties. Elife *2*, e00924.

Noubissi, F. K., Elcheva, I., Bhatia, N., Shakoori, A., Ougolkov, A., Liu, J., Minamoto, T., Ross, J., Fuchs, S. Y., and Spiegelman, V. S. (2006). CRD-BP mediates stabilization of betaTrCP1 and c-myc mRNA in response to beta-catenin signalling. Nature *441*, 898-901.

Noubissi, F. K., Goswami, S., Sanek, N. A., Kawakami, K., Minamoto, T., Moser, A., Grinblat, Y., and Spiegelman, V. S. (2009). Wnt signaling stimulates transcriptional outcome of the Hedgehog pathway by stabilizing GLI1 mRNA. Cancer Res *69*, 8572-8578.

Noubissi, F. K., Nikiforov, M. A., Colburn, N., and Spiegelman, V. S. (2010). Transcriptional Regulation of CRD-BP by c-myc: Implications for c-myc Functions. Genes Cancer *1*, 1074-1082.

Palanichamy, J. K., Tran, T. M., Howard, J. M., Contreras, J. R., Fernando, T. R., Sterne-Weiler, T., Katzman, S., Toloue, M., Yan, W., Basso, G.*, et al.* (2016). RNA-binding protein IGF2BP3 targeting of oncogenic transcripts promotes hematopoietic progenitor proliferation. J Clin Invest *126*, 1495-1511.

Pallante, P., Battista, S., Pierantoni, G. M., and Fusco, A. (2014). Deregulation of microRNA expression in thyroid neoplasias. Nat Rev Endocrinol *10*, 88-101.

Palyi, I., Peter, I., Daubner, D., Vincze, B., and Lorincz, I. (1993). Establishment, characterization and drug sensitivity of a new anaplastic thyroid carcinoma cell line (BHT-101). Virchows Arch B Cell Pathol Incl Mol Pathol *63*, 263-269.

Patel, K. N., and Shaha, A. R. (2006). Poorly differentiated and anaplastic thyroid cancer. Cancer Control *13*, 119-128.

Pereira, B., Billaud, M., and Almeida, R. (2017). RNA-Binding Proteins in Cancer: Old Players and New Actors. Trends Cancer *3*, 506-528.

Perycz, M., Urbanska, A. S., Krawczyk, P. S., Parobczak, K., and Jaworski, J. (2011). Zipcode binding protein 1 regulates the development of dendritic arbors in hippocampal neurons. J Neurosci *31*, 5271-5285.

Potschke, R., Gielen, G., Pietsch, T., Kramm, C., Klusmann, J. H., Huttelmaier, S., and Kuhnol, C. D. (2020). Musashi1 enhances chemotherapy resistance of pediatric glioblastoma cells in vitro. Pediatr Res *87*, 669-676.

Pozdeyev, N., Gay, L. M., Sokol, E. S., Hartmaier, R., Deaver, K. E., Davis, S., French, J. D., Borre, P. V., LaBarbera, D. V., Tan, A. C.*, et al.* (2018). Genetic Analysis of 779 Advanced Differentiated and Anaplastic Thyroid Cancers. Clin Cancer Res *24*, 3059-3068.

Prunier, C., Prudent, R., Kapur, R., Sadoul, K., and Lafanechere, L. (2017). LIM kinases: cofilin and beyond. Oncotarget *8*, 41749-41763.

Ragazzi, M., Ciarrocchi, A., Sancisi, V., Gandolfi, G., Bisagni, A., and Piana, S. (2014). Update on anaplastic thyroid carcinoma: morphological, molecular, and genetic features of the most aggressive thyroid cancer. Int J Endocrinol *2014*, 790834.

Rahib, L., Smith, B. D., Aizenberg, R., Rosenzweig, A. B., Fleshman, J. M., and Matrisian, L. M. (2014). Projecting cancer incidence and deaths to 2030: the unexpected burden of thyroid, liver, and pancreas cancers in the United States. Cancer Res *74*, 2913-2921.

Raman, L., Dheedene, A., De Smet, M., Van Dorpe, J., and Menten, B. (2019). WisecondorX: improved copy number detection for routine shallow whole-genome sequencing. Nucleic Acids Res *47*, 1605-1614.

Rathert, P., Roth, M., Neumann, T., Muerdter, F., Roe, J. S., Muhar, M., Deswal, S., Cerny-Reiterer, S., Peter, B., Jude, J.*, et al.* (2015). Transcriptional plasticity promotes primary and acquired resistance to BET inhibition. Nature *525*, 543-547.

References

Rebucci, M., Sermeus, A., Leonard, E., Delaive, E., Dieu, M., Fransolet, M., Arnould, T., and Michiels, C. (2015). miRNA-196b inhibits cell proliferation and induces apoptosis in HepG2 cells by targeting IGF2BP1. Mol Cancer *14*, 79.

Rodrigues, R. F., Roque, L., Krug, T., and Leite, V. (2007). Poorly differentiated and anaplastic thyroid carcinomas: chromosomal and oligo-array profile of five new cell lines. Br J Cancer *96*, 1237-1245.

Ron, E., Lubin, J. H., Shore, R. E., Mabuchi, K., Modan, B., Pottern, L. M., Schneider, A. B., Tucker, M. A., and Boice, J. D., Jr. (2012). Thyroid cancer after exposure to external radiation: a pooled analysis of seven studies. 1995. Radiat Res *178*, AV43-60.

Rosenfeld, Y. B., Krumbein, M., Yeffet, A., Schiffmann, N., Mishalian, I., Pikarsky, E., Oberman, F., Fridlender, Z., and Yisraeli, J. K. (2019). VICKZ1 enhances tumor progression and metastasis in lung adenocarcinomas in mice. Oncogene *38*, 4169-4181.

Runge, S., Nielsen, F. C., Nielsen, J., Lykke-Andersen, J., Wewer, U. M., and Christiansen, J. (2000). H19 RNA binds four molecules of insulin-like growth factor II mRNA-binding protein. J Biol Chem *275*, 29562-29569.

Rusinek, D., Chmielik, E., Krajewska, J., Jarzab, M., Oczko-Wojciechowska, M., Czarniecka, A., and Jarzab, B. (2017). Current Advances in Thyroid Cancer Management. Are We Ready for the Epidemic Rise of Diagnoses? Int J Mol Sci *18*.

Sarina Anne, P.-P., Jasgit, C. S., Minal, A. B., Patricia, L., Russell Zelig, S., Sapna Pradyuman, P., Mark, D. M., Johannes, E. W., Beibei, H., Anjla, S.*, et al.* (2018). Results of the first-in-human study of ABBV-075 (mivebresib), a pan-inhibitor of bromodomain (BD) and extra terminal (BET) proteins, in patients (pts) with relapsed/refractory (R/R) solid tumors. Journal of Clinical Oncology *36*, 2510-2510.

Schmid, D., Behrens, G., Jochem, C., Keimling, M., and Leitzmann, M. (2013). Physical activity, diabetes, and risk of thyroid cancer: a systematic review and meta-analysis. Eur J Epidemiol *28*, 945-958.

Schmidbauer, B., Menhart, K., Hellwig, D., and Grosse, J. (2017). Differentiated Thyroid Cancer-Treatment: State of the Art. Int J Mol Sci *18*.

Schneider, T., Hung, L. H., Aziz, M., Wilmen, A., Thaum, S., Wagner, J., Janowski, R., Muller, S., Schreiner, S., Friedhoff, P.*, et al.* (2019). Combinatorial recognition of clustered RNA elements by the multidomain RNA-binding protein IMP3. Nat Commun *10*, 2266.

Schoenberg, D. R., and Maquat, L. E. (2012). Regulation of cytoplasmic mRNA decay. Nat Rev Genet *13*, 246-259.

Schubbert, S., Shannon, K., and Bollag, G. (2007). Hyperactive Ras in developmental disorders and cancer. Nat Rev Cancer *7*, 295-308.

Scott, R. W., Hooper, S., Crighton, D., Li, A., Konig, I., Munro, J., Trivier, E., Wickman, G., Morin, P., Croft, D. R.*, et al.* (2010). LIM kinases are required for invasive path generation by tumor and tumor-associated stromal cells. J Cell Biol *191*, 169-185.

Shen, H., and Laird, P. W. (2013). Interplay between the cancer genome and epigenome. Cell *153*, 38-55.

Shi, H., Wei, J., and He, C. (2019). Where, When, and How: Context-Dependent Functions of RNA Methylation Writers, Readers, and Erasers. Mol Cell *74*, 640-650.

Shi, J., Liu, H., Wang, H. L., Prichard, J. W., and Lin, F. (2013). Diagnostic utility of von Hippel-Lindau gene product, maspin, IMP3, and S100P in adenocarcinoma of the gallbladder. Hum Pathol *44*, 503-511.

Singh, G., Pratt, G., Yeo, G. W., and Moore, M. J. (2015). The Clothes Make the mRNA: Past and Present Trends in mRNP Fashion. Annu Rev Biochem *84*, 325-354.

Smallridge, R. C., Ain, K. B., Asa, S. L., Bible, K. C., Brierley, J. D., Burman, K. D., Kebebew, E., Lee, N. Y., Nikiforov, Y. E., Rosenthal, M. S.*, et al.* (2012). American Thyroid Association guidelines for management of patients with anaplastic thyroid cancer. Thyroid *22*, 1104-1139.

Sparanese, D., and Lee, C. H. (2007). CRD-BP shields c-myc and MDR-1 RNA from endonucleolytic attack by a mammalian endoribonuclease. Nucleic Acids Res *35*, 1209-1221.

Stathis, A., and Bertoni, F. (2018). BET Proteins as Targets for Anticancer Treatment. Cancer Discov *8*, 24-36.

Stohr, N., Kohn, M., Lederer, M., Glass, M., Reinke, C., Singer, R. H., and Huttelmaier, S. (2012). IGF2BP1 promotes cell migration by regulating MK5 and PTEN signaling. Genes Dev *26*, 176-189.

Subbiah, V., Kreitman, R. J., Wainberg, Z. A., Cho, J. Y., Schellens, J. H. M., Soria, J. C., Wen, P. Y., Zielinski, C., Cabanillas, M. E., Urbanowitz, G.*, et al.* (2018). Dabrafenib and Trametinib Treatment in Patients With Locally Advanced or Metastatic BRAF V600-Mutant Anaplastic Thyroid Cancer. J Clin Oncol *36*, 7-13.

Subramanian, A., Tamayo, P., Mootha, V. K., Mukherjee, S., Ebert, B. L., Gillette, M. A., Paulovich, A., Pomeroy, S. L., Golub, T. R., Lander, E. S., and Mesirov, J. P. (2005). Gene set enrichment analysis: a knowledge-based approach for interpreting genome-wide expression profiles. Proc Natl Acad Sci U S A *102*, 15545-15550.

Takahashi, K., and Yamanaka, S. (2006). Induction of pluripotent stem cells from mouse embryonic and adult fibroblast cultures by defined factors. Cell *126*, 663-676.

Tang, A., Gao, K., Chu, L., Zhang, R., Yang, J., and Zheng, J. (2017). Aurora kinases: novel therapy targets in cancers. Oncotarget *8*, 23937-23954.

Tessier, C. R., Doyle, G. A., Clark, B. A., Pitot, H. C., and Ross, J. (2004). Mammary tumor induction in transgenic mice expressing an RNA-binding protein. Cancer Res *64*, 209-214.

Tiedje, V., Stuschke, M., Weber, F., Dralle, H., Moss, L., and Fuhrer, D. (2018). Anaplastic thyroid carcinoma: review of treatment protocols. Endocr Relat Cancer *25*, R153-R161.

Tiedje, V., Ting, S., Herold, T., Synoracki, S., Latteyer, S., Moeller, L. C., Zwanziger, D., Stuschke, M., Fuehrer, D., and Schmid, K. W. (2017). NGS based identification of mutational hotspots for targeted therapy in anaplastic thyroid carcinoma. Oncotarget *8*, 42613-42620.

Trabucco, S. E., Gerstein, R. M., Evens, A. M., Bradner, J. E., Shultz, L. D., Greiner, D. L., and Zhang, H. (2015). Inhibition of bromodomain proteins for the treatment of human diffuse large B-cell lymphoma. Clin Cancer Res *21*, 113-122.

Trendel, J., Schwarzl, T., Horos, R., Prakash, A., Bateman, A., Hentze, M. W., and Krijgsveld, J. (2019). The Human RNA-Binding Proteome and Its Dynamics during Translational Arrest. Cell *176*, 391-403 e319.

References

Tu, H. C., Schwitalla, S., Qian, Z., LaPier, G. S., Yermalovich, A., Ku, Y. C., Chen, S. C., Viswanathan, S. R., Zhu, H., Nishihara, R.*, et al.* (2015). LIN28 cooperates with WNT signaling to drive invasive intestinal and colorectal adenocarcinoma in mice and humans. Genes Dev *29*, 1074-1086.

Tybl, E., Shi, F. D., Kessler, S. M., Tierling, S., Walter, J., Bohle, R. M., Wieland, S., Zhang, J., Tan, E. M., and Kiemer, A. K. (2011). Overexpression of the IGF2-mRNA binding protein p62 in transgenic mice induces a steatotic phenotype. J Hepatol *54*, 994-1001.

Undeutsch, H., Lof, C., Offermanns, S., and Kero, J. (2014). A mouse model with tamoxifen-inducible thyrocyte-specific cre recombinase activity. Genesis *52*, 333-340.

Uren, P. J., Vo, D. T., de Araujo, P. R., Potschke, R., Burns, S. C., Bahrami-Samani, E., Qiao, M., de Sousa Abreu, R., Nakaya, H. I., Correa, B. R.*, et al.* (2015). RNA-Binding Protein Musashi1 Is a Central Regulator of Adhesion Pathways in Glioblastoma. Mol Cell Biol *35*, 2965-2978.

Van Nostrand, E. L., Pratt, G. A., Shishkin, A. A., Gelboin-Burkhart, C., Fang, M. Y., Sundararaman, B., Blue, S. M., Nguyen, T. B., Surka, C., Elkins, K.*, et al.* (2016). Robust transcriptome-wide discovery of RNA-binding protein binding sites with enhanced CLIP (eCLIP). Nat Methods *13*, 508-514.

Vanderpump, M. P. (2011). The epidemiology of thyroid disease. Br Med Bull *99*, 39-51.

Vervoorts, J., Luscher-Firzlaff, J., and Luscher, B. (2006). The ins and outs of MYC regulation by posttranslational mechanisms. J Biol Chem *281*, 34725-34729.

Vikesaa, J., Hansen, T. V., Jonson, L., Borup, R., Wewer, U. M., Christiansen, J., and Nielsen, F. C. (2006). RNA-binding IMPs promote cell adhesion and invadopodia formation. EMBO J *25*, 1456-1468.

Viola, D., Valerio, L., Molinaro, E., Agate, L., Bottici, V., Biagini, A., Lorusso, L., Cappagli, V., Pieruzzi, L., Giani, C.*, et al.* (2016). Treatment of advanced thyroid cancer with targeted therapies: ten years of experience. Endocr Relat Cancer *23*, R185-205.

Vu, L. P., Pickering, B. F., Cheng, Y., Zaccara, S., Nguyen, D., Minuesa, G., Chou, T., Chow, A., Saletore, Y., MacKay, M.*, et al.* (2017). The N(6)-methyladenosine (m(6)A)-forming enzyme METTL3 controls myeloid differentiation of normal hematopoietic and leukemia cells. Nat Med *23*, 1369-1376.

Wachter, K., Kohn, M., Stohr, N., and Huttelmaier, S. (2013). Subcellular localization and RNP formation of IGF2BPs (IGF2 mRNA-binding proteins) is modulated by distinct RNA-binding domains. Biol Chem *394*, 1077-1090.

Wagner, M., Kunsch, S., Duerschmied, D., Beil, M., Adler, G., Mueller, F., and Gress, T. M. (2003). Transgenic overexpression of the oncofetal RNA binding protein KOC leads to remodeling of the exocrine pancreas. Gastroenterology *124*, 1901-1914.

Wang, L., Rowe, R. G., Jaimes, A., Yu, C., Nam, Y., Pearson, D. S., Zhang, J., Xie, X., Marion, W., Heffron, G. J.*, et al.* (2018). Small-Molecule Inhibitors Disrupt let-7 Oligouridylation and Release the Selective Blockade of let-7 Processing by LIN28. Cell Rep *23*, 3091-3101.

Warner, K. D., Hajdin, C. E., and Weeks, K. M. (2018). Principles for targeting RNA with drug-like small molecules. Nat Rev Drug Discov *17*, 547-558.

Williams, D. (2008). Radiation carcinogenesis: lessons from Chernobyl. Oncogene *27 Suppl 2*, S9-18.

Wilson, P. M., Labonte, M. J., Russell, J., Louie, S., Ghobrial, A. A., and Ladner, R. D. (2011). A novel fluorescence-based assay for the rapid detection and quantification of cellular deoxyribonucleoside triphosphates. Nucleic Acids Res *39*, e112.

Woodward, E. L., Biloglav, A., Ravi, N., Yang, M., Ekblad, L., Wennerberg, J., and Paulsson, K. (2017). Genomic complexity and targeted genes in anaplastic thyroid cancer cell lines. Endocr Relat Cancer *24*, 209-220.

Wurth, L., and Gebauer, F. (2015). RNA-binding proteins, multifaceted translational regulators in cancer. Biochim Biophys Acta *1849*, 881-886.

Xuan, J. J., Sun, W. J., Lin, P. H., Zhou, K. R., Liu, S., Zheng, L. L., Qu, L. H., and Yang, J. H. (2018). RMBase v2.0: deciphering the map of RNA modifications from epitranscriptome sequencing data. Nucleic Acids Res *46*, D327-D334.

Yaniv, K., and Yisraeli, J. K. (2002). The involvement of a conserved family of RNA binding proteins in embryonic development and carcinogenesis. Gene *287*, 49-54.

Yates, A., Akanni, W., Amode, M. R., Barrell, D., Billis, K., Carvalho-Silva, D., Cummins, C., Clapham, P., Fitzgerald, S., Gil, L.*, et al.* (2016). Ensembl 2016. Nucleic Acids Res *44*, D710-716.

Yi, C., Li, G., Ivanov, D. N., Wang, Z., Velasco, M. X., Hernandez, G., Kaundal, S., Villarreal, J., Gupta, Y. K., Qiao, M.*, et al.* (2018). Luteolin inhibits Musashi1 binding to RNA and disrupts cancer phenotypes in glioblastoma cells. RNA Biol *15*, 1420-1432.

Yisraeli, J. K. (2005). VICKZ proteins: a multi-talented family of regulatory RNA-binding proteins. Biol Cell *97*, 87-96.

Yoo, S. K., Song, Y. S., Lee, E. K., Hwang, J., Kim, H. H., Jung, G., Kim, Y. A., Kim, S. J., Cho, S. W., Won, J. K.*, et al.* (2019). Integrative analysis of genomic and transcriptomic characteristics associated with progression of aggressive thyroid cancer. Nat Commun *10*, 2764.

Yu, J., Vodyanik, M. A., Smuga-Otto, K., Antosiewicz-Bourget, J., Frane, J. L., Tian, S., Nie, J., Jonsdottir, G. A., Ruotti, V., Stewart, R.*, et al.* (2007). Induced pluripotent stem cell lines derived from human somatic cells. Science *318*, 1917-1920.

Zaccara, S., Ries, R. J., and Jaffrey, S. R. (2019). Reading, writing and erasing mRNA methylation. Nat Rev Mol Cell Biol *20*, 608-624.

Zhan, T., Rindtorff, N., Betge, J., Ebert, M. P., and Boutros, M. (2019). CRISPR/Cas9 for cancer research and therapy. Semin Cancer Biol *55*, 106-119.

Zhao, B. S., and He, C. (2015). Fate by RNA methylation: m6A steers stem cell pluripotency. Genome Biol *16*, 43.

Zhou, X., Zhang, C. Z., Lu, S. X., Chen, G. G., Li, L. Z., Liu, L. L., Yi, C., Fu, J., Hu, W., Wen, J. M., and Yun, J. P. (2015). miR-625 suppresses tumour migration and invasion by targeting IGF2BP1 in hepatocellular carcinoma. Oncogene *34*, 965-977.

Zhu, X., Enomoto, K., Zhao, L., Zhu, Y. J., Willingham, M. C., Meltzer, P., Qi, J., and Cheng, S. Y. (2017). Bromodomain and Extraterminal Protein Inhibitor JQ1 Suppresses Thyroid Tumor Growth in a Mouse Model. Clin Cancer Res *23*, 430-440.

Zhu, X., Holmsen, E., Park, S., Willingham, M. C., Qi, J., and Cheng, S. Y. (2018). Synergistic effects of BET and MEK inhibitors promote regression of anaplastic thyroid tumors. Oncotarget *9*, 35408-35421.

Zhu, X., Park, S., Lee, W. K., and Cheng, S. Y. (2019). Potentiated anti-tumor effects of BETi by MEKi in anaplastic thyroid cancer. Endocr Relat Cancer.

7. APPENDIX

7.1 Supplementary tables

Table A1. Molecular and clinical characteristics of tumor cohorts

| | No. of Tumors (%) | | | | | | | | | |
| | RNA-seq (test cohort) | | | in-house tissue microarray (TMA I) | | | | commercial tissue microarray (TMA II) | | |
	ATC	PTC	FTC	ATC	PDTC	PTC	FTC	ATC	PTC	FTC
Total	10	6	6	20	18	82	29	6	43	20
Sex										
female	7 (70)	3 (50)	4 (66.7)	10 (50)	10 (55.6)	44 (53.7)	11 (37.9)	4 (66.7)	37 (86.1)	14 (70)
male	3 (30)	3 (50)	2 (33.3)	10 (50)	8 (44.4)	38 (46.3)	18 (62.1)	2 (33.3)	6 (13.9)	6 (30)
median age, years (range)	68.5 (48-81)	50 (23-81)	55.5 (41-79)	67 (33-89)	70 (27-83)	47 (7-90)	63 (17-89)	55.5 (30-86)	40 (18-76)	54.5 (20-77)
UICC stage										
I	0	1 (16.7)	1 (16.7)	0	2 (11.1)	49 (59.8)	10 (34.5)	0	23 (53.5)	4 (20)
II	0	2 (33.3)	1 (16.7)	0	1 (5.6)	6 (7.3)	4 (13.8)	0	13 (30.2)	4 (20)
III	0	2 (33.3)	4 (66.7)	0	6 (33.3)	13 (15.9)	6 (20.7)	0	7 (16.3)	11 (55)
IV	10 (100)	1 (16.7)	0	13 (65)	9 (50)	13 (15.9)	1 (3.4)	6 (100)	0	1 (5)
nd	0	0	0	7 (35)	0	1 (1.2)	8 (27.6)	0	0	0
pos. protein expression [A]										
IGF2BP1	10 (100)	0	0	14 (70)	1 (5.6)	0	0	3 (50)	0	0
MAGE3A	10 (100)	0	0	7 (35)	0	0	0	1 (16.67)	0	0
MYC	9 (90)	5 (83.3)	3 (50)	15 (75)	2 (11.1)	1 (1.2)	5 (17.24)	2 (33.3)	0	0
IGF2BP1 CN gain [B]	1 (10) [C]	0	1 (16.7)	nd				nd		

[A] Protein expression was detected by Western blot (samples prior used for RNA-seq) or via immunohistochemistry (TMAs).
[B] Copy numbers were determined by sWGS (only for samples prior used for RNA-seq).
[C] Only the promoter region, exon 1 and exon 2 were found to be gained.
Abbreviations: UICC, Union internationale contre le cancer; nd, not determined; CN, Copy Number; pos, positive.

Table A2. WDTC-content of TMA I samples

sample #	entity	IGF2BP1 protein	WDTC/PDTC content
1	ATC	pos	-
2	ATC	neg	-
3	ATC	neg	-
4	ATC	pos	PTC
5	ATC	pos	PTC
6	ATC	pos	-
7	ATC	pos	-
8	ATC	pos	PDTC
9	ATC	pos	-
10	ATC	neg	-
11	ATC	pos	-
12	ATC	pos	FTC + PDTC
13	ATC	pos	PDTC
14	ATC	neg	-
15	ATC	neg	-
16	ATC	pos	-
17	ATC	pos	-
18	ATC	pos	-
19	ATC	pos	-
20	ATC	neg	-

7.2 List of figures

7.3 List of tables

7.4 List of abbreviations

3'	3-prime
5'	5-prime
aCGH	array-comparative genomic hybridizatio
ActD	actinomycin D
AML	acute myeloid leukemia
ARE	AU-rich element
as	antisense
ATC	anaplastic thyroid carcinoma
ATP	adenosinetriphosphate
BET	bromodomain and extra-terminal motif
bp	base pair
BRD	bromodomain
cDNA	complementary DNA
CDS	coding sequence
ChIP	chromatin-immunoprecipitation
CLIP	crosslinking-immunoprecipitation
CRISPR	clustered regularly interspaced short palindromic repeats
CT	cycle threshold
Ctrl	control
dATP	deoxyadenosine triphosphate
dCTP	deoxycytosine triphosphate
dGTP	deoxyguanosine triphosphate
DMEM	Dulbecco's modified Eagle's medium
DMSO	dimethyl sulfoxid
DNA	desoxyribonuleic acid
dNTP	desoxyribonucleosid triphosphate
dTTP	deoxythymidine triphosphate
DOR	diagnostic odds ratio
dT	desoxythymidine
EC_{50}	half-effective concentration
eCLIP	enhanced crosslinking-immunoprecipitation
E. coli	*Escherichia coli*
ECM	extra-cellular matrix
EDTA	ethylenediaminetetraacetate

Appendix

E_{max}	maximal efficacy
EMT	epithelial-mesenchymal-transition
ENCODE	Encyclopedia of DNA Elements
ESC	embryonic stem cell
EtOH	ethanol
FACS	fluorescence-activated cell sorting
FBS	fetal bovine serum
FDA	Food and Drug Agency
FDR	false discovery rate
FFL	firefly luiferase
FTC	follicular thyroid carcinoma
g	relative centrifugal force
gDNA	genomic desoxyribonucleic acid
GFP	green fluorescent protein
GSEA	gene set enrichment analysis
h	hours
H3K4/27me3	histone H3 lysine 4/27 tri-methylation
HE	hematoxilin eosin
HSA	highest single agent
I^{131}	iodine-131
IgG	immunoglobulin G
IHC	immunohistochemistry
IP	immunoprecipitation
IRES	internal ribosomal entry site
iRFP	near-infrared fluorescent protein
KD	knockdown
kDa	kilo Dalton
KH	k-homology
KO	knockout
LB	lysogeny broth
log	logarithm
loxP	locus of X(cross)-over in P1
LSL	lox-stop-lox
LUT	look up table
m6A	N6-methyladenosine
MeOH	methanol

M	molar
min	minutes
miRNA	micro RNA
ml	millilitre
mm	millimeter
mM	millimolar
mRNA	messenger RNA
mRNP	messenger RNP
MTC	medullary thyroid carcinoma
n	number
NaDoc	sodium deoxycholat
ncRNA	non-coding RNA
nM	nanomolar
NPC	neural progenitor cell
nt	nucleotide
NT	non-malignant thyroid tissue
NTP	nucleoside triphosphate
OE	overexpression
PAGE	polyacrylamide gelelectrophoresis
PAR-CLIP	photoactivatable-ribonucleoside-enhanced crosslinking-immunoprecipitation
PBS	phosphate-buffered saline
PCR	polymerase-chain reaction
PDTC	poorly-differentiated thyroid carcinoma
pH	potential of hydrogen
PRC	polycomb-repressive complex
PROTAC	proteolysis-targeting chimeras
PTC	papillary thyroid crcinoma
R6	random hexamers
RBP	RNA-binding protein
RET	rearranged during transfection
RIP	RNA-immunoprecipitation
RISC	RNA-induced silencing complex
RNA	ribonucleic acid
RNase	ribonuclease
RNP	ribonucleoprotein

rpm	rounds per minute
RRM	RNA-recognition motif
RT	room temperature
RT-qPCR	real-time quantitative PCR
s	sense
sec	seconds
SDS	sodium dodecylsulfate
Ser	serine
Seq	sequencing, referring to next generation sequencing
sgRNA	small guide RNA
shRNA	small hairpin RNA
siRNA	small interfering RNA
sWGS	shallow whole genome-sequencing
T3	triiodothyronine
T4	thyroxine
TAE	Tris-Acetate-EDTA
TCGA	The Cancer Genome Atlas
TE	Tris-EDTA
Tg	thyroglobulin
TMA	tissue micro-array
TrxG	thrithorax group
UTR	untranslated region
UV	ultra violet
V	volt
WB	Western blot
WDTC	well-differentiated thyroid carcinoma
WT	wildtype
%	percent
% (w/v)	percent weight/volume
% (v/v)	percent by volume
°C	centigrade
μ	micro
μl	microliter
μm	micrometer
μM	micromola

Danksagung

An dieser Stelle möchte ich noch ein paar Personen danken: Mitwirkenden, Kollegen, Freunden, Familie.

Diese geschriebene Arbeit repräsentiert nur eine „Formsache". Die Abgabe war schon längst überfällig, aber Stefan hat es geschafft, dass ich für diesen Job 24/7 brenne und ich deshalb eher Experimenten nachgejagt bin, als zu schreiben. Was soll man auch machen, wenn die Laborausstattung und das Mindset der AG in Halle ihresgleichen suchen und man um die Welt jetten darf. Danke dafür.

Großer Dank gilt der gesamten AG, von der viele zu Freunden geworden sind.
Ich danke außerdem Allen, die dem ATC-Projekt Daten und Material geliefert haben: Niko, Marcus, Udo Siebolts, Claudia Wickenhauser, Kerstin Lorenz und Henning Dralle.

Ich danke meiner Familie für Unterstützung und Rückhalt.

Besonders möchte ich mich bei Rebecca bedanken, für das Science-Couple-sein, ihren Antrieb, ihr Verständnis, ihre Geduld und unsere Pläne inklusive Rosalind.

Curriculum Vitae

Personal Details

Name: Jacob Haase

Date of birth, birthplace: 31.03.1989, Karl-Marx-Stadt (Chemnitz)

Nationality: German

Education

1995 – 1999   Emanuel Gottlieb Flemming-Grundschule, Chemnitz

1999 – 2005   Emanuel – Gottlieb – Flemming Realschule, Chemnitz

2005 – 2008   BSZ für Wirtschaft II Berufliches Gymnasium, Chemnitz – Abitur

Scientific Education

2008 – 2011   B.Sc. studies in Biology at the Martin Luther University Halle-
                            Wittenberg
                            – 02/2011 - 08/2011: Thesis under supervision of Prof. Dr. Ulla Bonas
                            at the Martin Luther University Halle-Wittenberg; Title: „Die
                            Charakterisierung des letzten halben *repeats* in AvrBs3".

2012 – 2014   M.Sc. studies in Biology at the Martin Luther University Halle-
                            Wittenberg
                            08/2012 - 09/2012: Internship at the Zentrum für Diagnostik
                            (Humangenetik) at the Klinikum Chemnitz
                            03/2014 - 12/2014: Thesis under supervision of Prof. Dr. Mechtild
                            Hatzfeld; Title: „Investigation of the post-transcriptional regulation of δ-
                            catenin".

2014 – 2020   Doctoral studies (associated Ph.D. student at the RTG 1591) in the
                            Laboratory of Prof. Dr. Stefan Hüttelmaier at the Martin Luther
                            University Halle-Wittenberg
                            10/2019 - 11/2019: Research stay in the laboratory of Prof. Dr. Markus
                            Landthaler at the Max-Delbrück Center Berlin

Publications

Müller S., Glaß M., Singh A. K., **Haase J.**, Bley N., Fuchs T., Lederer M., Dahl A., Huang H., Chen J., Posern G., Hüttelmaier S. October 2018
IGF2BP1 promotes SRF-dependent transcription in cancer in a m6A- and miRNA-dependent manner. *Nucleic Acids Research* 47(1)

Lan Q., Liu P. Y., **Haase J.**, Bell J. L., Hüttelmaier S., Liu T. March 2019
The critical role of RNA m6A methylation. *Cancer Research* 79(7)

Presentations and workshops

19/03/2019, Wernigerode, Germany – "Next Level: Advanced CRISPR/Cas approaches and CRISPR Screen"

06/12/2019, Halle (Saale), Germany – "Identification of the first diagnostic marker for Anaplastic Thyroid Carcinoma"

Poster

06/2016 – RNA meeting, Kyoto, Japane – "The oncogenic role of the IGF2 mRNA-binding protein 1 (IGF2BP1) in anaplastic thyroid carcinoma (ATCs)"

05/2017 – RNA meeting, Prague, Czech Republic – "Different RNA-sequencing approaches lead to the identification and validation of downstream effectors of the oncogenic IGF2 mRNA-binding protein 1 (IGF2BP1) in anaplastic thyroid carcinoma (ATC)"

10/2018 – Annual Meeting of the American Thyroid Association, Washington D.C., USA – "IGF2BP1 is a novel targetable & MYC-dependent post-transcriptional enhancer of ATC"

Erklärung

Hiermit erkläre ich, dass ich meine Dissertationsschrift selbständig und ohne fremde Hilfe verfasst habe. Ich habe keine anderen als die von mir angegebenen Quellen und Hilfsmittel benutzt. Die aus den benutzten Werken wörtlich oder inhaltlich entnommenen Stellen habe ich als solche kenntlich gemacht.

Mit der vorliegenden Arbeit bewerbe ich mich erstmals um die Erlangung des Doktorgrades.

Halle (Saale), Juni 2020

Jacob Haase